Structure-activity relationship between *Klebsiella pneumoniae* β-Lactamase CTX-M-15 and selected β-lactam antibiotics: Evaluating the binding site promiscuity.

by

Veruschka Esau
(1473414)

Research Thesis

Submitted in fulfilment of the requirements for the degree

Master of Science

in

Molecular and Cell Biology

in the Faculty of Science, University of the Witwatersrand, Johannesburg, South Africa

Supervisor: Dr. Ikechukwu A. Achilonu
Co-supervisor: Prof Yasien Sayed

2023

Declaration

I declare that this dissertation is my own, unaided work. It is being submitted for the Degree of Master of Science at the University of the Witwatersrand, Johannesburg. It has not been submitted before for any degree or examination at any other University.

_____ _____
Veruschka Esau

Publication

Jeje, Olamide; Maake, Reabetswe; van Deventer, Ruan; **Esau, Veruschka**; Iwuchukwu, Emmanuel Amarachi; Meyer, Vanessa; Khoza, Thandeka; Achilonu, Ikechukwu; Effect of Divalent Metal Ion on the Structure, Stability and Function of Klebsiella pneumoniae Nicotinate-Nucleotide Adenylyltransferase: Empirical and Computational Studies, ***International journal of molecular sciences***, 23(116), 2022 MDPI.

Role: Assisted with conducting of Thermal shift assay experiments.

Abstract

Background: Nosocomial infections have become a major concern in Sub-Saharan Africa. Bacteria predominantly cause these infections due to resistance development attributed to lack of novel therapeutics. These resistant bacteria are classed as ESKAPE pathogens that gained resistance to most known antimicrobials; one such is the Gram-negative *Klebsiella pneumoniae*. *K. pneumoniae* developed resistant strategies against most known β-lactam antibiotics through the development of the enzyme, β-lactamase. Beta-lactamases hydrolyse the β-lactam ring of β-lactam antibiotics rendering them ineffective towards *K. pneumoniae*. This research aimed to investigate the structural and functional characteristics of *K. pneumoniae* β-lactamase and asses the conformational stability with penicillin and cefoperazone (CPZ). **Methods**: Overexpression of recombinant wild-type and mutant-(S70A) *K. pneumoniae* β-lactamase in *E. coli* T7 cells using a pET-28a vector and protein purification using Immobilised Metal Affinity Chromatography (IMAC), and enzyme activity assessed with nitrocefin. Secondary, tertiary, and quaternary structure studies were conducted with Far-UV CD, tryptophan fluorescence, ANS fluorescence and size exclusion HPLC respectively. The thermal stability and binding mechanisms were assessed with thermal shift assay and isothermal titration calorimetry (ITC). **Results**: The wild-type and mutant-(S70A) *K. pneumoniae* β-lactamase was successfully expressed and purified. S70A-KpBlac-1 showed no activity towards nitrocefin, and WT-KpBlac-1 was highly activity towards nitrocefin. The native structures were determined to be alpha-helical, but alpha-helical content is lost upon penicillin and CPZ binding to unorder and β-stranded conformations. The binding site was determined to be solvent exposed with one hydrophobic active site. The proteins were monomeric. CPZ induce thermal stability on S70A-KpBlac-1, whereas as penicillin binding had no effect on the thermal stability. Penicillin binding to S70A-KpBlac-1 was endothermic and the protein had low binding affinity for penicillin. CPZ binding was exothermic, and the protein had higher binding affinity for the substrate. **Conclusion**: Potential novel inhibitor design should be focused on CPZ. Through substrate-based drug discovery, potential drugs should confer a similar shape, size, or stereochemistry as CPZ. This would change the conformation of the protein, be tightly bound to the active site, and lower inhibitor concentration would be required. Therefore, these findings contribute, and provide insights on potential novel inhibitors against highly antibiotic resistant bacteria.

Acknowledgements

I would like to express my greatest gratitude toward my supervisor; Dr. Ikechukwu A. Achilonu, who has supported and guided me tremendously throughout my research project. He's guidance has helped in expanding my knowledge and passion for the field of biochemistry. I want to sincerely thank you for all the encouragement, patience and understanding.

The Protein-Structure Function Research Unit (PSFRU) for providing a platform for learning and growth within Protein Science.

Olamide Jeje, Reabetswe Maake, Blessing Oyiogu, and Dr Monare Thulo; thank you for all the aid and wisdom you all have imparted to me.

The National Research Foundation for funding.

A very special thanks to my family for all the support and continued encouragement through my tough times. Your love, faith and believe in me motivates me to achieve my dreams and goals.

Table of contents

List of figures and tables

List of Abbreviations

AMPs	Antimicrobial peptides
ANS	8-anilino-1-naphthalenesulfonic acid
BamHI	Restriction endonuclease from *Bacillus amyloliquefaciens*
CAUTI	Catheter-associated urinary tract infections
cDNA	Complementary DNA
CLABSI	Central line-associated bloodstream infections
Clp	Caseinolytic proteins
ClpK	Caseinolytic proteins found in *K. pneumoniae*
CPZ	Cefoperazone
CTX-M-15	Cefotaximase-Munich type (15)
DBO	Diazabicyclooctanes
DMSO	Dimethyl sulfoxide
EC	Enzyme class
EDTA	Ethylenediaminetetraacetic acid
ESBL	Extended-spectrum Beta-lactamases
ESKAPE	*Enterococcus faecium, Staphylococcus aureus, Klebsiella pneumoniae, Acinetobacter baumannii, Pseudomonas aeruginosa, and Enterobacter species*
Far-UV CD	Far-ultraviolet circular dichroism
FTIR	Fourier Transform Infrared
ΔG	Change in Gibbs free energy in standard conditions
ΔH	Change in enthalpy in standard conditions
HAIs	Health-care-associated infections
His	Histidine
IDA	Iminodiacetic acid
IMAC	Immobilized Metal Affinity Chromatography
IPTG	Isopropyl β-D-1-thiogalactopyranoside
ITC	Isothermal titration calorimetry
Ka	Association constant
KD	Dissociation constant
kDa	Kilodalton
KpBlac	*Klebsiella pneumoniae* Beta-Lactamase
KPCs	*Klebsiella pneumoniae* carbapenemases
lacUV5	Mutated variant form of the Lactose promoter (TATGTT----TAT**AA**T)
LB	Lysogeny broth
MDR	Multi-drug resistant
MRSA	Methicillin-resistant *Staphylococcus aureus*
n	Stoichiometry
NcoI	Restriction endonuclease from *Nocardia corallina*
NTA	Nitrilotriacetic acid
OD600	Optical density at 600 nm
OXA-	Family of Beta-lactamases which are able to hydrolyze cloxacillin or oxacillin

PBP	Penicillin-binding protein
PDB	Protein Data Bank
pET	Plasmid for expression by T7 RNA polymerase
RMSD	Root means square deviation
ΔH	Change in entropy in standard conditions
SDS-PAGE	Sodium dodecyl sulphate polyacrylamide gel electrophoresis
SE-HPLC	Size exclusion high-pressure liquid chromatography
SOC	Super optimal broth with catabolite repression
SSI	Surgical site infections
S70A-KpBlac-1	Mutant; Serine-70-Alanine *Klebsiella pneumoniae* Beta-Lactamase-1
TCEP	Tris(2-carboxyethyl)phosphine
TEMED	Tetramethylethylenediamine
TSA	Thermal shift assay
Tm	Melting temperature
T7 RNA	RNA polymerase from the T7 bacteriophage
VAP	Ventilator-associated pneumonia
VRE	Vancomycin-resistance *Enterococcus*
WHO	World Health Organization
WT-KpBlac-1	Wild-type *Klebsiella pneumoniae* Beta-Lactamase-1

Chapter 1
Introduction

1.1 Problem statement

Hospital-acquired infections (HAIs), or nosocomial infections, have become a major concern in Sub-Saharan Africa. These infections are commonly contracted due to prolonged hospitalisation and are noticed in approximately 50% of patients (Tolera *et al*., 2018). These infections are difficult to combat due to the causative microorganisms' evolutionary ability to escape the biocidal action of antibacterial drugs (Mulani *et al.,* 2019). Statistics from the World Health Organisation (WHO); revealed that nosocomial infections result in 10% and 7% of fatalities in developing and developed countries, respectively (Khan *et al*., 2017). Sources of infections are contaminated areas, medical equipment, and antibiotic overuse, which leads to antibiotic-resistant bacteria, more so multidrug-resistant (MDR) pathogens (Tolera *et al*., 2018). Common nosocomial infections include surgical site infections (SSI), catheter-associated urinary tract infections (CAUTI), ventilator-associated pneumonia (VAP), and central line-associated bloodstream infections (CLABSI) (Agaba *et al*., 2017). Bacteria that cause nosocomial infections have developed strategies to evade the biocidal activity of antimicrobials and thus are difficult to prevent. These bacteria are classified as ESKAPE pathogens (Mulani *et al*., 2019).

ESKAPE pathogens are evolutionarily developed Gram-positive and Gram-negative bacteria which have escaped antimicrobial effects. *Enterococcus faecium, Staphylococcus aureus, Klebsiella pneumoniae, Acinetobacter baumannii, Pseudomonas aeruginosa* and *Enterobacter species* are grouped into the acronym "ESKAPE" pathogens (Mulani *et al.*, 2019). Continuous use of antibiotics causes resistant bacterial strains due to selective pressure. Resistance genes are obtained from other resistant bacterial chromosomes through plasmids, transposons (transformation, conjugation, or transduction), efflux pumps or *de novo* mutations (Santajit and Indrawattana, 2016). Downregulation of bacterial porin genes due to mutations or alterations in cell wall permeability prevents intracellular entry of antimicrobials (Santajit and Indrawattana, 2016). Ventilator-associated pneumonia is caused by Gram-negative *Klebsiella pneumoniae* (*K. pneumoniae*) and is attributed to 86% of pneumonia-related nosocomial infections (Fischbach,

2011). *K. pneumoniae* commonly causes respiratory and urinary tract infections, as well as bloodstream infections. Penicillin, cephalosporin, and carbapenem-resistant bacteria are categorised as extended-spectrum beta-lactamases (ESBLs) (Dirar *et al.*, 2020). WHO reported that third-generation cephalosporins resistance in African countries by *K. pneumoniae* was 27.6%, and *K. pneumoniae* resistance to carbapenems was 8.5% (Prestinaci *et al*., 2015). In 1996, *K. pneumoniae* was identified that was able to hydrolyse every beta-lactam drug and was classified as carbapenemase-hydrolysing *K. pneumoniae* (Nordmann *et al.,* 2009). Ciprofloxacin is a commonly prescribed drug for urinary tract infections (Aditi Priyadarshini *et al.*, 2019). Due to overuse, the resistance of *Klebsiella pneumoniae* towards ciprofloxacin has spiked from 4.1% to 79.4% and 8.4% to 92.9% in *Escherichia coli* (Yang *et al*., 2014). Antimicrobial resistance makes bacterial infection treatment increasingly complicated; due to limited therapeutic options. Therefore, designing new novel therapeutic drugs targeted against nosocomial infection treatment are required to combat MDR strains such as *Klebsiella pneumoniae.*

1.2 **Rationale of the study**

The increasing pathogenicity of ESKAPE pathogens due to antibiotic resistance is a major concern in Sub-Saharan Africa; thus, new drug therapies should be developed (Santajit and Indrawattana, 2016). Also, since prevailing antibiotics utilise DNA synthesis and cellular functions like interfering with the cell wall as targets; thus, newer alternatives need to be explored (Vaara *et al.,* 2013). At present, β-lactam antibiotics are the first-line therapy against ESKAPE pathogens (Mulani *et al.*, 2019). And due to resistance development within these bacterial species, newer antibiotics are required. Combinational drug therapy, bacteriocins, silver nanoparticles, bacteriophage therapy and antimicrobial peptides (AMPs) are potential innovative alternatives for nosocomial infections caused by ESKAPE pathogens (Fischbach, 2011). The use of two or more antibiotics is the basis of combination therapy predominately targeted against Gram-negative MDR bacteria. Bacterial strains produce these peptides or proteins, which impede the growth of a similar related bacterial strain (Zharkova *et al.*, 2021). These peptides or proteins are called Bacteriocins, including microcins and colicins (Benítez-Chao *et al.,* 2021). Small silver (or gold) materials with biophysical and chemical properties are called silver nanoparticles; which have bactericidal properties and have been revealed to enhance bacteriocin and antibiotic function

(Zharkova *et al.*, 2021). Bacteriophage therapy involves using bacteriophages (viruses that inject a bacterium) specific to a strain of bacteria to attack the bacterium through cell lysis (Principi *et al*., 2019). Mode of action includes interfering with protein and DNA synthesis, destabilising cell membranes or forming transmembrane channels (Principi *et al.*, 2019).

Antimicrobial peptides are small peptides that form part of the innate system of some organisms and have varied inhibitory mechanisms against microbes (Zharkova *et al*., 2021). However, several research concerns and limitations have been established for these techniques, as in vitro and in vivo trial data produced contradicting results (Zharkova *et al*., 2021). Also, these techniques are more focused on MDR bacteria and not ESKAPE pathogens as an entity. As well as that, new classes of antibiotics have proven to be ineffective against Gram-negative bacteria. Thus, novel approaches through rational drug design should be explored for targeting ESKAPE pathogens. These approaches are designing novel drugs targeted against bacterial metabolism or biomolecules vital for the survival of the bacterium. One such compound is the enzyme, Beta-lactamase.

Beta-lactams are the most applied antibiotics in treating bacterial infections due to their high bioavailability and efficacy, low toxicity, and broad activity (Bush, 1989). Beta-lactams are a class of antibiotics that share a common four-membered β-lactam ring in their structures, such as carbapenems, penicillins, monobactams, and cephalosporins (Kadonaga *et al.,* 1984). The β-lactam ring act as a covalent inhibitor of the transpeptidase enzyme, known as the penicillin-binding protein (PBP), preventing cell membrane synthesis and thereby exhibiting bactericidal activities (Prestinaci *et al*., 2015). The major mechanism of β-lactam resistance is the plasmid acquisition of genes encoding the enzyme β-lactamase by the clinically important Gram-negative bacteria among the ESKAPE pathogens. The β-lactamase enzyme catalyses the hydrolysis of the amide bond of the four-member β-lactam rings, rendering the antibiotics inactive and incapable of inducing bactericidal activity (Tooke *et al.*, 2019b). The β-lactamases are categorised into four groups by the Ambler system based on conserved amino acid motifs, molecular structure, and sequence homology. Classes A, C, and D β-lactamases are classified as serine β-lactamases. Class B β-lactamases are classified as Metallo-β-lactamases (Ambler *et al.,* 1991).

More than a thousand β-lactamases have been identified to degrade β-lactam antibiotics, and one such is the Gram-negative *Klebsiella pneumoniae* β-lactamase-1. No research has been done on utilising Thermal shift assay and Isothermal titration calorimetry (ITC) on the binding of *Klebsiella pneumoniae* β-lactamase-1 to β-lactam; cefoperazone. Therefore, this research aims to provide structural and biophysical information on *Klebsiella pneumoniae* β-lactamase-1 binding stability and dynamics amongst two β-lactams (including penicillin). With this, we gain vital information on the mechanism of β-lactamase resistance, which will help design new and improved β-lactamase inhibitors in *K. pneumoniae,* which would ultimately reduce the resistance of ESKAPE pathogens in nosocomial infections.

1.3 **Aims and Objective**

The research aims to characterise wild-type and mutant-(S70A) Beta-lactamase from *Klebsiella pneumoniae* structurally and functionally. The following objectives were conducted to assess their biophysical characterisation and conformational stability in the absence and presence of penicillin and cefoperazone with empirical studies such as thermal shift assay and analysis of thermodynamic parameters associated with the binding interaction using isothermal titration calorimetry (ITC),:

- To overexpress recombinant wild-type and mutant-(S70A) *K. pneumoniae* β-lactamase in competent *E. coli* T7 cells using a pET-28a translational vector. To purify wild-type and mutant-(S70A) *K. pneumoniae* β-lactamase using Immobilised Metal Affinity Chromatography (IMAC) and assess the purity using sodium dodecyl sulfate-polyacrylamide gel electrophoresis (SDS-PAGE).
- Assess the function of wild-type and mutant-(S70A) *K. pneumoniae* β-lactamase with nitrocefin.
- Protein secondary and tertiary structural determination with Far-ultraviolet (UV) circular dichroism (CD), tryptophan fluorescence and ANS-fluorescence spectroscopy in the presence and absence of penicillin and cefoperazone. Quaternary structure determination with Size exclusion high-performance liquid chromatography (SE-HPLC).
- To assess the thermal stability of wild-type and mutant-(S70A) *K. pneumoniae* β-lactamase with thermal shift assay (TSA).

- To characterise the thermodynamics of penicillin and cefoperazone binding to *K. pneumoniae* β-lactamase using isothermal titration calorimetry (ITC).

1.4 **Novelty**

Understanding the mechanism of enzyme catalysis is vital to design new antimicrobials or to validate known inhibitors to druggable targets. Limited information is available on the β-lactamase ability to hydrolyse different kinds (i.e., different shapes and sizes) of β-lactams. This led to my research's aim, which was to characterise the binding site of *Klebsiella pneumoniae* β-lactamase and establish a binding mechanism with penicillin and cefoperazone.

Chapter 2
Literature Review

2.1 ESKAPE pathogens and nosocomial infections

Healthcare inflictions in Sub-Saharan Africa are a major concern due to the surge of hospital-acquired infections (HAIs) or nosocomial infections. These infections are difficult to combat due to the evolutionary ability of causative bacteria to escape the biocidal action of antibacterial drugs. Thus, orthodox antibiotics have become less effective in treating nosocomial infections. Nosocomial infections are contracted due to prolonged hospitalisation and are noticed in approximately 50% of patients, such as neonates, chronic immunocompromised persons, and old-aged and surgical-induced patients (Tolera *et al*., 2018). Infection development generally occurs 48 hours and 73 -hours after admittance and release, respectively, and 30 days post-surgery. Statistics from the World Health Organisation (WHO, 2011); revealed that nosocomial infections result in 10% and 7% of fatalities in developing and developed countries, respectively, with a 75% incidence rate and 28-45.8% prevalence in Sub-Saharan Africa (Khan *et al.,* 2017). Surgical site infections are the most predominant in Sub-Saharan Africa as depicted in Figure 2.1 (Elizabeth et al., 2019). The prevalence rate of nosocomial infection in Ghana, Mali, and Uganda were 6.7%, 9.6-18.7%, and, 10.9%, respectively (Elizabeth *et al*., 2019). The low prevalence observed in these countries are due to incorporation of infection controls practices between medical staff and patients which alleviated the spread of nosocomial infections. In 2020; these infection control practices were in full effect in Ghana to reduce occurrence and re-occurrence of hospital acquired infections (Sunkwa-Mills *et al.*, 2020).

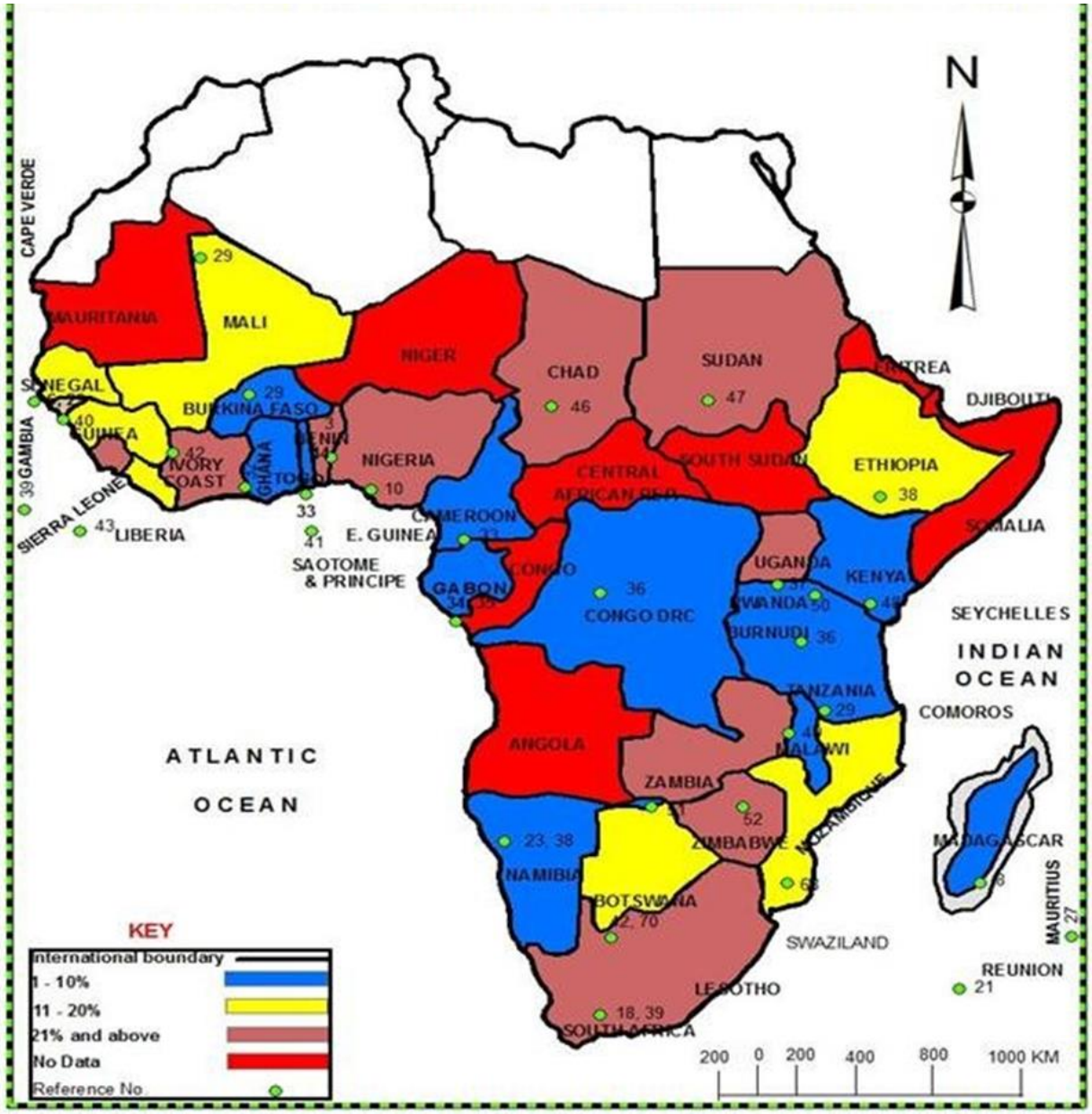

Figure 2. 1 Distribution of nosocomial infections in Sub-Saharan Africa. Surgical site infections are the dominant nosocomial infections in Sub-Saharan Africa, with Nigeria reported to have the highest prevalence in Africa**.** (Elizabeth et al., 2019).

Opportunistic fungi and viruses cause 5% of nosocomial infections, whereby bacteria are the leading cause of these infections, making up 90%. Bacteria are the leading cause of these infections due to their continuous antibiotic resistance mechanisms and their ability to grow and form biofilms on surgical instruments and medical equipment (catheters and ventilators), and overuse

of antibiotics, which have led to multidrug-resistant (MDR) bacteria (Tolera *et al*., 2018). A study conducted in Ethiopia reported that bacterial isolates causing nosocomial infections were from *Escherichia coli and Staphylococcus aureus* (89% methicillin-resistant *S. aureus*) (Tolera *et al*., 2018). A study conducted in Kenya reported that common isolates causing patient infections were *Staphylococcus pneumoniae*, *Citrobacter*, *Klebsiella*, *E. coli*, *P. aeruginosa, S. aureus* and *Acinetobacter* (Agaba *et al.*, 2017).

Common nosocomial infections include surgical site infections (SSI) with a 30% morbidity incidence rate; and catheter-associated urinary tract infections (CAUTI) with a morbidity incidence rate of 23% (Agaba *et al*., 2017). As well as ventilator-associated pneumonia (VAP) with a 9-12% incidence rate; and central line-associated bloodstream infections (CLABSI) with an incidence rate of 12-25% globally. Fluoroquinolones, cephalosporins and carbapenems are common treatments for these infections (Agaba *et al.,* 2017). However, the emergence of multi-drug resistance (MDR) strains, such as methicillin-resistant *S. aureus* (MRSA) and vancomycin-resistance *Enterococcus* (VRE), causes uncertainty of future treatment. Resistance development is through the acquisition of resistance genes through the conjugation of plasmids harboring these resistance genes from an inter-bacterial exchange. Bacteria that cause nosocomial infections have developed strategies to evade the biocidal activity of antimicrobials, thus, are difficult to prevent; are classified as ESKAPE pathogens (Mulani *et al*., 2019).

ESKAPE pathogens are evolutionarily developed Gram-positive and Gram-negative bacteria which have escaped antimicrobial effects. *Enterococcus faecium*, *Staphylococcus aureus*, *Klebsiella pneumoniae*, *Acinetobacter baumannii*, *Pseudomonas aeruginosa* and *Enterobacter species* are grouped into the acronym "ESKAPE" pathogens (Mulani *et al*., 2019). Frequently used antibacterial drugs obstruct nucleic acid and microbial cell wall synthesis, inhibit metabolic pathways and protein synthesis, and disrupt microbial membrane structures (Tenover, 2006). Continuous use of antibiotics causes resistant bacterial strains due to selective pressure. Resistance genes are obtained from other resistant bacterial chromosomes through plasmids, transposons (transformation, conjugation, or transduction), efflux pumps or *de novo* mutations (Santajit and Indrawattana, 2016). Downregulation of bacterial porin genes due to mutations or alterations in cell wall permeability prevents intracellular entry of antimicrobials (Santajit and Indrawattana,

2016). Gram-positive *Staphylococcus aureus* (*S. aureus*) and *Enterococcus faecium* (*E. faecium*) have developed methicillin (MRSA) and vancomycin (VRE) resistance, respectively. Ventilator-associated pneumonia is caused by Gram-negative *Klebsiella pneumoniae* (*K. pneumoniae*), attributing to 86 % of pneumonia-related nosocomial infections (Fischbach, 2011). *K. pneumoniae* commonly causes respiratory and urinary tract infections, as well as bloodstream infections. Penicillin, cephalosporin, and carbapenem-resistant bacteria are categorised as extended-spectrum beta-lactamases (ESBLs) (Dirar *et al*., 2020). *K. pneumoniae* have gained resistance to aminoglycoside, fluoroquinolones, and β-lactam antibiotics such as carbapenems and cephalosporins, which has led to the development of resistant *K. pneumoniae* extended-spectrum β-lactamases (ESBL) (Dirar *et al.*, 2020). WHO reported that third generation cephalosporins resistance in African countries by *K. pneumoniae* were 27.6% and *K. pneumoniae* resistance to carbapenems were 8.5% (Prestinaci *et al*., 2015). In 1996, *K. pneumoniae* was identified as able to hydrolyse every beta-lactam drug, which was classified as carbapenemase-hydrolysing *K. pneumoniae* (Nordmann *et al.,* 2009). Due to the lack of novel therapeutic antimicrobials, carbapenem-resistant *K. pneumoniae* has emerged as the leading cause of multidrug-resistant infections worldwide. Chaperone proteins: Caseinolytic proteins (Clp) found in *K. pneumoniae* are sought to have acquired the Clpk gene encoding for ClpK, leading to the emergence of heat-resistant *K. pneumoniae* (Prestinaci *et al.*, 2015). Ciprofloxacin is a commonly prescribed drug for urinary tract infections (Aditi Priyadarshini *et al*., 2019). Due to overuse, the resistance of *Klebsiella pneumoniae* towards ciprofloxacin has spiked from 4.1 % to 79.4 % and 8.4% to 92.9% in *Escherichia coli* (Yang *et al.*, 2014). Antimicrobial resistance makes bacterial infection treatment increasingly complicated; due to limited therapeutic options. Therefore, designing new novel therapeutic drugs targeted against nosocomial infection treatment are required to combat MDR strains such as *Klebsiella pneumoniae.*

2.2 Drug-resistance mechanisms in ESKAPE pathogens

Resistance genes are carried on bacterial chromosomes, plasmids, and transposons. Antimicrobial resistance mechanisms involve multidrug resistance, development of efflux pumps, drug inactivation, alterations in the bacterial membrane permeability, modifications on drug binding sites and biofilm formation (Prestinaci *et al.*, 2015). These antimicrobial resistance strategies are

shown in Figure 2.2. Modifications of drug-binding sites are produced through gene mutations in localised bacterial cell membrane proteins and penicillin-binding proteins (PBP) (Santajit and Indrawattana, 2016). Alterations of drug channels and subsequent production of efflux pumps enable the reduced uptake of antimicrobials by extrusion of these drugs out of the intracellular environment (Prestinaci *et al*., 2015). Irreversible drug inactivation is carried out by β-lactamases which hydrolyse β-lactam rings of carbapenems, monobactams, penicillin, and cephalosporins (Bush, 1989). Microorganisms have developed a strategy to form a mechanical shield by forming biofilm communities. These biofilms grow at conditions that a non-physiological to antibiotics (e.g. low oxygen, pH and water levels and high carbon dioxide levels) (Santajit and Indrawattana, 2016). Acquired resistant gene mutations can downregulate bacterial porin genes and alter the permeability of the cell wall thus, prevent intracellular antimicrobial entry (Prestinaci *et al.*, 2015). Treatment of bacterial infections has become a problem due to the rapid surge of resistant bacteria and the continued use of common therapeutics. Examples of such resistant bacteria are β-lactam resistant bacteria such as methicillin-resistant *S. aureus* (MRSA), which cause sepsis and pneumonia (Kumarasamy *et al.*, 2010). Gut infections are caused by cephalosporin-resistant *E. coli,* carbapenem-resistant *Enterobacteriaceae and* Vancomycin-resistant (Kumarasamy *et al*., 2010).

Gram-negative *Klebsiella pneumoniae* formed resistance toward β-lactams such as carbapenem, penicillin and cephalosporin through the acquisition of genes encoding for the protein β-lactamases (Blahová *et al.*, 2002). For example, the resistant *K. pneumoniae* against carbapenems antibiotics was acquired through *blaKPC* genes (Nordmann *et al.*, 2009). *Acinetobacter baumannii's* ability to hydrolyse carbapenems was through the acquisition of *blaOXA* genes producing the protein oxacillinase serine *β*-lactamases and *blaIMP* resistant gene acquisition encoding the metallo *β*-lactamases (Nordmann *et al.*, 2009). Polymyxins are commonly used in combination therapy to reduce resistant bacteria development. The drug is commonly used in conjugation with tigecycline (novel glycylcycline) for treating KPC-producing bacterial infections; however, the surge of resistance has become a limiting factor (Arnold *et al.,* 2011). As resistant KPC-producing bacteria have emerged resistant to polymyxin, tigecycline, and aminoglycosides (Mehta *et al.,* 2015).

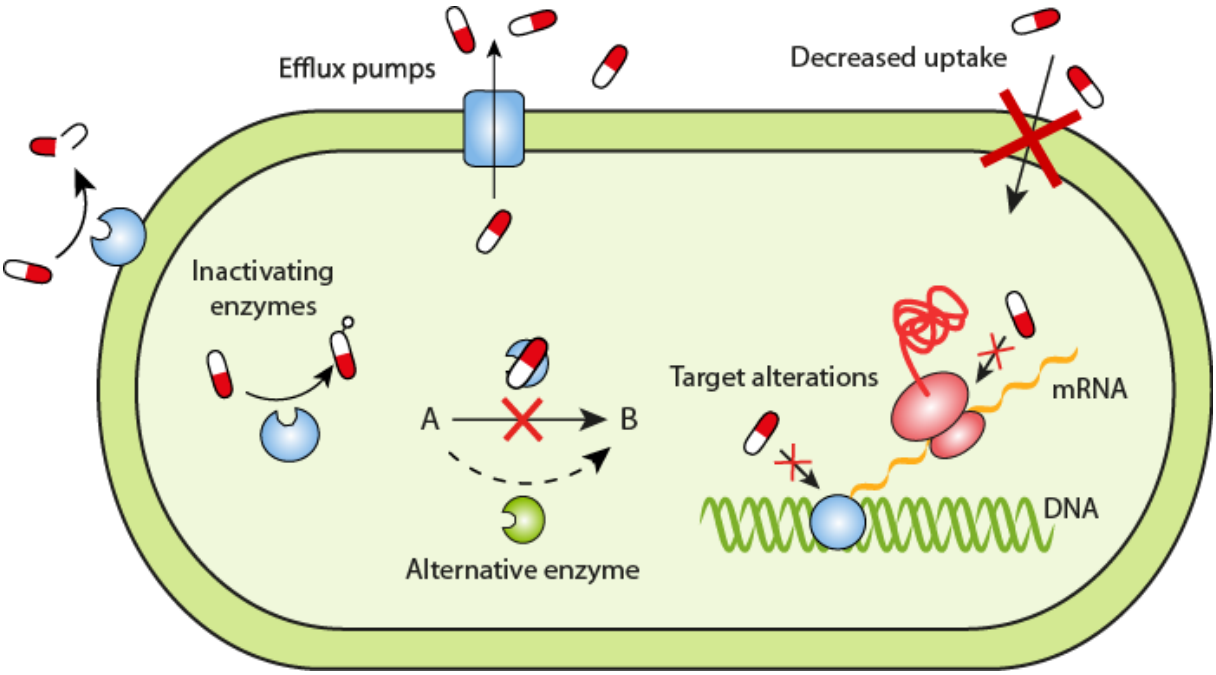

Figure 2. 2 Antimicrobial resistance strategies adopted by resistant bacteria. Bacteria evolved resistance through reduced membrane permeability, increased efflux pump activity and altering drug binding sites.

Clavulanic acid, a β-lactamase inhibitor, has been shown to be ineffective against the surge of resistant KPC-producing bacteria (Arnold *et al.*, 2011). Thus, novel approaches are in development, and one such is a β-lactamase inhibitor, NXL104. The development of novel aminoglycosides (ACHN-490.38) and novel tetracyclines (PTK-0796,37) are exciting approaches against resistant bacteria *(Li et al.*, 2019). NAB740 and NAB739 are synthetic polymyxin derivatives developed to inhibit resistant KPC-producing bacteria (Vaara *et al*., 2013). These inhibitor classes are only suited for KPC-producing strains and not suited for all classes of multi-drug resistant gram-negative bacteria strains (Vaara *et al*., 2013).

2.3 Beta-lactamase

β-lactams are antimicrobials that can facilitate bactericidal activity on microbes due to their evolutionary conserved four-membered β-lactam ring (Ambler *et al.*, 1991). As depicted in Figure 2.3; common β-lactams include monobactams, cephalosporins, penicillins and carbapenem. The

carbapenems contain a fused five-membered ring to the β-lactam ring with a distinctive 6-α-hydroxyethyl sidechain (Figure 2.3; structure 3), which is responsible for the broad-spectrum activity of the carbapenem antibiotics (Youjun Yang *et al.*, 1999). Cephalosporins (fused six-membered ring) and penicillins (fused five-membered ring) contain a 7-β- or 6-β-acylamino sidechain, respectively (Figure 2.3; structure 2 and 1 respectively) (Youjun Yang *et al.*, 1999).

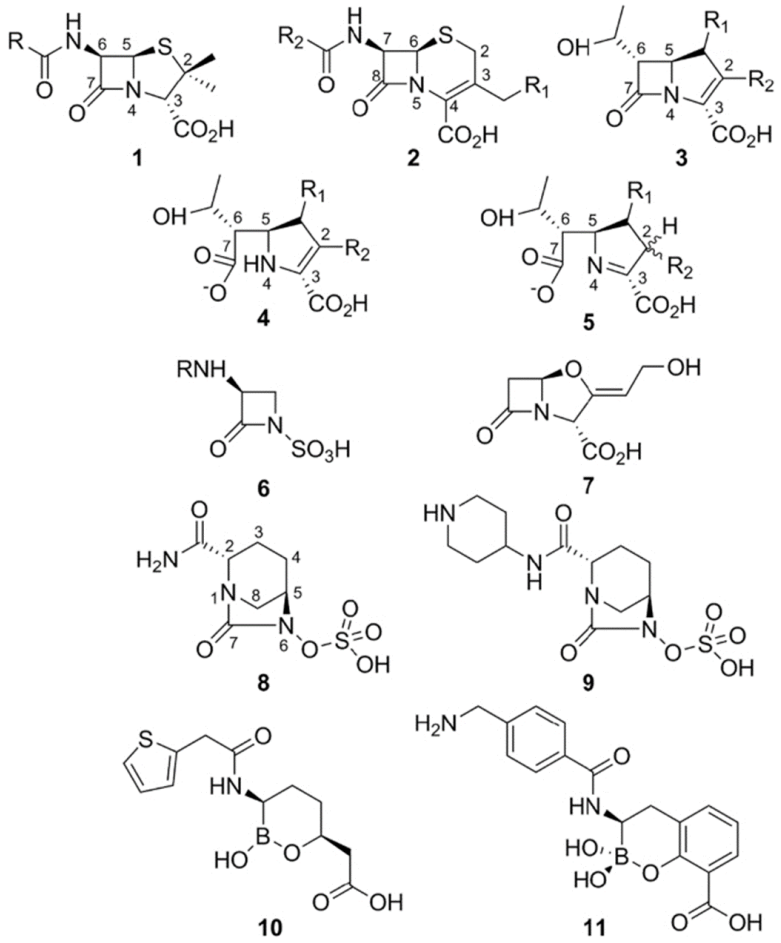

Figure 2. 3 Two-dimensional structures of β-lactamase inhibitors and β-lactam antibiotics. Structures 1 to 6 represent β-lactams in respective order; Penicillin, Cephalosporin, (1-methyl) Carbapenem, Hydrolysed carbapenem (Δ2-pyrroline form), Hydrolysed carbapenem (Δ1-pyrroline form) and Monobactam scaffold. Structures 7 to 10 represent β-lactamase inhibitors in respective order; Clavulanic acid, Avibactam, Relebactam, Vaborbactam and Bicyclic boronate (Tooke *et al.,* 2019a)

β-lactams covalently bind to the active site serine of the transpeptidase enzyme, known as the penicillin-binding protein (PBP) (Boyd *et al*., 2020). Therefore, inhibit bacterial cell wall

peptidoglycan biosynthesis (by attenuating peptidoglycan strand crosslinking) via covalent binding to the active site serine of penicillin-binding proteins, leading to membrane lysis thereby exhibiting bactericidal activities (Prestinaci *et al.*, 2015). β-lactam antibiotics are widely used and prescribed drugs against a wide range of infections. Due to their widespread usage, bacteria have found ways to escape the antimicrobial abilities of these drugs (Oelschlaeger, 2021). This has led to a global surge of resistant Gram-negative bacteria, with escape mechanisms such as, the plasmid acquisition of genes encoding the enzyme β-lactamase (Wang *et al.*, 1999). Beta-lactamases is a hydrolase enzyme (EC no. 3.5.2.6) capable of hydrolysing a broad range of β-lactam antibiotics via hydrolysis of the amide bond of the four-membered β-lactam rings, rendering the antibiotics inactive and incapable to induce bactericidal activity (Shapiro, 2017).

Due to evolutionary conserved amino acid motifs, functional mechanisms, and primary sequences; groups β-lactamases into Ambler classes (A to D). As shown in Figure 2.5a,c,d; Classes A, C, and D are categorised as Serine β-lactamases (Ambler *et al.*, 1991). These classes of enzymes have a conserved Ser–X–X–Lys motif (X-any other amino acid) (Ambler *et al.*, 1991). The serine moiety acts as a nucleophile which covalently binds and hydrolyses the β-lactam carbonyl, leading to opening of the ring structure forming an irreversible acyl enzyme intermediate by acylating the active-site serine (Figure 2.4) (Tooke et al., 2019a). Therefore, prevents formation of peptidoglycan cross-linking. As shown in Figure 2.5b; Metallo-Beta-lactamases are zinc dependent and grouped into Class B (Chiou *et al.,* 2015). This class of enzymes depend on one or two active site zinc ions to coordinate and ionise a nucleophilic hydroxide ion (or polarised water molecule) to mediate β-lactam hydrolysis (Ambler *et al.*, 1991).

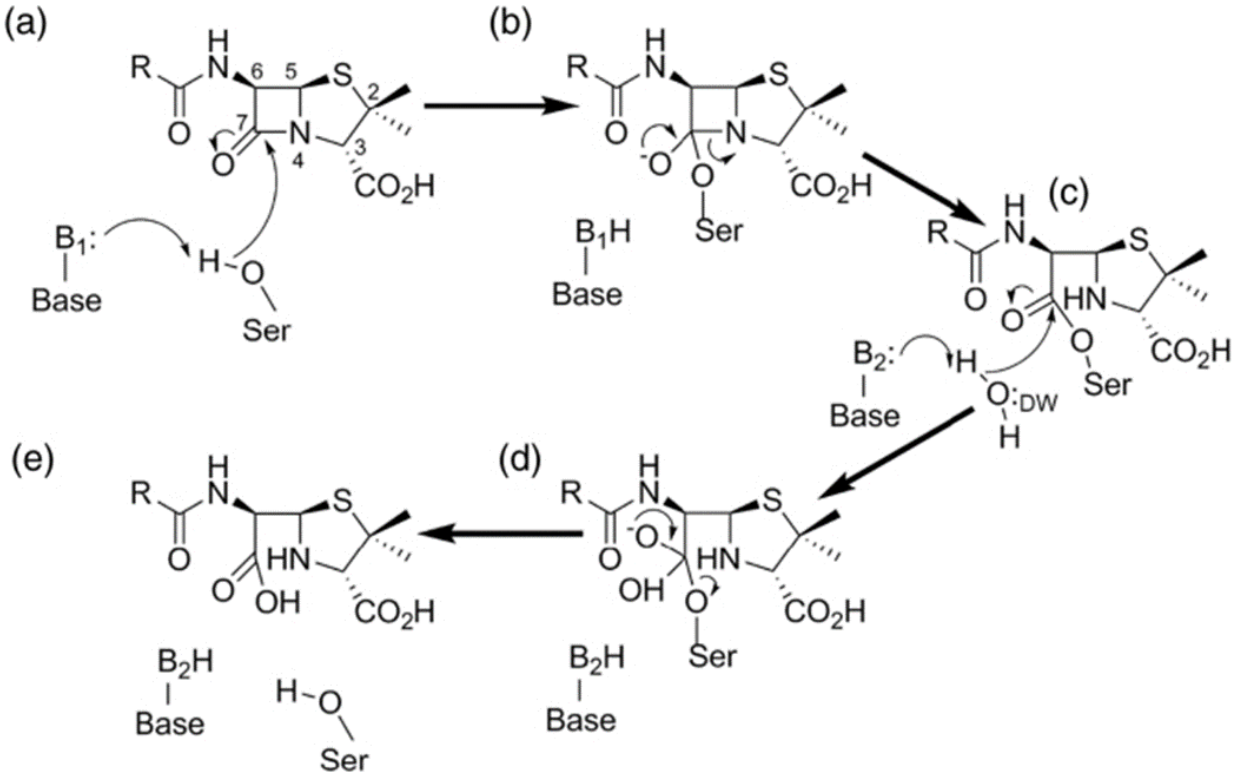

Figure 2. 4 Mechanism of action of a β-lactam (penicillin) hydrolysis by serine β-lactamase (a) B1 represents a β-lactamase base which initiates a nucleophilic attack on the serine on the C-7 amide carbonyl carbon of penicillin producing the covalent acylenzyme (b) through a tetrahedral acylation (oxyanionic) transition state. (c) water molecules (DW) are deacylated by a second base (B2) from the enzyme to activate them for nucleophilic attack of the acylenzyme carbonyl producing a penicilloate product (d) through a deacylation tetrahedral transition state. (e) hydrolysed penicillin (Tooke *et al.*, 2019a).

The subfamily categorisation of metallo-β-lactamases are determined by the number of bound zinc ions and sequence identity (Sacha *et al*., 2008). Class A serine β-lactamases encompass the most pathogenic Gram-negative bacteria that cause resistance and pose a clinical threat globally (Dirar *et al.*, 2020). Class As made up of *Klebsiella pneumoniae carbapenemases* (KPCs) (as seen in Figure 2.5a) and extended-spectrum CTX-M predominantly disseminated in *Pseudomonas aeruginosa, Escherichia coli* and *Klebsiella pneumoniae* (Bush, 1989). CTX-M-15 extended-spectrum β-lactamases (ESBL) can hydrolyse a spectrum of widely used antimicrobials. *Klebsiella pneumoniae* carbapenemases (KPCs) are common *in Enterobacteriaceae,* more so the KPC-2, KPC-3 (H274Y) and KPC-4 (P104R/V240G) (Mehta *et al.*, 2015). The subgroup activity and specificity are altered due to mutation incorporated into the sequences of KPC-2 (Mehta *et al*.,

2015). Class D serine β-lactamases such as enzymes OXA-23 and OXA-48 (as seen in Figure 2.5d) are carbapenemases derivatives, can hydrolyse last line defence antibiotics (Bush and Jacoby, 2010).

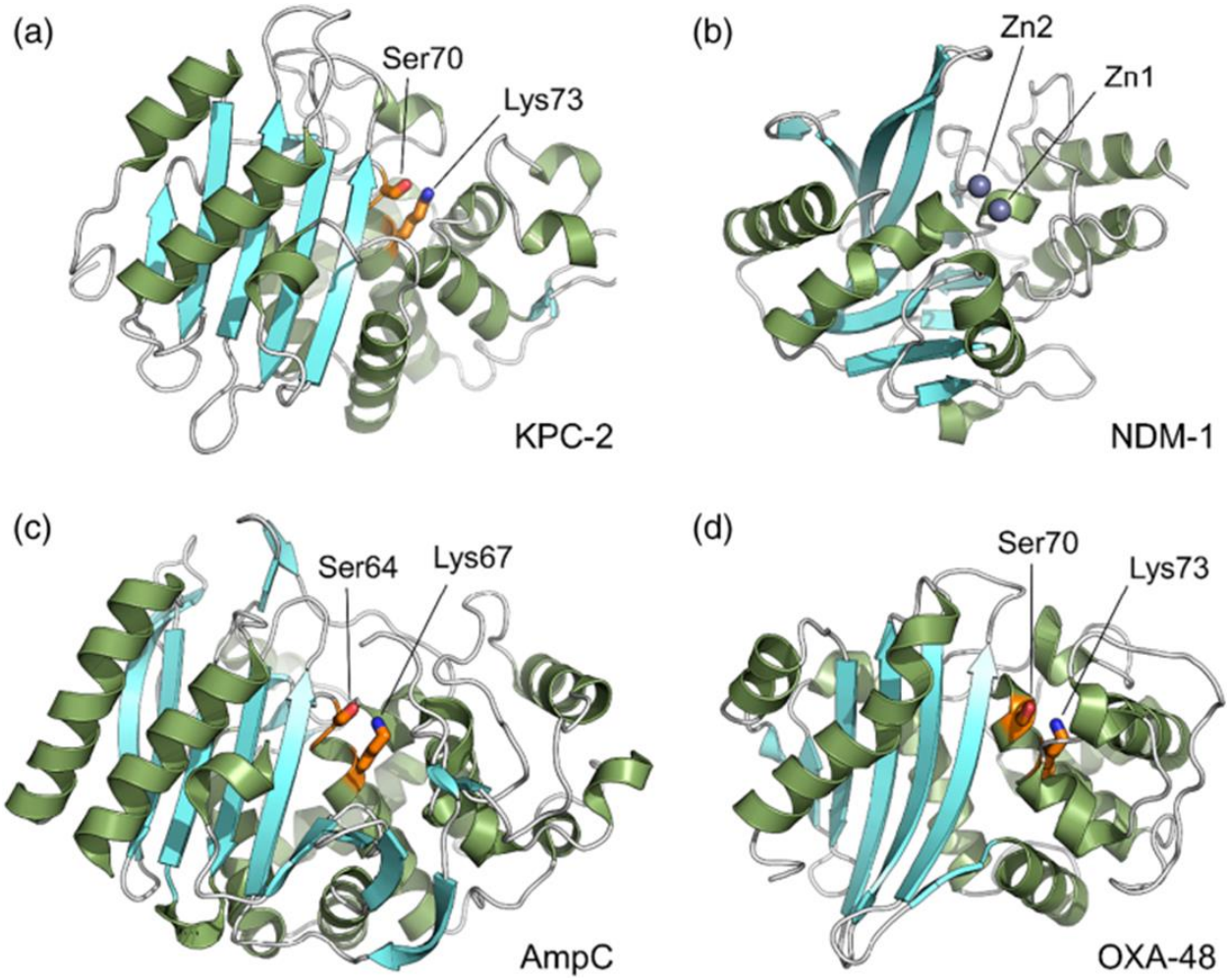

Figure 2. 5 Crystal β-lactamase structures from classes A, B, C and D. Crystal structures from each class of β-lactamases with their respective catalytically important amino acids. (a) to (d) represents the respective Classes A to D. (Tooke et al., 2019a)

Sulbactam, tazobactam and clavulanic acid are present-day β-lactam inhibitors against class A serine β-lactamases (Hinchliffe *et al*., 2022). They confer inhibition by forming an irreversible covalent bond with the active site serine residue (King and Strynadka, 2011). Resistance

development strategies have enabled the irreversible bonds to be broken in clavulanic acid inhibitors by acyl-exchange between serine β-lactamases which leads to decarbamylation (Y. Yang *et al.*, 1999). This is seen in KPC-2 and CTX-M 15, conferring resistance for the inhibitor. However, with the surge of resistance within the class A enzymes, novel inhibitors need to be designed that target class A and have the inhibitory potential for all serine β-lactamase classes. Newer non-β-lactam inhibitors with inhibitory potential for a wide range of serine β-lactamases are diazabicyclooctanes (DBOs), such as sulbactam, and avibactam (Tooke *et al.*, 2019b). These inhibitors contain a bicyclic DBO core with an addition of a piperidine ring on relebactam. They mediate inhibition through their DBO ring, which opens and forms a carbamyl ester bond with the active site serine (Tooke *et al.,* 2019b). Metallo-β-lactamases have hydrolytic potential against all β-lactam antibiotics except for monobactams due to low hydrolytic affinity (Wang *et al*., 1999). No inhibitors are available for metallo-β-lactamases; thus, strategies such as dual action inhibitors were in development targeted against metallo-and serine-β-lactamases (Boyd *et al.*, 2020). However, this therapeutic approach would be difficult to accomplish due to the visible structural and functional mechanisms between the two β-lactamases. Recently it was established that cyclic boronates could inhibit both metallo-and serine-β-lactamases classes by acting as the tetrahedral intermediate analogue present in both β-lactamase classes (Lence and González-Bello, 2021).

Recently a crystal structure of the *Klebsiella pneumoniae* β-lactamase was deposited (Figure 2.6). The CTX-M-15 (cefotaximase-Munich-15) enzyme was co-crystalised with an inhibitor; enmetazobactam (Hinchliffe *et al.,* 2022). From the crystalised structure the protein is predominantly alpha-helical, monomeric, and approximately 31 kDa. It was also determined from this crystal structure and previously published structures that the conserved active site amino acids are Serine-70, Lysine-73, Serine-130, Asparagine-132 and Threonine-237. More so, the Ser-70 and Lys-73 amino acids are catalytically important for forming a lysinoalanine cross-link (Hinchliffe *et al.*, 2022).

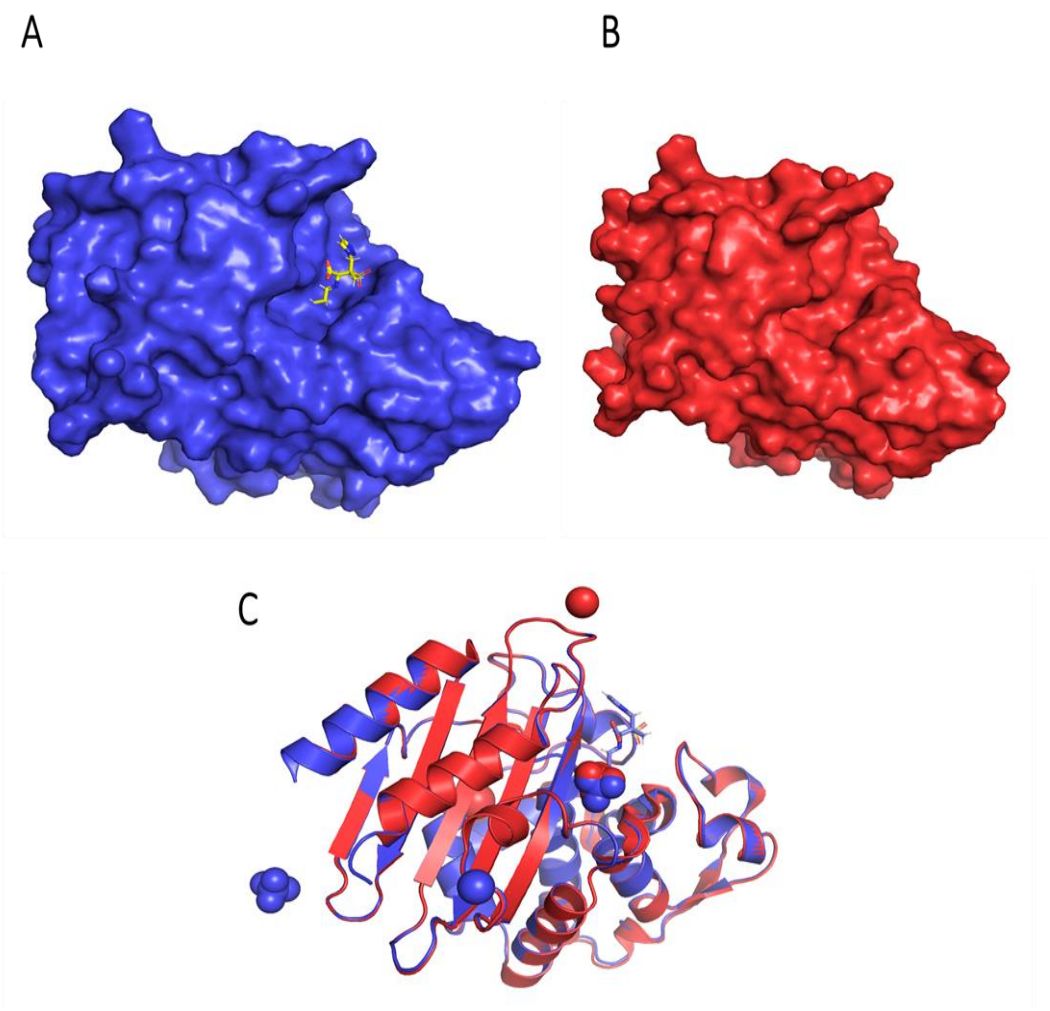

Figure 2. 6 Crystal structure of CTX-M-15. The structure was obtained through X-ray diffraction method with a resolution of 1.14 Å. Uniport ID: W1DN50, PDBe ID: 6z7j. Images generated with PyMol A) co-crystallised enzyme structure with emmetazobactam. B) hydrophobic surface structure. C) ribbon structure.

Chapter 3
Materials and methods

3.1 Materials

Unless stated otherwise, all materials were supplied by Sigma-Aldrich. W1DN50_pET28a and W1DN50_S70A_pET28a vectors (GenScript), T7-express *E. coli* (New England Biolab), kanamycin, SOC media (super optimal broth with catabolite repression), Tryptone, yeast extract, Agar (Merck Biosciences), NaCl, penicillin, and cefoperazone. Isopropyl-β-thiogalactopyranoside (IPTG), Tween-20, lysozyme, imidazole, nickel sulphate hexahydrate, bromophenol blue, Page Ruler Plus Prestain protein ladder (Thermo scientific (South Africa), glycine, acrylamide, β-mercarptoethanol, tetramethylethylenediamine (TEMED), bis-acrylamide, Coomassie Brilliant Blue R-250, sodium dodecyl sulphate (SDS), and glacial acetic acid. Snakeskin™ dialysis tubing (10 kDa MWCO) (Thermo scientific, South Africa), urea, sodium phosphate monobasic, 8 Anilino-1-naphthalenesulfonic acid (ANS), electrophoresis casting apparatus (Bio-Rad), nitrocefin, SYPRO-orange dye, 96-well plates, TCEP, DMSO, Gel filtration standards (Bio-Rad). IMAC Sepharose 6 Fast Flow resin (GE Healthcare, Chicago, Illinois, USA), Econo-Column Chromatography column (Bio-Rad), Phenomenex Gel Filtration/Size Exclusion silica column, Gravity flow pump (Bio-Rad Model EP-1 EconoTM). Yarra 3u SEC-2000 coupled to Phenomenex Security Guard ULTRA guard column. TSKgel SuperSW2000 SEC column (Tosoh Corporation Tokyo, Japan) and FLUOstar Omega Multimode Microplate Reader (BMG LABTECH).

3.2 Methods

3.2.1 Vector design

The complementary DNA (cDNA), which encodes the wildtype-Kpβlac-1 (UniProt code: W1DN50) and mutant version (S70A-Kpβlac-1), was extracted from GenBank (ID: CDL10227.1). The S70A-Kpβlac-1 was constructed using the wildtype-Kpβlac-1 as a template for site-directed mutagenesis. The 28-amino acid signal sequence was removed from each sequence, and a non-

cleavable hexa-histidine-tag was incorporated into the N-terminus of each sequence (Figure 3.1). The two gene sequences were incorporated into pET-28a vectors using NcoI and BamHI cleavage sites (Figure 3.2). The vectors have kanamycin antibiotic selection, expression controlled with T7 polymerase promoter and an origin of replication for host cell replication of the target gene sequences.

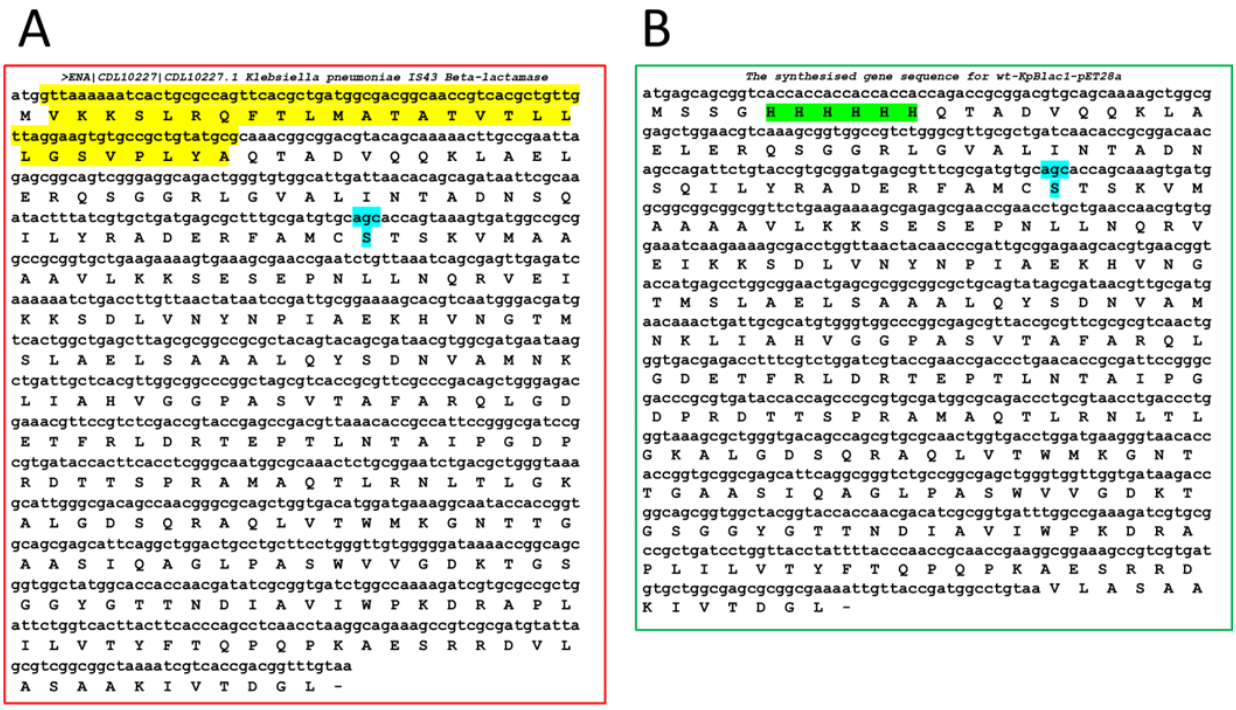

Figure 3. 1 Gene sequence of wildtype-Kpβlac-1 and mutant (S70A)-Kpβlac-1. (A) Depicts the extracted gene sequence of *K. pneumoniae* β-lactamase (GenBank ID: CDL10227.1). The yellow highlighted region predicts the 28-amino acid sequence. B) Depicts the manipulated sequence of *K. pneumoniae* β-lactamase whereby the signal peptide was removed, and a hexa-histidine tag attached (highlighted in green), also the position of the Serine (highlight in blue) which was mutated to an Alanine residue for the mutant construct.

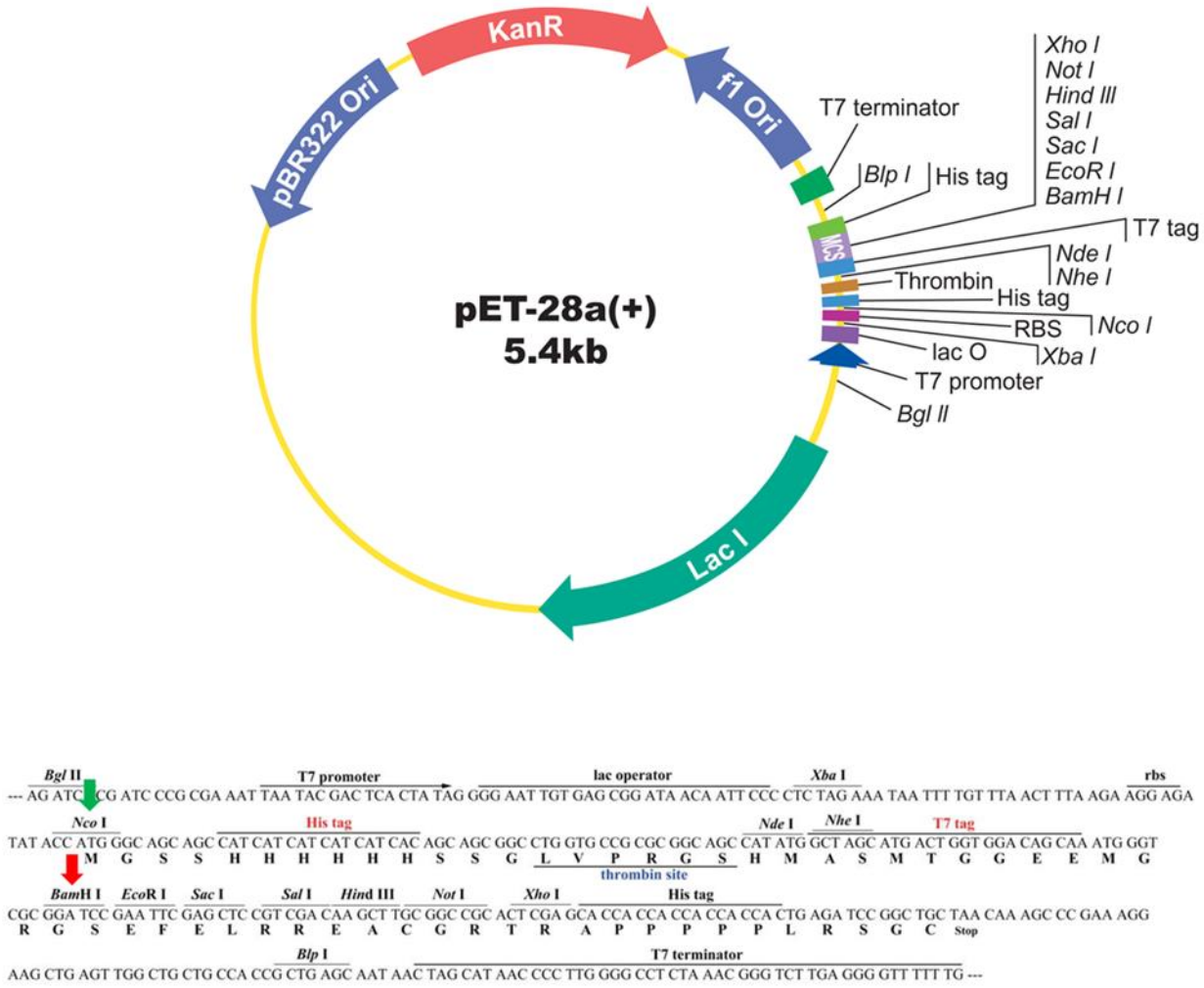

Figure 3. 2 Map of pET-28a translational vector. The gene sequences of the wildtype-Kpβlac-1 and mutant (S70A)-Kpβlac-1 was incorporated with *Nco*I (green arrow) and *Bam*HI (red arrow) restriction enzymes onto the multiple cloning regions of the vector. The gene sequences with the non-cleavable his-tag on the N-terminus will be controlled by the T7-promoter for expression and have resistance towards kanamycin.

3.2.2 Transformation of the *E. coli* expression host

Competent T7-*E. coli* T7 cells were used as hosts for transformation of wildtype-Kpβlac-1 and mutant (S70A)- Kpβlac-1 using pET28a-vectors. The pET expression vectors are pBR322 plasmid derivatives that contain a T7 bacteriophage promoter, and with the T7 RNA polymerase, great expression efficiencies are prompted (Kram and Finkel, 2015). The *E. coli* cloning host has a well-known metabolism, quick exponential growth rate, easy-to-manipulate genes, and cost-effective and expresses protein at a fast rate. Therefore it is routinely used in recombinant protein technology

and to ensure high copy number of cells with the target vector gene constructs are produced for expression of these proteins (Kram and Finkel, 2015). Transformation was conducted as follows:

Two Eppendorf tubes containing Competent T7 *E. coli* cells (100 µL each) were left on ice for 10 minutes. Lyophilised wildtype-Kpβlac-1 and mutant (S70A)- Kpβlac-1 vectors were rehydrated with ultra-pure Milli-Q water (100 µL) to a concentration of 40 ng/µL and centrifuged (12 000 × *g*, 25 °C, 30 seconds). Respective wildtype-Kpβlac-1 (2 µL) and mutant (S70A)- Kpβlac-1 (2 µL) vector was added to the T7 cells and incubated on ice (30 minutes). The cell-vector mixture was heat shocked (42 °C, 40 seconds) and incubated on ice for another 5 minute to allow for cell recovery from the thermal shock. The heat shocking increased the permeability and porosity of the bacterial cell membrane (increased membrane fluidity) to allow for uptake of the constructed DNA vectors. SOC media (1 mL) was added into each of the tubes, and incubated while shaking (1 hour, 220 rpm, 37°C) to provide nutrients for bacterial growth. The incubated suspension (100 µL) was spread plated on 35 µg/mL chloramphenicol and 30 µg/mL kanamycin supplemented lysogeny broth (LB)-agar plates. Then without flaming the plate spreader, the spreader was spread across four additional plates to dilute the number of cells from the stock solution to obtain isolated colonies. The plates were sealed with parafilm and incubated for 15 hours at 37 °C. Single colonies of transformed wildtype-Kpβlac-1 and mutant (S70A)- Kpβlac-1 were cultured overnight in 2× yeast tryptone media (16 hours, 37 °C, 230 rpm) supplemented with 30 µg/mL kanamycin.

3.2.3 Recombinant expression of KpBLac1 in *E. coli*

Like the pET28a vector, the *E. coli* expression host contains a copy of the T7 RNA polymerase gene, which is controlled by the lacUV5 promoter which is frequently used in blue-white screening (Gupta and Shukla, 2016). The vector construct within the *E. coli* host contains an origin of replication, which is the replication initiation site and impacts the plasmid copy number. The expression of wildtype and mutant *Klebsiella pneumoniae* Beta-Lactamase-1 (*KpBlac-1*) was carried out via induction with a non-hydrolysable lactose analogue; Isopropyl β-D-thiogalactoside (IPTG). IPTG induces the pET vectors; by binding to and therefore inactivating the lac repressor protein (encoded by the *lacI* gene) (Gupta and Shukla, 2016). This inactivation will mediate T7 RNA polymerase accessibility to the T7 promoter for transcriptional binding. The expression of the WT-*KpBlac-1* and S70A-*KpBlac-1* proteins with specific antibiotic resistance was carried out

within *E. coli*. A qualitative SDS-PAGE analysis should depict molecular weight bands correlating to the expressed proteins. The recombinant WT-*KpBlac-1* and S70A-*KpBlac-1* used for this experiment have a theoretical isoelectric point (pI) of 8.95 and are made up of 273 amino acids (inclusive of the N-terminal histidine tag). The molecular weights are 29293,11 Da and 29277,11 Da, respectively, using ProtParam ExPASY tool.

From the overnight growth cultures of WT-*KpBlac-1* and S70A-*KpBlac-1,* 20 mL of each culture were diluted (1/50 dilution) into two separate flasks of fresh 2xYT media (1 L) supplemented with 30 µg/mL kanamycin and incubated (230 rpm, 37°C). The optimal density at 600 nm (OD_{600}) was measured until cells reached approximately 0.45-0.6. The flasks were placed on ice for 10 minutes, induced with 0.5 mM IPTG, and incubated (6 hours, 230 rpm, 30°C). Cells were harvested (5000 ×*g*, 15 minutes, 4 °C), pellet weighed, and recorded, whereas the supernatant was discarded. The weight of wet cell pellet from the 1 L cell cultures was obtained by weighing the centrifuge bottles containing the wet cell pellets (in grams) after the supernatant was discarded. The pellet weights were corrected by the mass of an empty centrifuge bottle to obtain exact weight of cell pellet solely in each of the 1 L cell culture expression. The pellet was resuspended in 30 mL 1× phosphate buffer saline (PBS) pH 7.4 (137 mM NaCl, 0.02% (w/v) sodium azide, 10 mM Na_2HPO_4, 1.8 mM KH_2PO_4, 2.7 mM KCl, 25 mM imidazole) and 6.25 mg/mL lysozyme (1 mL) was added to assists in weakening the bacterial cell wall. The resuspension was mixed and frozen at -80 °C.

3.2.4 Purification of KpBLac1 using IMAC

To characterise a protein's biophysical and biochemical properties, protein purification must be conducted to separate the recombinant protein from naturally occurring bacterial proteins. Immobilised Metal Affinity Chromatography (IMAC) was discovered in 1975; and separates proteins based on their divalent metal ion affinity (Porath *et al.*, 1975). The imidazole ring of histidine-tagged proteins would have affinity and interact with either nickel, zinc, ferrous, copper or cobalt embedded within the resin (Kaur and Reinhardt, 2012). These metal ions are immobilised onto the resin via chelation with chelating agents such as nitrilotriacetic acid (NTA) or iminodiacetic acid (IDA) which use the oxygen and nitrogen atoms to coordinate the metal ions onto the column; in such that the metal ion binding regions are free from either histidine,

tryptophan, or cysteine binding (Wong *et al.,* 1991). Nickel-based resins are commonly used as the metal is highly selective for histidine-tagged proteins: thus, purification efficiency is optimal (Goh *et al*., 2017). The imidazole ring of histidine binds to the metal ion by acting as an electron-pair donor (Kaur and Reinhardt, 2012). The histidine tag not only assists in purification but also in the solubility of the protein (Goh *et al.*, 2017). The protein can be eluted either by the addition of free imidazole, the addition of chelating agents (ethylenediaminetetraacetic acid (EDTA)) or by lowering the buffer's pH (Porath *et al.*, 1975). A serine protease: Thrombin, can be used to remove a cleavable histidine tag by causing non-specific insertions between arginine and glycine residues (Zhu *et al.,* 2013). The cleaved protein would then be bypassed through a benzamidine column and interact with thrombin in the protein solution (Zhu *et al.*, 2013). Protein quantity is lost with every purification; thus, multiple purification procedures should be avoided to obtain a crude protein with a high yield. N-terminal histidine tags can remain on proteins since their interference with protein structure and function is negligible.

Crude cell suspension of WT-*KpBlac-1* and S70A-*KpBlac-1* were thawed from -80 °C and sonicated on ice (to prevent heat denaturation) until cell suspension became free-flowing. This is to ensure mechanical cell lysis of the *E. coli* cells by the high sound frequency wave causes shearing of the bacterial cell walls. The lysate was harvested by centrifugation (4 °C, 18000 × *g*, 20 minutes) to separate the soluble from insoluble cell fractions which were analysed on a 12.5% (w/v) sodium dodecyl sulphate polyacrylamide gel electrophoresis (SDS-PAGE). Immobilised metal affinity chromatography (IMAC) was employed to purify *KpBlac-1*, which exhibits the N-terminal His-tag on the vector construct. IMAC Sepharose 6 Fast Flow resin (9 mL) was added to an Econo-Column Chromatography column and washed with a 10× column volume of ddH_2O to remove preservative ethanol in the resin. The resin was Ni^{2+} charged by passing 0.1 M $NiSO_4$, followed by a ddH_2O wash. The column was equilibrated with equilibration PBS buffer (137 mM NaCl, 0.02% (w/v) sodium azide, 10 mM Na_2HPO_4, 1.8 mM KH_2PO_4, 2.7 mM KCl, 25 mM imidazole, pH 7.4). The supernatant was passed through the column at a 4 mL/min flow rate and flowthrough was collected. The column was washed with equilibration buffer and a 0.5% (v/v) Tween-20 containing equilibration buffer to reduce hydrophobic interactions. These wash steps ensure that non-specific proteins are washed off the column. WT-*KpBlac-1* and S70A-*KpBlac-1* were eluted with an elution buffer (10 mM PBS, 500 mM imidazole, pH 7.4) and 20 (1.5 mL)

fractions were collected. The histidine amino acids on the tagged WT-*KpBlac-1* and S70A-*KpBlac-1* are outcompeted by high imidazole concentrations for nickel ion binding. Therefore, the proteins are eluted off the resin. The purification samples: the supernatant, pellet, flow-through, washes and eluted protein fractions were analysed on a 12.5% SDS-PAGE.

3.2.5 Qualitative and quantitative analysis of the expressed KpBLac1

After successful purification, both the quality and the quantity of the recombinant protein is assessed to ensure that the protein is devoid of aggregation, nucleic acid, or protein contamination. Sodium dodecyl sulphate-polyacrylamide gel electrophoresis (SDS-PAGE) is a protein quality assessment (Laemmli, 1970). This technique introduces a uniform negative charge on proteins and cleaves non-covalent disulphide bonds due to the ionic SDS surfactant; therefore, protein separation is based on molecular size (Nowakowski *et al.,* 2014). Reducing agents such as β-mercaptoethanol is used to further denature the proteins by disrupting disulphide bonds between cysteine residues (Nowakowski *et al.*, 2014). The SDS detergent binds proteins with a 1 SDS molecule per 2 amino acid ratio, thus conferring a net negative charge which attracts proteins to the anode (positively charged electrode) in the presence of an electric field current (Laemmli, 1970). Smaller proteins migrate further on the gel matrix compared to larger proteins. A discontinuous buffer system composed of stacking and separating gel buffer of Tris-HCl at pH 6.8 and 8.8, respectively, is used for protein separation. The running gel buffer is composed of glycine and Tris-HCl at pH 8.3 (Laemmli, 1970). The protein is retarded in the stacking gel due to interaction with the glycine and chloride ions in the stacking and tank buffer before it enters the separating gel (Laemmli, 1970). Further assessment of the quality and the quantity of WT-*KpBlac-1* and S70A-*KpBlac-1* will be conducted using UV-vis spectroscopy from which the amount of light absorbed by the recombinant proteins are ascertained. This is due to aromatic residues (tryptophan, phenylalanine, and tyrosine) within the protein sequence's ability to absorb at 280 nm. The protein concentration is determined using the Beer Lamberts law of equation:

$$A = \varepsilon c l$$

Where A = Absorbance

ε = molar extinction coefficient at 280 nm (WT-*KpBlac-1* and S70A-*KpBlac-1* = 23950 $M^{-1}cm^{-1}$ (ProtParam ExPASY).)

c = concentration (M)

l = path length (cm) (width or thickness of cuvette)

The 20-elution fractions were measured for absorbance with a UV- vis Spectrophotometer (*Jasco V-630*) at 280 nm to determine the fractions in which the highly recombinant protein is in. These highly absorptive fractions were ran on a gel and later pooled together and dialysed. Reducing buffer (50 µL) (125 mM Tris-HCl, 10% (v/v) β-mercaptoethanol, 20% (v/v) glycerol, 4% (w/v) SDS, pH 6.8) was added to the purification samples (50 µL) of WT-*KpBlac-1* and S70A-*KpBlac-1*. The composition of the gel is outlined in Table 3.1. Samples were incubated (100 °C) and 5 µL of each sample was loaded on a discontinuous 12.5% SDS-PAGE. Prestain PageRuler Plus protein ladder (5 µL) was also loaded onto the gel. Gel was transferred into a gel casket filled with tank buffer and gel run with a Bio-Rad Mini Protean electrophoresis system at 120 V until dye front reached 0.5 cm from the gel edge. The gel was soaked in Coomassie stain [0.2% Coomassie Brilliant Blue R in 1:5:4 (v/v/v) acetic acid: methanol: distilled water] for 30 minutes and destained [1:5:4 (v/v/v) acetic acid: methanol: distilled water] for 2 hours. Gel bands were observed with the Bio-Rad Gel Doc XR+ system. The bands were measured to estimate the molecular weight of the recombinant proteins. A linear curve was plotted of the logarithm of the known molecular weights standards against the relative migration distance (Rf):

$Rf = Distance$ travelled $of\ the$ macromolecule/$Distance$ travelled by $the\ dye\ front$

The fitted linear equation determined the molecular weight of WT-KpBlac-1 and S70A-KpBlac-1. The pooled fractions were dialysed in SnakeSkin dialysis tubing with a 10 kDa molecular weight cut-off against and a sodium phosphate buffer (5 mM NaH_2PO_4, and 0.02% (w/v) sodium azide, pH 7.2) for 12-16 h at 4 °C. Protein concentration was measured spectroscopically at 280 nm by a 1/20 serial dilution of both proteins. The purified protein was monitored between 240 nm to 350 nm at 20 °C to determine any contamination within the protein. A plot of corrected absorbance (A_{280nm}) against the dilution factor was generated. A linear regression line was fitted, and the

gradient from the fitted equation was used in conjugation with the Beer lamberts equation to deduce the concentration of WT-*KpBlac-1* and S70A-*KpBlac-1*.

Table 3. 1 Composition of a discontinuous 12.5% (w/v) separating and 4% (w/v) stacking gels.

Reagent	12.5% (w/v) Separating gel	4% (w/v) Stacking gel
Monomer solution	6.25 mL	940.00 µL
Separating gel buffer (pH 8.8)	3.75 mL	0.00
Stacking gel buffer (pH 6.8)	0.00	1.75 mL
Distilled Water	4.75 mL	4.30 mL
10% (w/v) SDS	150.00 µL	70.00 µL
TEMED (N,N,N′,N′-Tetramethylethylenediamine)	20.00 µL	50.00 µL
10% (w/v) Ammonium Persulfate (initiator reagent)	75.00 µL	35.00 µL

3.2.6 Enzyme activity assay

Intact beta-lactam antibiotics (including third-generation cephalosporins) disrupt peptidoglycan synthesis by binding and inactivating penicillin-binding proteins (PBPs) (Bush, 1989). The nitrogen-carbonyl carbon amide bond in the beta-lactam ring of these antibiotics is hydrolysed by Beta-lactamases (Bush and Jacoby, 2010). Hydrolysis of the amide bond renders the beta-lactams incapable of bactericidal activity (Bush and Jacoby, 2010). Visual detection of the hydrolysis event is difficult with most cephalosporins due to the ultraviolet absorption shift from intact to the hydrolysed product being outside the visible spectrum range (Chow *et al.,* 2013). However, a chromogenic cephalosporin, Nitrocefin, provides absorption shifts within the visible range upon hydrolysis and a colour change from intact yellow-producing nitrocefin to red-producing hydrolysed product (Zhang *et al.*, 2018) (outlined in Figure 3.3). Nitrocefin has a highly reactive β-lactam ring but has no antimicrobial properties. The colour change upon hydrolysis is consequence of the hydrolysis of the vinyl dinitrobenzene substituent attached to the C3 position (Boehle *et al*., 2017). Nitrocefin at neutral pH conditions produces two absorption peaks at 386 nm and 217 nm (due to the 7-acyl group) (Boehle *et al.*, 2017). After β-lactamase hydrolysis, the 386 nm peak is lessened, and the appearance of a new peak at 482 nm is produced, which relates

to the hydrolysed product. This absorption shift is measured rapidly over time, enabling quantifying β-lactamase activity based on the rate of nitrocefin degradation (Franceschini *et al.*, 2002).

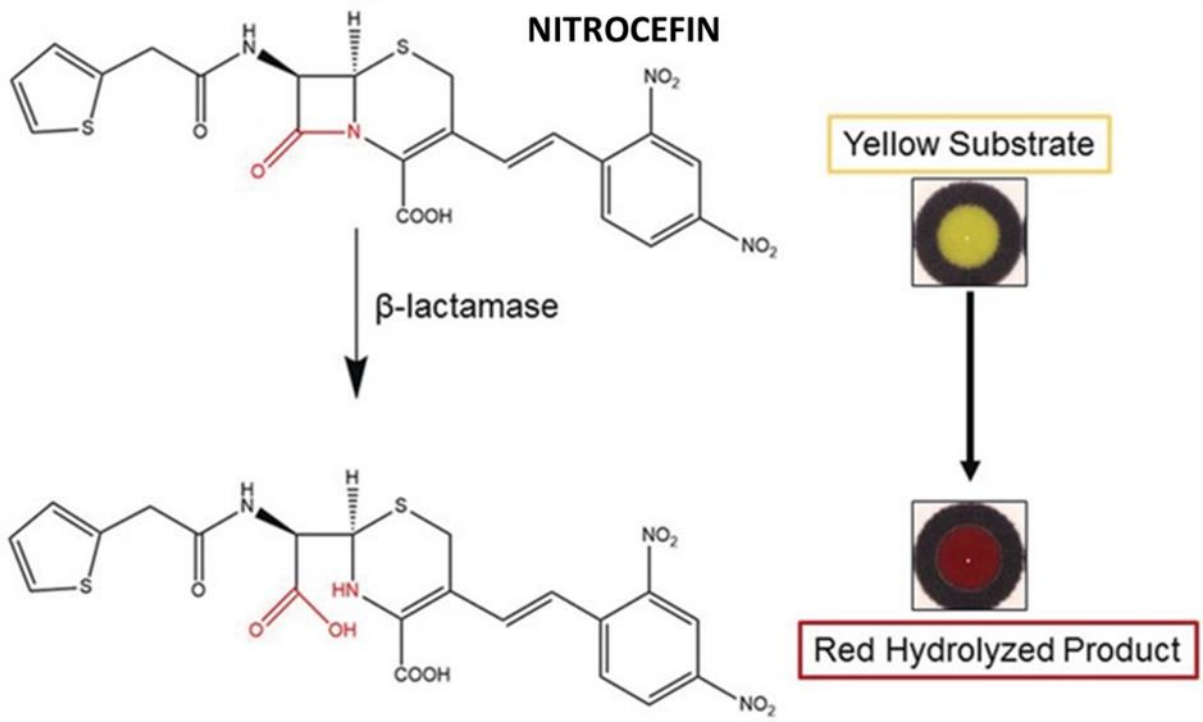

Figure 3. 3 Hydrolysis of nitrocefin by Beta-lactamase. The beta-lactam ring of Nitrocefin is hydrolysed in the presence of a β-lactamase. This hydrolytic event is observed by a color change from yellow to red at 482 nm. (Boehle et al., 2017).

DMSO (1 mL) was added to lyophilised nitrocefin (10 mg). A working concentration of 0.5 mg/mL nitrocefin was produced with the addition of 50 µL of 10 mg/mL stock nitrocefin to 950 µL sodium phosphate buffer, pH 7. The remaining stock nitrocefin was wrapped in foil and stored at -20°C for use within 2 weeks. The experimental setup was conducted as outlined in Figure 3.4. WT-*KpBlac-1* and S70A-*KpBlac-1* (50 µL) concentrations were varied (0 nM to 1600 nM) and prepared in sodium phosphate buffer, and 150 µL of 0.5 mg/mL nitrocefin was injected stepwise into each well to make final reaction volume of 200 µL. The absorbance was measured at 482 nm with a Plate reader.

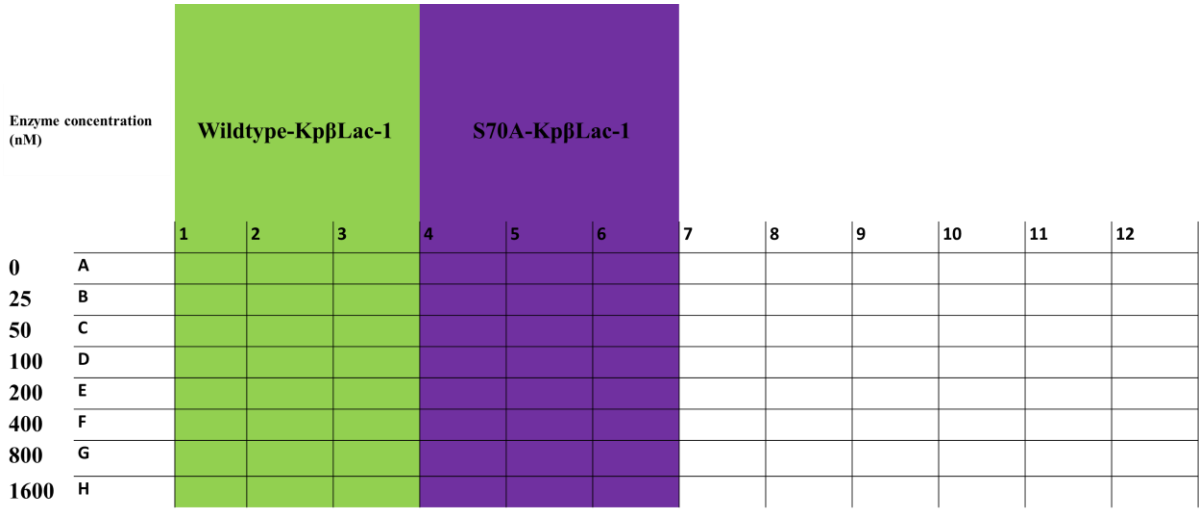

Figure 3. 4 Experimental setups of Beta-lactamase activity in the presence of nitrocefin. The activity of WT-*KpBlac-1* and S70A-*KpBlac-1* was assessed at various concentrations (0 µM to 1600 µM) in the presence of 0.5 mg/mL of Nitrocefin.

3.2.7 Secondary structure content analysis

Protein conformational stability due to environmental changes (increased temperature or denaturant addition), sequence alterations with mutations or ligand interaction is monitored using Far-Ultraviolet circular dichroism (Far-UV CD) (Munishkina and Fink, 2007). Far-UV CD assess the secondary structure of proteins, in which the peptide backbone bonds of the hydrogen bonding between carbonyl-oxygen and the nitrogen-hydrogen atoms are chromophores that absorb in the spectral regions of 190 to 250 nm (Micsonai *et al*., 2015). The basis of Far-UV CD is the ability of phi (Φ) and psi (Ψ) angles of backbone peptide bonds which act as chromophores ability to absorb differences of left-and right-handed circularly polarised light and signal output denoted as the ellipticity (θ) (Micsonai *et al.,* 2015).

A beta-sheeted protein produces a positive and negative band at 195 nm and 218 nm, respectively. An alpha-helical protein produces a spectrum with a positive band at 193 nm and two negative bands at 208 nm and 222 nm. Positive and negative bands are captured at 195 nm and 210 nm, respectively, for Random coils (Munishkina and Fink, 2007) (Figure 3.5). The experimental data is expressed in molar ellipticity with the following equation:

$$[\theta]=100\times\theta Cnl$$

Where θ represents ellipticity (millidegree), *n* represents the number of residues in protein, *C* represents protein concentration (mM), and *l* represents path length (cm).

This technique is cost-effective, easy experimental setup and has rapid data output. Far-UV CD does not quantify the secondary structure of proteins; thus, online algorithms such as Dichroweb is used. This tool deconvolutes the experimental data against built-in reference protein sets with Contin-LL and produces a percent analysis report.

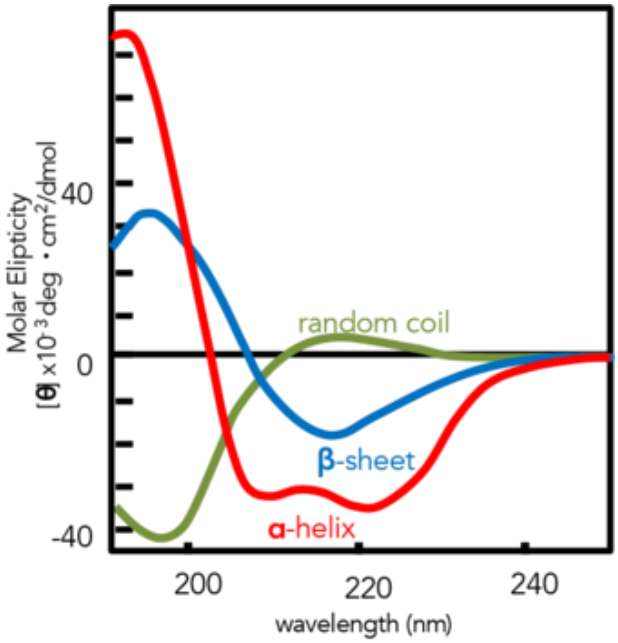

Figure 3. 5 Spectral properties of protein secondary structural content using Far-UV CD. The random coil (green spectrum) produces positive and negative peaks at 195 and 210 nm, respectively. The β-sheeted structure (blue spectrum) with a positive peak at 195 nm and a negative peak between 218 nm. The α-helical structure (red spectrum) produces a positive peak at 193 nm and negative peaks at 222 nm and 208 nm.

Secondary structure analysis of native, denatured and ligand-bound WT-*KpBlac-1* and S70A-*KpBlac-1* states were evaluated. For the analysis, 5 µM WT-*KpBlac-1* and S70A-*KpBlac-1*, 8 M urea (for denatured states), 100 µM penicillin and cefoperazone were prepared in sodium

phosphate buffer. The experiment was conducted in triplicates and monitored on a Jasco J-1500 CD Spectrometer connected to a Peltier temperature controller (Jasco, UK) at 20°C from 180 to 255 nm (3 accumulations, 0.5 data pitch, 2.5 nm bandwidth, 100 nm/min scan speed). The appropriate buffer blanks were subtracted from the protein samples, and data were converted from ellipticity θ (millidegrees; m.deg) to mean residue ellipticity [θ] ($deg.cm^2.dmol^{-1}$). The resultant spectra were deconvoluted in the DichroWeb analysis program- CONTIN-LL to obtain the percent secondary content of WT-*KpBlac-1* and S70A-*KpBlac-1* in the absence and presence of penicillin and cefoperazone.

3.2.8 Tertiary structure analysis

3.2.8.1 tryptophan fluorescence

Fluorescence is the ability of biomolecules to absorb light at a certain wavelength (shorter wavelength) at a higher energy level and subsequently emit light at a different longer wavelength (Vivian and Callis, 2001). The emission spectra are due to the excited electrons returning to the ground state due to energy minimisation and vibrational relaxation (Jablonski, 1933). The Jablonski diagram in Figure 3.6 outlines this. The difference in emission and absorption wavelengths is referred to as a Stokes shift (Vivian and Callis, 2001). Delocalised electrons in aromatic amino acids such as tyrosine, tryptophan and phenylalanine contribute to the fluorescence. These amino acids are intrinsic probes as the ring structures are solvent sensitive and can be monitored at 280 nm (Möller and Denicola, 2002). Tryptophan is generally buried in hydrophobic areas within a protein and is therefore frequently used to probe the microenvironment of proteins due to it exhibiting high quantum signals and minimised environmental quenching; thus, the probe is highly environmentally sensitive (Vivian and Callis, 2001). The indole ring of tryptophan is excited at 295 nm, and due to changes within the microenvironment of the protein, such as substrate binding or protein unfolding, the emission spectrum is monitored from 300 nm to 500 nm (Sindrewicz *et al*., 2019). When the tryptophan probe is situated in hydrophobic areas within the protein, a hypsochromic shift (blue shift) is established with a high quantum yield signal. When the tryptophan probe is polarly exposed, a bathochromic shift (redshift) results in a lowered quenched quantum yield (Ghisaidoobe and Chung, 2014).

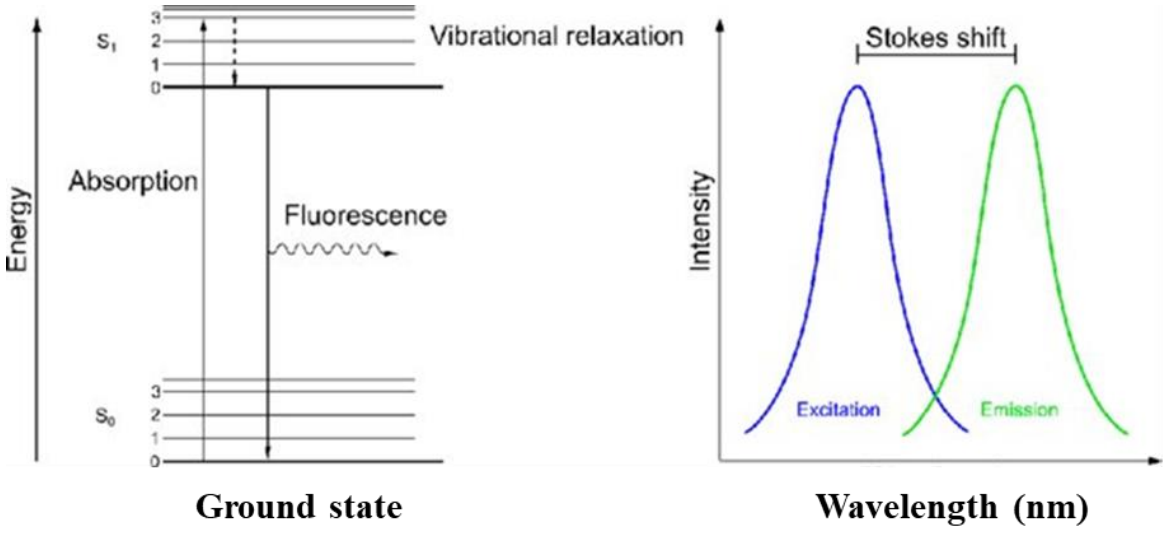

Figure 3. 6 Fluorescence spectroscopy illustrated with the Jablonski diagram. The electrons of the ring structures of aromatic amino acids are excited by light of a particular wavelength with high energy input. These electrons absorb the light and are coordinated from the ground state to higher energy level states. At a certain energy state, the electrons loss energy due to vibrational relaxation and return to the ground state. This return of electrons emits light at a certain wavelength (emission), and this is monitored with the fluorescence spectroscope. The difference between the excitation and emission wavelength is referred to as a stokes shift.

Conformational changes in the three-dimensional structures of WT-*KpBlac-1* and S70A-*KpBlac-1* in the presence and absence of penicillin, urea (denatured state) and cefoperazone were monitored with Jasco FP-6300 spectrofluorometer. For the analysis, 5 µM WT-*KpBlac-1* and S70A-*KpBlac-1*, 8 M urea (for denatured states), 100 µM penicillin and cefoperazone were prepared in sodium phosphate buffer. The experiment was conducted in triplicates and monitored at 20°C. The proteins were excited, at 295 nm and emission spectra were captured from 300 to 500 nm (3 accumulations, 0.5 data pitch, 2.5 nm emission bandwidth and 5 nm excitation bandwidth, 200 nm/min scan speed). The spectra were corrected with appropriate buffer blanks.

3.2.8.2 ANS fluorescence

The protein tertiary structure can be studied using extrinsic fluorescent dyes such as the anionic dye; 8-anilino-1-naphthalene sulfonic acid (ANS). The dye attracts and binds to hydrophobic clefts, protein-active sites, or solvent exposed hydrophobic pockets within the proteins. Upon binding produces a high quantum yield and a blue-shifted spectrum (Hawe *et al.*, 2008). The dye covalently or non-covalently bind to the thiol group, or α-amino group of cysteine residues or the ε-amino group of lysine residues within the protein (Douminge *et al.,* 2013). With this extrinsic probe, conformational changes within the protein, such as protein unfolding or misfolding, protein aggregation, or substrate binding can be monitored as the dye is weakly fluorescence when freely in polar environments (Hawe *et al.,* 2008). The dye is excited at 395 nm, and emission is monitored from 400 nm to 600 nm.

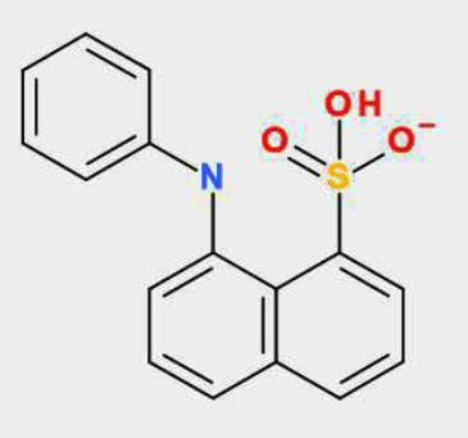

Figure 3. 7 Structure of 8-anilino-1-naphthalenesulfonic acid (ANS). The ANS structure contains a sulfonate group and a highly polar-sensitive naphthalene ring. (Image extracted from PubChem).

Stock ANS solution was prepared in sodium phosphate buffer, and concentration was measured spectroscopically at 350 nm (MW= 299,34; Ɛ= 5000 M^{-1} cm^{-1}) to prevent photodecomposition, the dye was wrapped in foil to protect it from the light because it is a light-sensitive dye. Conformational changes of WT-*KpBlac-1* and S70A-*KpBlac-1* in the presence and absence of penicillin, urea (denatured state) and cefoperazone were monitored with Jasco FP-6300 spectrofluorometer. For the analysis, 5 µM WT-*KpBlac-1* and S70A-*KpBlac-1*, 8 M urea (for denatured states), 100 µM penicillin and cefoperazone and 100 µM ANS were prepared in sodium

phosphate buffer. The experiment was conducted in triplicates and monitored at 20°C. The proteins were excited, at 395 nm and emission spectra were captured from 400 to 600 nm (3 accumulations, 0.5 data pitch, 2.5 nm emission bandwidth and 5 nm excitation bandwidth, 200 nm/min scan speed). The spectra were corrected with appropriate buffer blanks.

3.2.9 Quaternary structure analysis

Macromolecule separation based on size was described in 1975 and was termed Gel filtration (Porath *et al.*, 1975). High-performance liquid chromatography (HPLC) is conducted with inert silica resins enclosed with steel supports which enable higher flow rates with fast data outputs (Pérez-Escalante *et al.,* 2018). The quaternary structure of the proteins is assessed with size-exclusion high-pressure liquid chromatography (SE-HPLC), which is non-reactive with protein samples and thus can provide reliable information on the oligomeric state of native proteins (Porath *et al.*, 1975). This technique separates molecules based on size through a porous molecular sieve (stationary phase of column) based on their hydrodynamic volume or Stokes radius, which takes into account the molecule's volume and the solvent volume (Marinescu *et al.*, 2018).

Larger molecules with higher hydrodynamic volumes attenuate faster than smaller molecules, as their movement is retarded in the porous beads in the column. SE-HPLC resins include agarose (Sepharose), polyacrylamide polymers, and dextran (sephacryl/sephadex) (Corbett and Roche, 1984). A commonly used agarose resin, Superdex, provides high-resolution efficiencies. The technique is advantageous as it can separate small volumes of proteins, is time effective, and requires less sample manipulation. Increasing column width results in higher column capacity, whereby increasing the column length results in greater resolution (Corbett and Roche, 1984). The pore sizes can be obstructed or minimised by packing the column, whereas a packed column reduces the surface area of the column and thus leads to reduced retention times of samples. SE-HPLC is monitored via the absorption of proteins at 280 nm over time (Corbett and Roche, 1984).

The size and oligomeric state of WT-*KpBlac-1* and S70A-*KpBlac-1* were assessed on a TSKgel SuperSW2000 SEC column (resolution range of 5–150 kDa) connected to a TSKgel SWXL guard column and absorption at 280 nm monitor on a Shimadzu ultrafiltration liquid chromatography

(UFLC) SPD-20A SE-HPLC system. The column was equilibrated with HPLC running buffer [5 mM sodium phosphate monobasic, 0.02 % (w/v) sodium azide and 500 mM NaCl, pH 7.2]. WT-*KpBlac-1* (20 µL) and S70A-*KpBlac-1* (20 µL) were injected onto the column and ran for 30 minutes. Gel filtration standards (20 µL) were injected into the column, which consists of thyroglobulin (670 kDa), γ-globulin (158 kDa), ovalbumin (44 kDa), myoglobin (17 kDa) and vitamin B12 (1.35 kDa) and ran for 30 minutes. The experiment was conducted at a flow rate of 1 mL/min. A linear regression curve was constructed with the logarithm molecular weight of the gel filtration standards against their retention time. From the fitted linear regression equation, the sizes of WT-*KpBlac-1* and S70A-*KpBlac-1* were calculated.

3.2.10 Effect of Penicillin and CPZ binding on the stability of KpBLac1

The thermal stability of proteins upon substrate or cofactor binding, as well as environmental changes such as various buffers or pH ranges, can be assessed with thermal shift assay. This technique uses a fluorescent dye, SYPRO Orange, to probe the hydrophobic clefts of the protein under several conditions (Huynh and Partch, 2015). In polar environments, these dyes exhibit a low fluorescent signal and a higher fluorescence signal in non-polar environments (Jafari *et al*., 2014). As the temperature increases from 20°C to 90°C, the protein becomes unfolded, and hydrophobic core residues are exposed; thus, SYPRO orange binds non-specifically to these hydrophobic pockets within the protein (Huynh and Partch, 2015). The binding of SYPRO orange to the hydrophobic sites increases the fluorescence intensity. Over time at higher temperatures, the protein starts to aggregate and misfold; as a result, the dye becomes displaced, and the fluorescent intensity is decreased (Huynh and Partch, 2015). The transition point before the protein aggregates is called the melting temperature (Tm), which is used to assess thermal stability. The T_m indicates the temperature at which the protein is 50% unfolded (Jafari *et al.*, 2014). A protein that results in a higher T_m is considered more stable as higher temperature fluctuation is needed to unfold the protein (Jafari *et al.*, 2014).

The thermal stability of WT-*KpBlac-1* and S70A-*KpBlac-1* were assessed using CFX96 Touch Real-Time PCR Detection System. The experimental setup in 96-well plates is outlined in Figure

3.8. Samples were prepared in sodium phosphate buffer with a reaction volume of 25 µL. The reaction was carried out with 10 µL sodium buffer containing varied concentrations (0 µM to 2000 µM) of penicillin and cefoperazone, 5µL of 50x SYPRO orange dye, 10 µL of 50 µM (final enzyme concentration of 20 µM) WT-*KpBlac-1* and S70A-*KpBlac-1*. Samples were run for 1 hour from 20°C to 75°C with increments of 0.5 °C for 10 seconds. The samples were corrected with appropriate buffer blanks. Melting curves of the relative fluorescence unit (RFU) and their derivative curves (-d(RFU)/dT) were obtained through the CFX Maestro software.

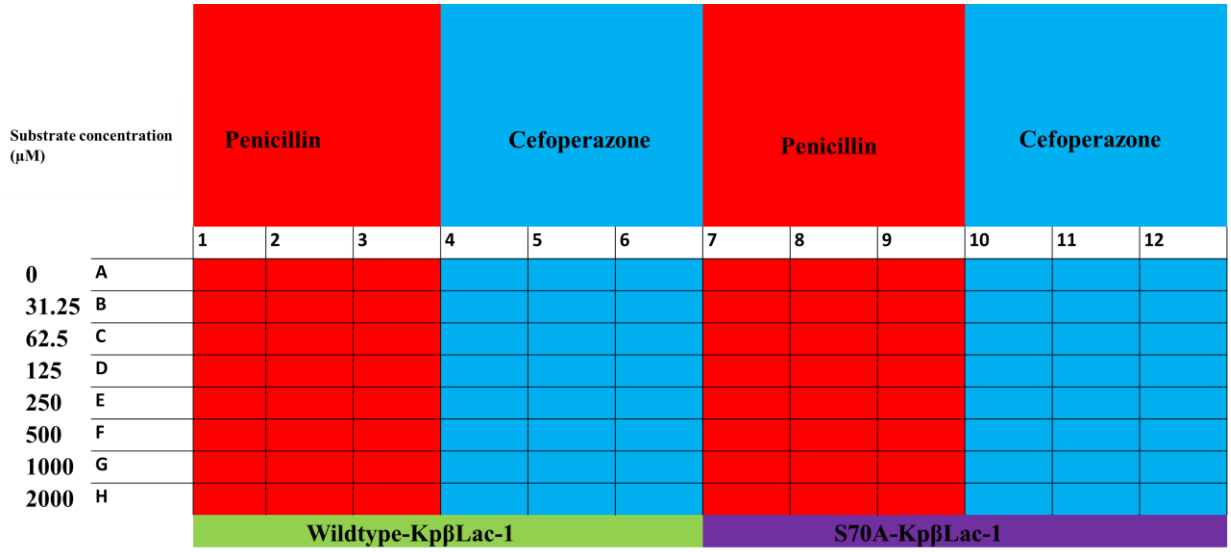

Figure 3. 8 A depiction thermal shift assay setup for *WT-KpBlac-1 and S70A-KpBlac-1*. The reaction was conducted in 96-multi well plates with varied concentrations of penicillin and cefoperazone.

3.2.11 Thermodynamics of KpBLac1 interaction with penicillin and CPZ

Isothermal titration calorimetry (ITC) is used to assess protein-protein or protein-ligand binding interactions, monitored through heat released or absorbed during the interaction at a constant temperature (Zhang *et al.,* 2018). The important thermodynamic parameters yielded from this technique are the binding affinities (K_a or K_D), stoichiometry (n) and enthalpy (ΔH), from which the entropy ($\Delta S°$) and Gibbs free energy ($\Delta G°$) is obtained (Pierce et al., 1999). ITC utilises the following equations for the determination of thermodynamic parameters:

$$\Delta G° = \Delta H° - T\Delta S°$$

where ΔG; change in Gibbs free energy (kJ/mol). ΔS; change in entropy(kJ/mol). T; temperature (K). ΔH; change in enthalpy (kJ/mol).

$$\Delta G° = -RT ln\ (K_a)$$

or

$$\Delta G° = -RT \ln(1/K_d)$$

Where $\Delta G°$; change in Gibbs free energy. T; temperature (K). R; gas constant (8.314 J/mol/K). K_a (M^{-1}) and K_D (M); affinity and dissociation constants.

The ITC instrument is composed of a reference cell containing the solvent in which samples are loaded, which also maintains the heat distribution within the cells (Freire *et al.,* 1990). The sample cell holder; contains the protein of interest. The compartments are enclosed in an adiabatic jacket. The ligand used in the experiment is titrated into the sample cell with a syringe attached to a burette (Freire *et al.*, 1990) (as shown in Figure 3.9). As the reaction starts and substrate binding to the protein simulates relative heat, either released or absorbed. The heats are proportional to the type of binding (exothermic or endothermic) (Grolier and del Río, 2012). With every substrate titration event, heat is supplied to the sample cell and is observed with signal peaks correlating to the binding events. The resulting interaction produces a thermogram (Freire *et al.,* 1990). This curve is then fitted to a mathematical model (e.g. Independent model) to obtain thermodynamic parameters (Figure 3.9). ITC give insights into the favourability of non-covalent and covalent interactions and the spontaneity of protein-ligand binding (Grolier and del Río, 2012). It also gives insight into substrate affinity and solvent environment interactions. ITC can also be used for enzyme kinetics to assess the activity of an enzyme (Chow *et al.*, 2013). This is advantageous as it does not require protein alterations, activity measurements are produced in real-time, and no addition of chromogenic substrates is required, as adversely seen in spectrophotometry techniques (Freire *et al.,* 1990).

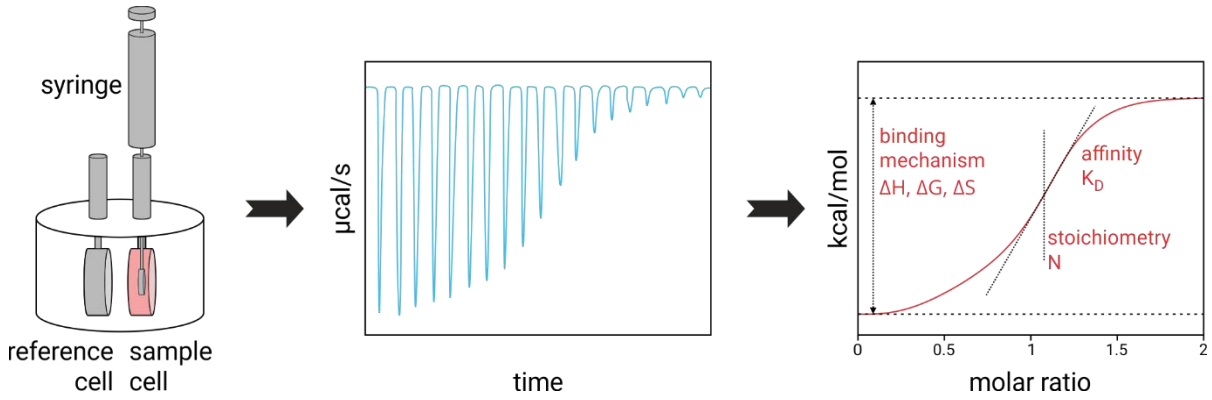

Figure 3. 9 The instrumental design and data output of an Isothermal titration calorimeter. The ITC instrument is composed of a reference cell and sample cell in which the protein is loaded into. The syringe containing the substrate is attached to a burette and titrated into the sample cell. Raw data from the interactions are shown with negative peaks (can also be positive) on a thermogram. The data is fitted through a mathematical model to obtain thermodynamic parameters. https://2bind.com/itc/.

The binding interaction between penicillin and cefoperazone with S70A-*KpBlac-1* at 25°C (298.15 K) was conducted with a Nano ITC instrument. The S70A-*KpBlac-1* was dialysed in sodium phosphate buffer containing 1 mM TCEP. For the two binding reactions, 2 mL samples were prepared in the dialysis buffer, filtered, and degassed (635 mmHg) for 15 minutes. For binding of cefoperazone to S70A-*KpBlac-1*, stock cefoperazone was dissolved in 100 % DMSO. To prevent protein damage and buffer mismatch, the final DMSO concentration for this binding reaction was 0.5% (v/v) in both samples, as 60 µM S70A-*KpBlac-1* and 1 mM cefoperazone were prepared. For binding of penicillin to S70A-*KpBlac-1*, 100 µM S70A-*KpBlac-1* and 5 mM penicillin were designed. Deionised water was loaded into the reference cell, protein samples were loaded in the sample cell, and penicillin and cefoperazone were loaded into the 250 µL syringe. The reactions were conducted with 5 µL injection volumes, 200 rpm stirring rate and 300-s increments between the 45 injections. Data were analysed through NanoAnalyse software, and the integrated heats per injection were corrected for heats of dilution and fitted with an independent model.

Chapter 4
Results

4.1 Recombinant expression of KpBLac-1 in *Escherichia coli*

Recombinant wild-type (WT)-and mutant *(S70A)-KpBlac-1* was expressed in T7 express competent *Escherichia coli* (*E. coli)* cells for 6 hours at 30 °C using a pET-28a vector with kanamycin selection. The expression was induced with 0.5 mM Isopropyl-β-D-thiogalactopyranoside (IPTG). The expressed enzyme, with a theoretical molecular weight of 29kDa (ProtParam), contains an N-terminal hexa-histidine tag pivotal for purification. The wet cell pellets obtained from expressed recombinant WT-KpBLac-1 and S70A-KpBlac-1 were 9.79 g/L and 12,64 g/L, respectively. Following purification preparation via sonication and centrifugation of expressed protein samples, the supernatant and pellet of each protein were run on a 12.5% (w/v) SDS-polyacrylamide gel (Figure 4.1 A and B (lanes 2 and 3). The SDS-PAGE gel showed that the expressed proteins were predominately evident in the soluble fraction (supernatant) in comparison to the insoluble (pellet) fraction (Figure 4.1 A and B (lanes 2 and 3) with the presence of a prominent band corresponding to the theoretical molecular weight (29 kDa). This is indicative that expression was successful, and protein can be utilised for downstream purification techniques (i.e., Ni^{2+}-IMAC).

4.2 Purification of KpBLac1 using Immobilised nickel affinity chromatography

The presence of an N-terminal hexahistidine tag on both WT and S70A-*Kp*βLac-1 enables purification through immobilised metal ion affinity chromatography (IMAC). A nickel-embedded column was used to separate the expressed recombinant protein from naturally occurring *E. coli* proteins. The targeted proteins would be bound to the resin's nickel ions due to histidine's affinity (more so the imidazole ring) to the metal ions. The solubilised his-tag protein cell fractions were effectively purified using Ni^{2+}- affinity chromatography as most of the protein remained attached to the column, and no protein was isolated in the flow-through (Figure 4.1 A and B (lanes 4)).

Column wash steps were employed to isolate any contaminants and weakly or unbound proteins (Figure 4.1 A and B (lanes 5-7)). WT-and S70A-KpβLac-1 were eluted off the column with a single-step elution with imidazole, and purified samples were run on a 12.5% (w/v) polyacrylamide SDS-PAGE gel (Figure 4.1 A and B (lanes 8-13). No impurities were visible, as only single thick bands were noticed at ~29 kDa (corresponding to theoretical molecular weights of protein). Thus, a one-step Ni^{2+}-IMAC column successfully purified clean WT-and S70A-KpBLac- from the supernatant of homogenised T7 Express *E. coli* cells.

The molecular weights of purified WT-and S70A-KpBlac-1 were confirmed using a standard curve of logarithm molecular weights of the PageRuler Plus Prestained Protein ladder standards from the SDS-PAGE (Figure 4.1 A and B (lanes 1) against relative distance migrated (Rf) of those standards. The constructed calibration curve (Figure 4.1 C) yielded a fitted linear regression with a linear equation of $\gamma = -1.39773x + 2.5612$ and an R-squared value of 0.9416. The WT-and S70A-KpBLac-1 sizes were confirmed to be 28 kDa and 27.7 kDa, respectively.

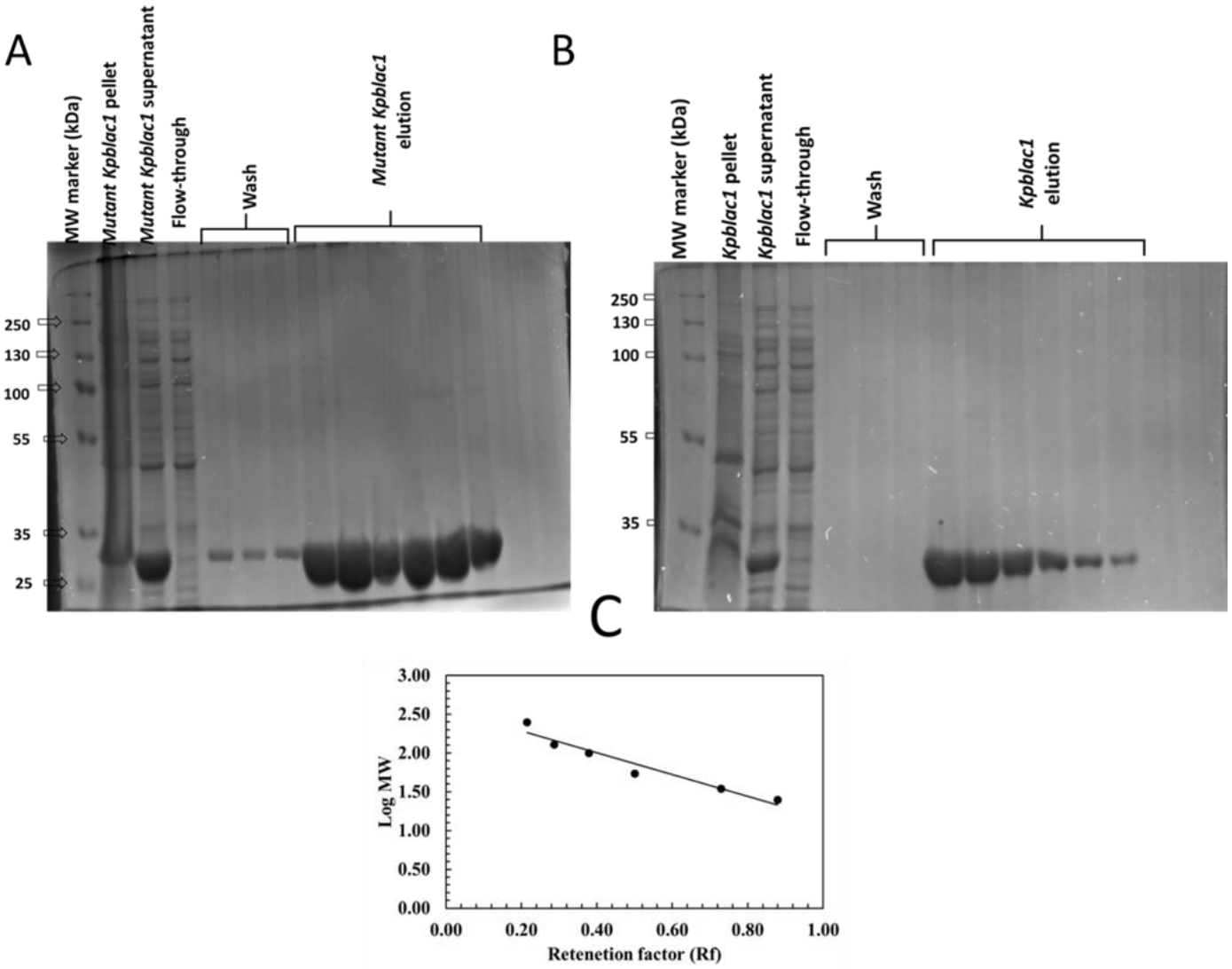

Figure 4. 1 SDS-PAGE analysis of over-expression and Ni^{2+}-IMAC purification of recombinant WT-KpBLac-1 and S70A-KpBLac-1. Crude lysate of *E. coli* containing overexpressed WT-and S70A-KpBLac-1 was subjected to sonication and centrifugation to separate the insoluble (pellet) from the soluble fraction (supernatant). Ni^{2+}-IMAC was used to purify the solubilised fraction and elution prompted with 500 mM imidazole in 1xPBS buffer (pH 7.4). **A)** 12.5% glycine SDS-PAGE gel analysis visualised with Coomassie brilliant blue staining of purification samples of WT-KpBLac-1 ran against PageRuler Plus Prestained Protein ladder standards (lane 1). The pellet (lane 2) and supernatant (lane 3) samples showed that the recombinant target protein was present in the soluble (supernatant) fraction indicated by thick band ~29 kDa (lane 3). The homogenised soluble fraction was injected on the column and flow-through collected (lane 4). Multiple wash steps were employed (lanes 5-7), with the equilibration buffer (PBS, 25 mM imidazole pH 7.4) and a detergent (Tween-20) wash. Elution fractions of pure WT-KpBLac-1 (lanes 8-13) was obtained, indicated with thick single bands ~29 kDa. **B)** 12.5% glycine SDS-PAGE gel analysis of S70A-KpBLac-1. Contents of gel lanes and technique were like WT-kpBLac-1 (A) gel analysis. **C)** The predicted molecular weights of WT-KpbLac-1 and S70A-kpBLac-1 was determined with a constructed standard curve of logarithm molecular weight marker standards on the SDS-PAGE gels against their relative

migration distance (Rf). The fitted curve yielded a linear curve ($\gamma = -1.39773x + 2.5612$ and a R^2 value of 0.9416) and WT-KpBLc-1 and S70A-kpBLac-1 sizes were determined as 28 kDa and 27.7 kDa respectively, which is comparable to the theoretical weights of 29 kDa (ProtParam).

4.3 Qualitative and quantitative analysis of the expressed KpBLac1

WT-*Kp*BLac-1 and S70A-KpBLac-1 contain a significantly high number of aromatic residues (tyrosine, phenylalanine, and tryptophan) in their primary amino acid sequence; therefore, they would absorb light maximally at 280 nm. The eluted fractions of WT and S70A-KpBLac-1 were dialysed in a sodium phosphate buffer using a Snakeskin dialysis tubing with a 10 kDa molecular weight cut-off. The qualitative assessment of WT-and S70A-KpBLac-1 was monitored with Ultraviolet (UV)-visible absorbance spectroscopy between 240 nm to 350 nm (Figure 4.2). This was significant in detecting the level of interference from protein aggregation (Rayleigh scatter) and nucleic acid contamination at 320 nm and 260 nm, respectively. Single peaks were revealed at 280 nm for both WT and S70A-KpBLac-1 at 280 nm indicating that the purified recombinant proteins were devoid of any interference from protein aggregation or nucleic acid contamination (Figure 4.2). Therefore, the protein concentration of WT-and S70A-KpBLac-1 can be more accurately determined.

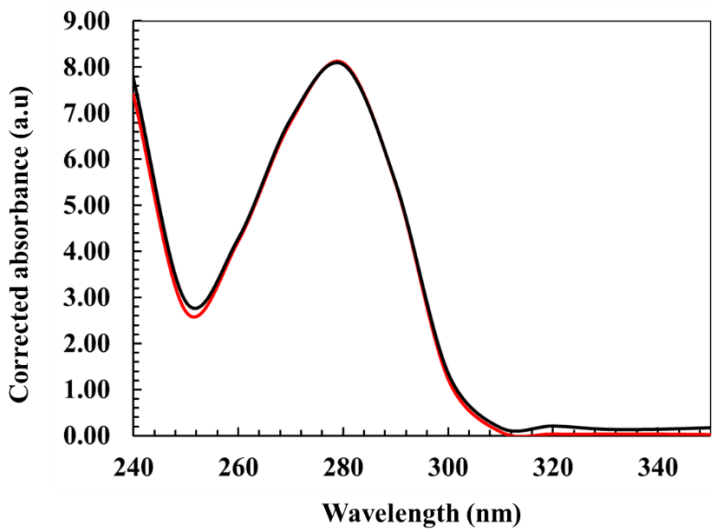

Figure 4. 2 Qualitative analysis of WT-and- S70A-KpβLac-1 via UV absorption spectrum. The purity was assessed with A UV spectrum (240-350 nm) of the WT-KpβLac-1 (black spectrum) and S70A-KpβLac-1 (red spectrum) revealed single peaks at 280 nm. JASCO V-630 spectrophotometer was utilised for the detection and revealed that protein aggregation or nucleic acid contaminants were not evident as no peaks and a flat trajectory were revealed at 260 nm and 320 nm-350 nm, respectively.

The concentration of WT-and S70A-*Kp*βlac-1 was further determined spectroscopically using a 1/20 serial dilution of the dialysed proteins and absorbance measured at 280 nm (Figure 4.3). This resulted in a linear regression curve with fitted linear equation of $y = 2.8175x - 0.0016$; R^2 value of 0,99 for WT-*Kp*βLac-1 and $y = -8.8551x - 0.0018$; R^2 value of 1 for S70A-*Kp*βLac-1. The Beer-Lamberts law equation, in conjunction with the gradient derived from the fitted linear equation and the extinction coefficient of WT-and S70A-Kpβlac-1 (23950 $M^{-1}cm^{-1}$) derived from ProtParam, was used to determine the concentration of the proteins. The concentrations were revealed to be 3.4 mg/mL and 10.8 mg/mL for WT-Kpβlac-1 and S70A-Kpβlac-1, respectively. The expression yield was revealed to be 3.4 mg of WT-Kpβlac-1 per g of wet *E. coli* cells; and 4.3 mg of S70A-Kpβlac-1 per g of wet *E. coli* cells.

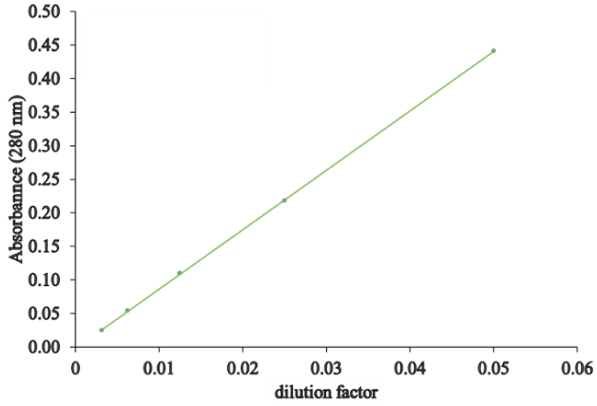

Figure 4. 3 Quantification assessment of recombinant WT-and S70A-Kpβlac-1. Absorbance measured at 280 nm was plotted against the dilution factor of 1:20 fold serially diluted Kpβlac-1 proteins carried out in sodium phosphate buffer (5 mM NaH_2PO^4 (monobasic), 0.01% (w/v) NaN_3, pH 7.2). A linear repression curve was obtained with fitted linear equations of $\gamma = 2{,}8175x - 0{,}0016$; R^2 value of 0,99 for WT-Kpβlac-1 and $\gamma = -8{,}8551x - 0{,}0018$; R^2 value of 1 for S70A-Kpβlac-1. Due to R-squared values being in good relation the protein concentration can be more accurately determined. The relationship between concentration and absorbance from the Beer-lamberts law was employed to acquire the concentrations of WT-Kpβlac-1 and S70A-Kpβlac-1 which were revealed to be 3.4 mg\mL and 10.8 mg/mL respectively.

4.4 Enzyme activity assay

The specific activity of WT-*KpBlac-1* and S70A-*KpBlac-1* were assessed spectroscopically using chromogenic cephalosporin, and nitrocefin, as the substrate. KpBlac-1 and the hydrolytic event readily degrade Nitrocefin is indicated by a colour change from yellow (intact Nitrocefin) to red (hydrolysed compound) (supplementary Figure S1). The assessment was measured at 482 nm under varied WT-*KpBlac-1* and S70A-*KpBlac-1* concentrations (Figure 4.4 and Supplementary Figure S1). Linear regression curves were obtained from the activity of the proteins and from the gradient of the linear regression equation, the specific activity of WT-*KpBlac-1* was 12.009 mg/µmol/min and S70A-*KpBlac-1* was 0,0028 mg/µmol/min.

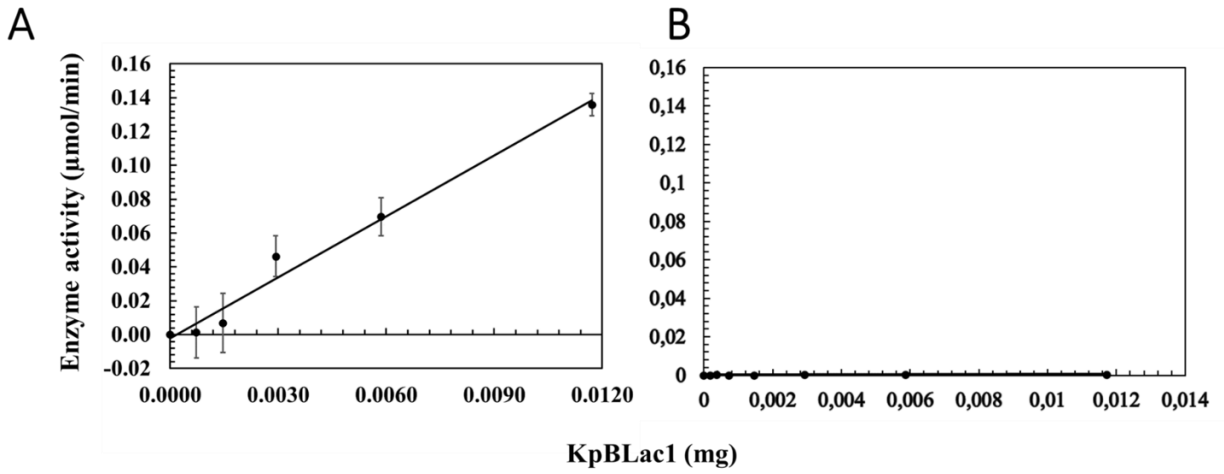

Figure 4. 4 Specific activity of WT-*KpBlac-1* and S70A-*KpBlac-1 was* assessed with nitrocefin. The ability of WT-*KpBlac-1* and S70A-*KpBlac-1* to hydrolyse nitrocefin was assessed. The experiment was conducted with varied WT-*KpBlac-1* and S70A-*KpBlac-1* concentrations (0 µM to 1600 µM) and 0.5 mg/mL Nitrocefin at 482 nm **A)** The activity of WT-*KpBlac-1* was assessed, and a fitted linear regression curve obtained an equation of $y = 12.009x - 0{,}00022$; R^2 value of 0.9826. **B)** The activity of S70A-*KpBlac-1* was assessed, and a fitted linear regression curve obtained an equation of $y = 0.0028x - 0.00001$; R^2 value of 0.5276. From the data it is evident that WT-*KpBlac-1* was highly active, and S70A-*KpBlac-1* was comparably inactive, which was expected.

4.5 Secondary structure content analysis of Kpblac-1

Secondary structure analysis of WT-Kpβlac-1 and S70A-Kpβlac-1 was monitored using far-ultraviolet circular dichroism (Far-UV CD). Hydrogen bonding of the peptide backbone stabilises the protein's secondary structure. Therefore, due to the ability of the peptide bonds to polarise light, the Kpβlac-1 proteins serve as the chromophore for Far-UV CD analysis. Beta-sheeted proteins have a positive peak at 195 nm and a trough at 218 nm. Alpha helical proteins exhibit a positive peak at 193 nm and trough at 222 nm and 208 nm. Random coils have a positive peak at 195 nm and a trough at 212 nm. Analysis was done under native conditions (Apo-proteins), denatured conditions with 8 M urea, and protein-ligand conditions with cefoperazone (CPZ) and penicillin (pen) (Figure 4.5). The experiment was conducted at 20 °C, and the spectrum measured from 180 nm to 255 nm (Figure 4.5). The analysis revealed that both the native WT-Kpβlac-1 and S70A-Kpβlac-1 were predominantly alpha-helical. Urea (8 M) was also successful in unfolding the proteins completely. Kpβlac-1 bound to cefoperazone (CPZ) introduced a distortion of the secondary structure (Figure 4.5). Native WT-Kpβlac-1 exhibited troughs at 218,5 nm and 208,5 nm and peaked at 192.5 nm. Native S70A-Kpβlac-1 exhibited troughs at 218 nm and 208 nm and peaked at 192.5 nm. Both native protein results were relatively close to the theoretical characteristics of alpha proteins. In the presence of penicillin, WT-Kpβlac-1 exhibited troughs at 221,5 nm and 209 nm and peaked at 196 nm; S70A-Kpβlac-1 exhibited troughs at 217 nm and 208.5 nm and peaked at 197 nm. In the presence of cefoperazone, WT-Kpβlac-1 and S70A-Kpβlac-1 exhibit troughs at 220 nm and 222 nm, respectively. Emission results of Kpβlac-1 bound to cefoperazone from 195 to 210 nm reveal that the secondary structure was disturbed as the peak was disrupted by high voltage compensation signalled by the HT spectrum (supplementary Figure S2). Kpβlac-1 denaturation with 8 M urea completely unfolded the protein. However, emission results between 195 to 210 nm are unreliable as urea absorbs light at 210 nm.

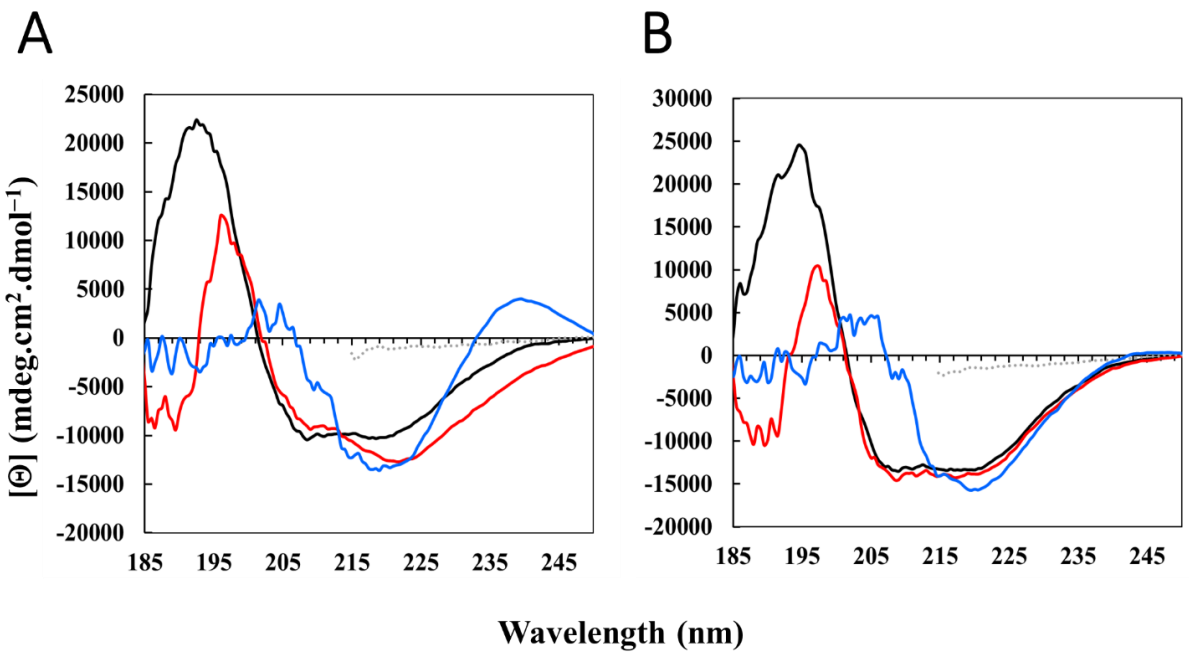

Figure 4. 5 Secondary structural, spectral analysis of WT-Kpβlac-1 and S70A-Kpβlac-1. The analysis was conducted in 5 mM sodium phosphate buffer **A)** The native WT-Kpβlac-1 profiles (black spectra) are predominantly alpha helical with negative ellipticity at 218,5 nm and 208,5 nm; and positive ellipticity at 192.5 nm. In the presence of substrates, penicillin (red spectra) and cefoperazone (blue spectra), the secondary structure is distorted, more so in the presence of CPZ. The protein was unfolded completely (grey dotted-line spectra) in 8 M urea. **B)** The native S70A-Kpβlac-1 profiles (black spectra) are predominantly alpha helical with troughs at 218 nm and 208 nm; and peaks at 192.5 nm. In the presence of substrates, penicillin (red spectra) and cefoperazone (blue spectra), there is visible loss of secondary structural features, more so in the presence of CPZ. The protein was unfolded completely (grey dotted-line spectra) in 8 M urea as a complete loss of secondary structural elements were obtained.

DichroWeb was utilised to assess the percentage of secondary structural content of WT-Kpβlac-1 and S70A-Kpβlac-1 in conjunction with the CONTIN-ILL algorithm. This software calculates the content of the protein secondary structure of the submitted data to the actual secondary structure. In revealing secondary structural content, the software also provides the normalised root mean square deviation (NRMSD). The NRMSD depicts the fit of the predicted data with the experimental data, i.e. it provides the best data fit or "goodness of fit". The lower the NRMSD value (<0.1), the more reliable the data fit. The experimental data were deconvoluted through DichroWeb (CONTIN-ILL algorithm, reference set 6) and revealed that the native Kpβlac-1 were predominantly alpha-helical and NRMSD values were in close range to a good fit (Table 4.1).

However, the presence of substrates (penicillin and cefoperazone) revealed a conformational shift to a more unordered and/or beta-stranded protein. Thus, revealing that the introduction of substrates distorts the secondary structure of Kpβlac-1, alluding to NRMSD values greater than 0.1 (Table 4.1).

Table 4. 1 DichroWeb analysis for Kpβlac-1 secondary structure content. The Normalised Root-Mean-Square Deviation (NRMSD) was determined with use of the CONTIN-ILL algorithm (reference set 6); which compares the obtained experimental data with calculated data and measures the goodness of fit; where values <0.1 are more accurate as they have a good fit.

KpβLac-1	α-helix (%)	β-stands (%)	β-turns (%)	Unordered (%)	NRMSD
Wild-type (WT)-Apo	63.4	7.4	24.1	5.1	0.161
WT-Cefoperazone	24.1	19.8	13.6	42.5	0.340
WT-Penicillin	25.5	12.5	1.09	51.1	0.394
Mutant (S70A)-Apo	60.9	7.8	21.5	9.3	0.166
S70A-Penicillin	44.5	19.0	2.6	33.9	0.494
S70A-Cefoperazone	0	100	0	0	0.363

4.6 Tertiary structure analysis

4.6.1 Tryptophan fluorescence of WT-Kpβlac-1 and S70A-Kpβlac-1

The tertiary structure of WT-Kpβlac-1 and S70A-Kpβlac-1 was assessed using aromatic tryptophan residues as a fluorophore probe for intrinsic fluorescence spectroscopy. This technique gives insight into the polarity of the global and local microenvironment of tryptophan residues within Kpβlac-1 in the presence of penicillin, cefoperazone, and native and denatured states. The tryptophan indole ring's electrons are excited at 295 nm, and light emission is monitored between 300 nm and 500 nm. Both WT-Kpβlac-1 and S70A-Kpβlac-1 have three tryptophan residues (Trp195, Trp214, and Trp235). The fluorescence spectra were measured at 20 °C, and the native WT-Kpβlac-1 had maximum emission at 339,5 nm (supplementary Table S1). When denatured, a redshift and fluorescence quenching was depicted as the tryptophans were more solvent-exposed (Figure 4.6 A). In the presence of penicillin and CPZ, no changes were significantly apparent as the maximum emission were 340.5 nm and 341. 5 respectively (supplementary Table S1), which

were expected since the WT-Kpβlac-1 actively hydrolyses the substrates and never is completely bound to the Kpβlac-1 binding site. The S70A-Kpβlac-1 was analysed as well (Figure 4.6 B); and similar to WT-Kpβlac-1, the native and denatured state exhibit similar behaviour, with a redshifted quenched fluorescence spectra for the denatured (λmax of 350 nm) compared to the native (λ_{max} of 339.5 nm) (supplementary Table S1). In the presence of penicillin and CPZ, there were slightly quenched spectra more noticeable for CPZ bound state (blue spectra) (Figure 4.6 B).

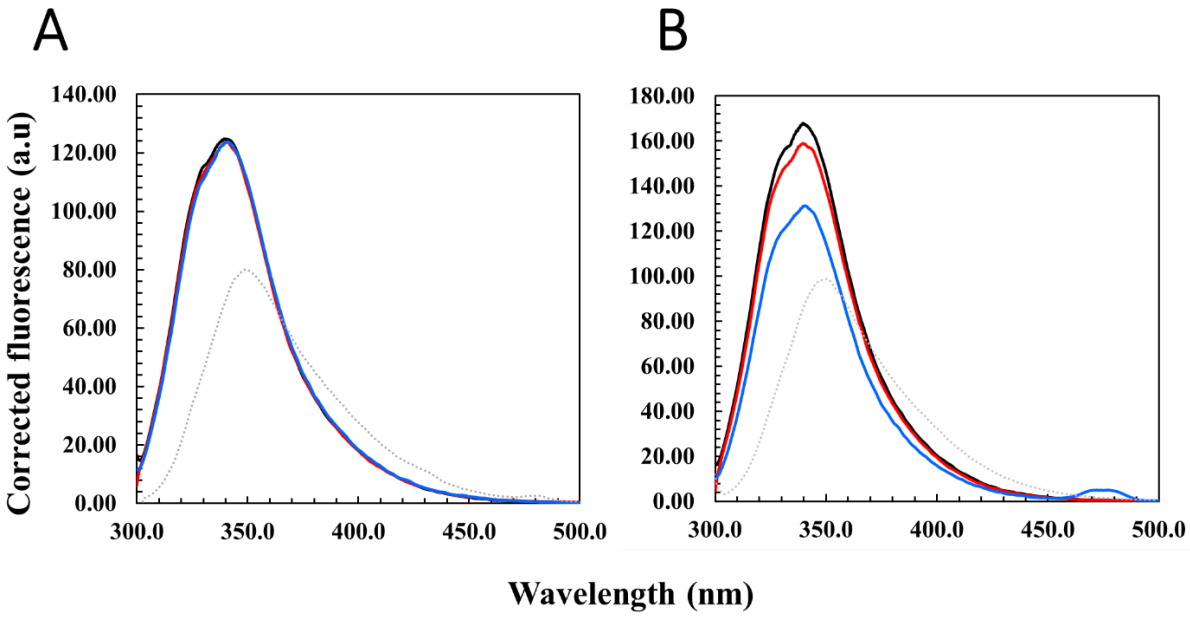

Figure 4. 6 Intrinsic fluorescence emission spectra of WT-Kpβlac-1 and S70A-Kpβlac-1. The analysis was conducted in 5 mM sodium phosphate; with 5 µM WT-Kpβlac-1 and S70A-Kpβlac-1, with excitation wavelength of 295 nm. **A)** The native WT-Kpβlac-1 (black line) vs denatured (grey dotted line) spectra indicated that the protein is completely unfolded in the presence of 8M urea and emission produced a redshift; from 339.5 nm (for native) to 348.5 nm (unfolded) with a lower quantum yield. In the presence of 100 µM penicillin (red line) and CPZ (blue line), no significant impact was shown as the spectra overlay with the native spectra. **B)** The native S70A-Kpβlac-1 (black line) vs denatured (grey dotted line) spectra indicated that the protein is completely unfolded in the presence of 8 M urea and produced an emission redshift; from 339.5 nm (for native) to 350 nm (unfolded) with lower quantum yield. In the presence of 100 µM penicillin (red line) and CPZ (blue line), decreased quenching of quantum yields were evident, with CPZ showing a significant decrease with respect to the native state. This could indicate that the presence of the substrate causes conformational changes within S70A-Kpβlac-1 exposing the tryptophan's to the aqueous environment.

4.6.2 ANS spectroscopy of WT-Kpβlac-1 and S70A-Kpβlac-1

Extrinsic fluorescence was assessed with an anionic dye, 8-anilino-1-naphthalenesulfonic acid (ANS). ANS fluorescence gives insight into the hydrophobicity of the protein as a fluorescence signal is obtained when ANS binds to hydrophobic clefts (such as the active site/s) within the protein. It can give insight into folding intermediates and surface hydrophobicity and detect aggregation events. The higher the degree of hydrophobicity, the higher the fluorescence signal. Kpβlac-1 is known to have one active site; thus, ANS spectroscopy can be utilised. The fluorescence was assessed for the native and denatured WT-Kpβlac-1 and S70A-Kpβlac-1 in the presence of penicillin and CPZ (Figure 4.7 A and B). The fluorescence spectra were measured at 20 °C, excited at 395 nm and light emission was captured between 400 nm to 600 nm. The native WT-Kpβlac-1 had maximum emission at 509 nm (supplementary Table S2). When denatured, a redshift (519 nm) and an increase in fluorescence were depicted as the hydrophobic patches are more solvent exposed and thus ANS has more ease of access to these clefts (Figure 4.7 A). In the presence of penicillin and CPZ, no changes were significantly apparent as the minimum emission were 510 nm and 508 nm, respectively (Supplementary Table S2), which were relative to the native spectra. This was expected since the WT-Kpβlac-1 actively hydrolyses the substrates; thus, the active sites are free for ANS to be bound, conferring a native-like spectrum. For S70A-Kpβlac-1 (Figure 4.7 B), the native and denatured states were analysed, and the denatured state showed a blueshift from 520 nm (native max emission) to 517 nm (supplementary Table S2), the fluorescence intensity was higher as the hydrophobic sites are more exposed for ANS binding (Figure 4.7 B). In the presence of penicillin and CPZ, a slight blueshift was observed (512 nm and 517.5 nm, respectively) (Supplementary Table S2). The fluorescence intensity of penicillin was similar to the native state, but a slight lowering in quantum yield was observed in the presence of CPZ (Figure 4.7 B). This could mean that in the presence of CPZ, conformational change was induced in that the ANS was displaced into the aqueous environment. In the presence of penicillin, the ANS dye could bind to the hydrophobic pockets as the spectra were similar to the native state. Since the quantum yields were not significantly different, it can be postulated that the active site of Kpβlac-1is polar exposed.

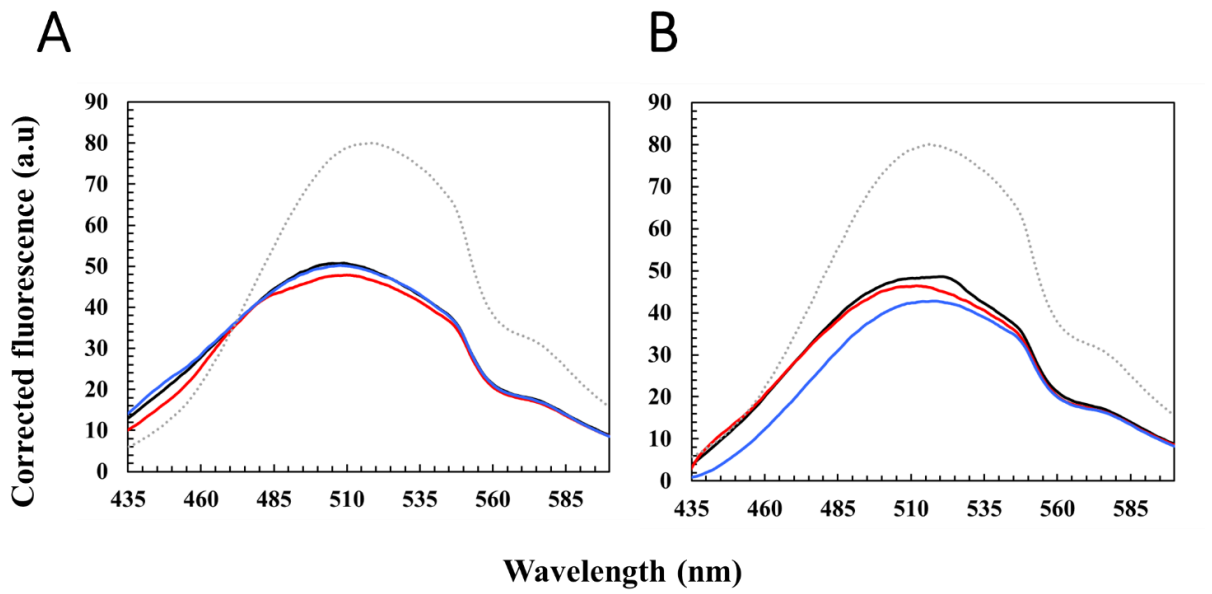

Figure 4. 7 Extrinsic ANS binding fluorescence emission spectrum of WT-Kpβlac-1 and S70A-Kpβlac-1. The analysis was conducted in 5 mM sodium phosphate buffer; with 5 µM WT-Kpβlac-1 and S70A-Kpβlac-1, 100 µM ANS excited at 395 nm and 100 µM penicillin and CPZ. **A)** The native WT-Kpβlac-1 (black line) vs denatured (grey dotted line) spectra indicated that the protein is completely unfolded in the presence of 8M urea with a redshifted emission; from 509 nm (for native) to 519 nm (unfolded) and increased quantum yield. In the presence of penicillin (red line) and CPZ (blue line), no significant impact was shown as the spectra overlay with the native spectra. **B)** The native S70A-Kpβlac-1 (black line) vs denatured (grey dotted line) spectra indicated that the protein completely unfolded in the presence of 8M urea with a slight blue shifted emission; from 520.5 nm (for native) to 519 nm (unfolded) and increased quantum yield. In the presence of penicillin (red line) and CPZ (blue line), no significant impact was observed for the penicillin bound state as the spectra overlay close with the native spectra. However, with CPZ a slight decreased with respect to the native state was observed.

4.7 Quaternary structure analysis of the expressed KpBLac1

Size exclusion HPLC was used to assess the quaternary structure of WT-Kpβlac-1 and S70A-Kpβlac-1. Gel filtration standards were injected into the column (Figure 4.8 A and B (grey dotted line). A chromatogram of the absorbance at 280 nm was used to construct a calibration curve of the logarithm molecular weight of the standards against their retention time (Figure 4.8 C). The WT-Kpβlac-1 was injected into the column and eluted as a single peak with a retention time of 18.31 minutes (Figure 4.8 A (blue line).

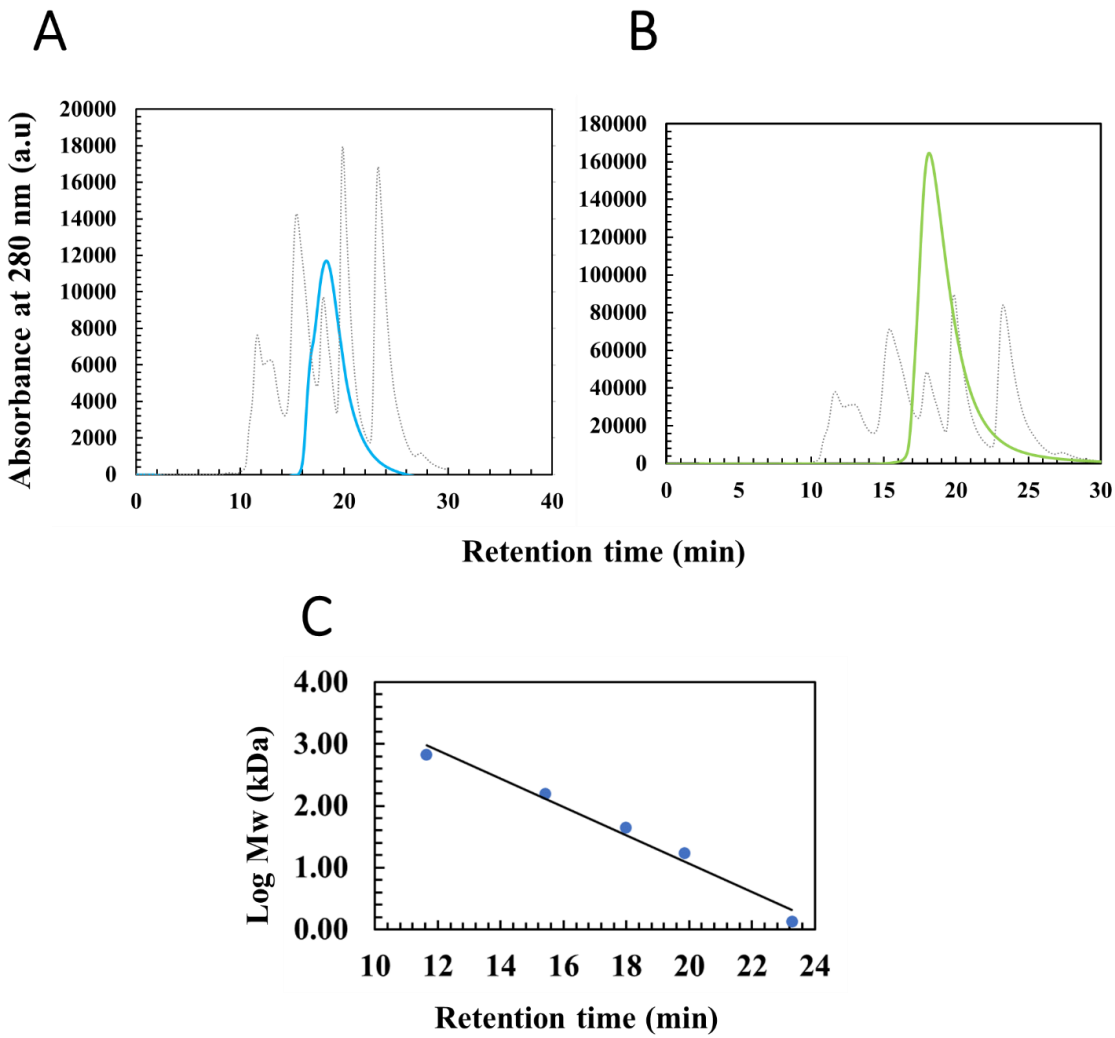

Figure 4. 8 Verification of the oligomeric state of WT-Kpβlac-1 and S70A-Kpβlac-1 by Size Exclusion-HPLC. A) Chromatogram profile of the eluted gel filtration standards (grey dotted profile) and 4.3 mg/mL WT-Kpβlac-1 (blue profile) prepared in 5 mM NaH_2PO^4 , 500 mM NaCl, and 0.02% (w/v) NaN_3, pH 7.2, at 20 °C. Composition of the standards from left to right peaks were thyroglobulin (670 kDa), γ-globulin (158 kDa), ovalbumin (44 kDa), myoglobin (17 kDa), and vitamin B12 (1.5 kDa). The eluted WT-Kpβlac-1 (blue profile) had a single peak at a retention time of 18.31 minutes. **B)** Chromatogram profile of the eluted gel filtration standards (grey dotted profile) and 10.8 mg/mL S70A-Kpβlac-1 (green profile). Composition of the standards from left to right peaks were stated in A. The eluted S70A-Kpβlac-1 (green profile) had a single peak at a retention time of 18.13 minutes. **C)** The constructed standard curve of logarithm molecular weight of the gel filtration standards against their retention time (minutes). A fitted curve was attained with linear regression equation of $\gamma = -0{,}2288x + 5{,}6414$ and a R-squared value of 0,9766. The equation was used to determine the size of WT-Kpβlac-1 and S70A-Kpβlac-1 which were reported as 28.3 kDa and 31 kDa respectively.

From the gel filtration standard curve with known standards (thyroglobulin, ɣ-globulin, ovalbumin, myoglobin and vitamin B12), a fitted curve was attained with a linear regression equation of $y = -0.2288x + 5.6414$ and an R^2 value of 0.9766 (Figure 4.8 C). The size of WT-Kpβlac-1 was determined to be 28.5 kDa. S70A-Kpβlac-1 was injected into the column and eluted as a single peak on the chromatogram with a retention time of 18.13 minutes [Figure 4.8 B (green line)]. From the linear regression equation, the protein oligomeric size was determined to be 31 kDa. Therefore, WT-Kpβlac-1 and S70A-Kpβlac-1 were determined to be monomeric.

4.8 Effect of Penicillin and CPZ binding stability on KpBLac1

The thermal stability of WT-Kpβlac-1 and S70A-Kpβlac-1 was assessed with SYPRO-orange dye from 20 °C to 75°C. WT-Kpβlac-1 and S70A-Kpβlac-1 thermal denaturation were monitored with a melt curve in the presence of various concentrations of penicillin and CPZ (supplementary Figure S3) using a Real-Time PCR Detection System. From these different conditions, 2 mM penicillin and CPZ were used for assessment of thermal denaturation of WT-Kpβlac-1 and S70A-Kpβlac-1. WT-Kpβlac-1 produced a sigmoidal melt curve (Figure 4.9A left graph) and melt peak (Figure 4.9 A right graph). The melt curve showed that the protein unfolded well (Figure 4.9A left graph), exposing hydrophobic pockets to SYPRO orange dye, thus, increasing the fluorescence signal. There is a transition point, resulting in decreased fluorescence signal as protein aggregation is attained. The melt peak (Figure 4.9A right graph) showed no significant effect in the presence of penicillin (red profile) and CPZ (blue profile) as no temperature shifts occurred and melt peak profiles overlay on the native profile (black profile). From the melt peak profiles, the melting temperatures were obtained (Table 4.2), which showed that a 0.5°C shift in the presence of penicillin and CPZ compared to the native WT-Kpβlac-1 was not significant. From the assessment of S70A-Kpβlac-1, a melt curve (Figure 4.9B left graph) and melt peak (Figure 4.9 B right graph) was obtained. The melt curve showed that the protein unfolded well (Figure 4.9B left graph). The melt peak (Figure 4.9B right graph) showed no significant effect in the presence of penicillin (red profile). However, an increased temperature shift was noticed in the presence of CPZ (blue profile) compared to the native profile (black profile). The melting temperatures were obtained from the melt peak profiles (Table 4.2) and showed that native and penicillin-S70A-Kpβlac-1 states had T_m of 52.5°C. In the presence of CPZ a 5.5 °C increased temperature shift was reported (Table 4.2).

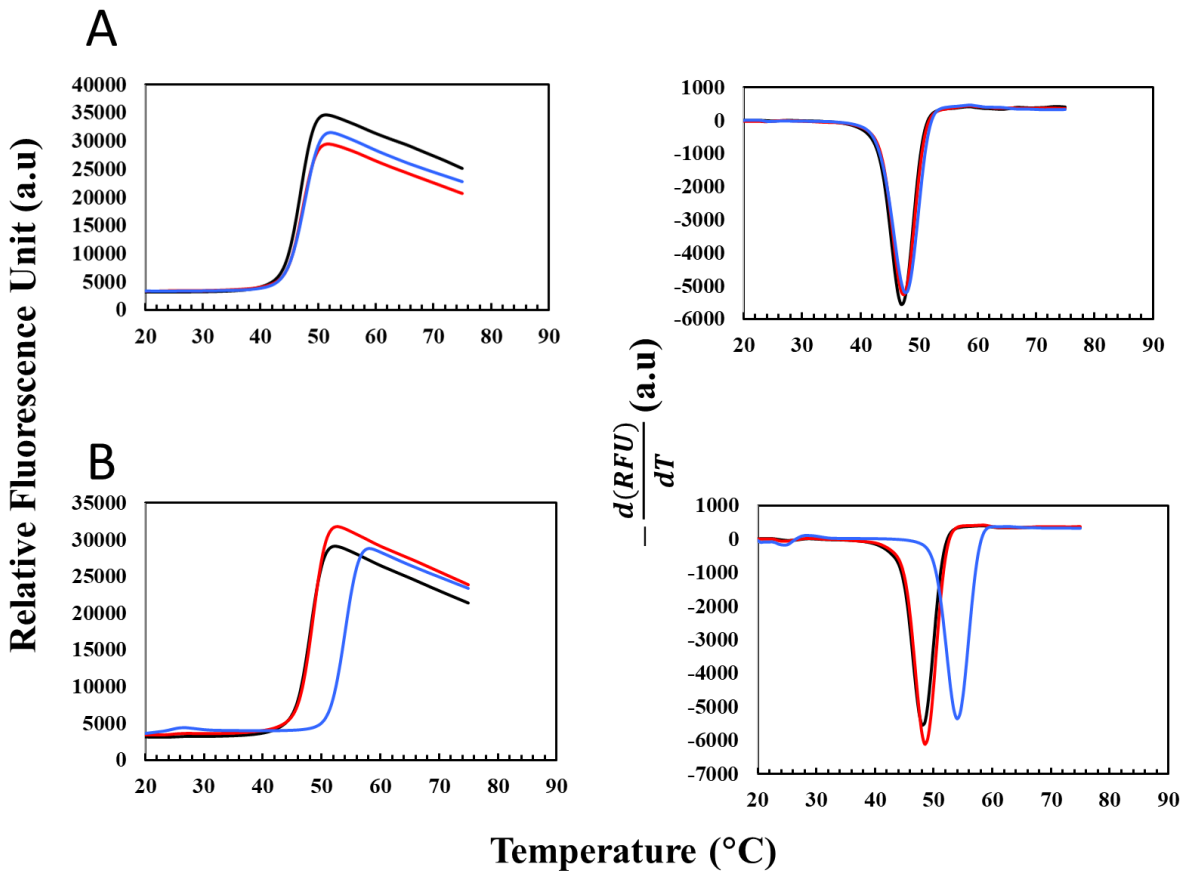

Figure 4. 9 Thermal denaturation stability of WT-Kpβlac-1 and S70A-Kpβlac-1 with Thermal shift assay. The stability and ligand interactions of native WT-Kpβlac-1 and S70A-Kpβlac-1 in the presence of penicillin and CPZ were monitored using SYPRO orange dye from 20 to 75 °C. **A)** Assessment of WT-Kpβlac-1 produced a sigmoidal melt curve (left graph) and melt peak (right graph). The melt curve showed cooperative protein unfolding, exposing hydrophobic pockets to SYPRO orange dye thus, increasing the fluorescence yield. The melt peak (right graph) depicted no significant effect in the presence of penicillin (red profile) and CPZ (blue profile) as only a 0.5 °C temperature shift compared to the native profile (black profile) was observed. **B)** S70A-Kpβlac-1 assessment produced both a melt curve (left graph) and melt peak (right graph). The melt curve showed the unfolding of the protein with a single transition. The melt peak (right graph) showed that no significant effect was noticed in the presence of penicillin (red profile). However, an increased 5.5°C temperature shift was noticed in the presence of CPZ (blue profile) compared to the native profile (black profile). Thus, can reveal that S70A-Kpβlac-1 is more thermally stable bound to CPZ.

Table 4. 2 Melting temperatures (Tm) for WT-Kpβlac-1 and S70A-Kpβlac-1 in the presence of penicillin and CPZ. The presence of penicillin and CPZ to WT-Kpβlac-1 showed a 0.5°C rightward temperature shift. However, for S70A-Kpβlac-1 no shift was evident in the presence of penicillin. In the presence of CPZ a significant 5.5°C rightward temperature shift was prominent.

		Melting temperature (T_m) (°C)
WT-KpBLac-1	**Apo**	51.5
	Penicillin	52.0
	Cefoperazone	52.0
S70A-KpBLac-1	**Apo**	52.5
	Penicillin	52.5
	Cefoperazone	58.0

4.9 Thermodynamics of KpBLac1 interaction with penicillin and CPZ

The thermodynamic parameters associated with penicillin and CPZ binding to S70A-Kpβlac-1 were assessed using isothermal titration calorimetry (ITC). The titration was conducted under controlled temperature conditions at 25°C. Penicillin and CPZ were titrated into the sample cell containing S70A-Kpβlac-1 until the protein binding sites were thoroughly saturated with the substrates. Penicillin-S70A-Kpβlac-1 and CPZ-S70A-Kpβlac-1 interactions were monitored and depicted on a thermogram (Figure 4.10 A and B top graphs). The raw data from the thermogram was fitted to an independent model to obtain a fitted isotherm and thermodynamic parameters were attained (Figure 4.10 A and B top graphs). CPZ-S70A-Kpβlac-1 interaction produced a typical sigmoidal curve, and interaction was revealed to be exothermic ($\Delta H<0$), entropically favourable ($\Delta S>0$) and spontaneous ($\Delta G>0$) and had a stoichiometry (n) of ~0.8 molecules of CPZ per mole of S70A-Kpβlac-1, with dissociation of 7.5777 µM (Figure 4.10 A and Table 4.3). Penicillin-S70A-Kpβlac-1 interaction did not produce a typical smooth sigmoidal curve, possibly due to weak penicillin-binding to S70A-Kpβlac-1. The interaction was revealed to be endothermic ($\Delta H<0$), entropically driven ($\Delta S>0$) and spontaneous ($\Delta G>0$) and had a stoichiometry (n) of ~ four molecules of penicillin per mole of S70A-Kpβlac-1, with a dissociation of 44.92 µM (Figure 4.10 B and Table 4.3).

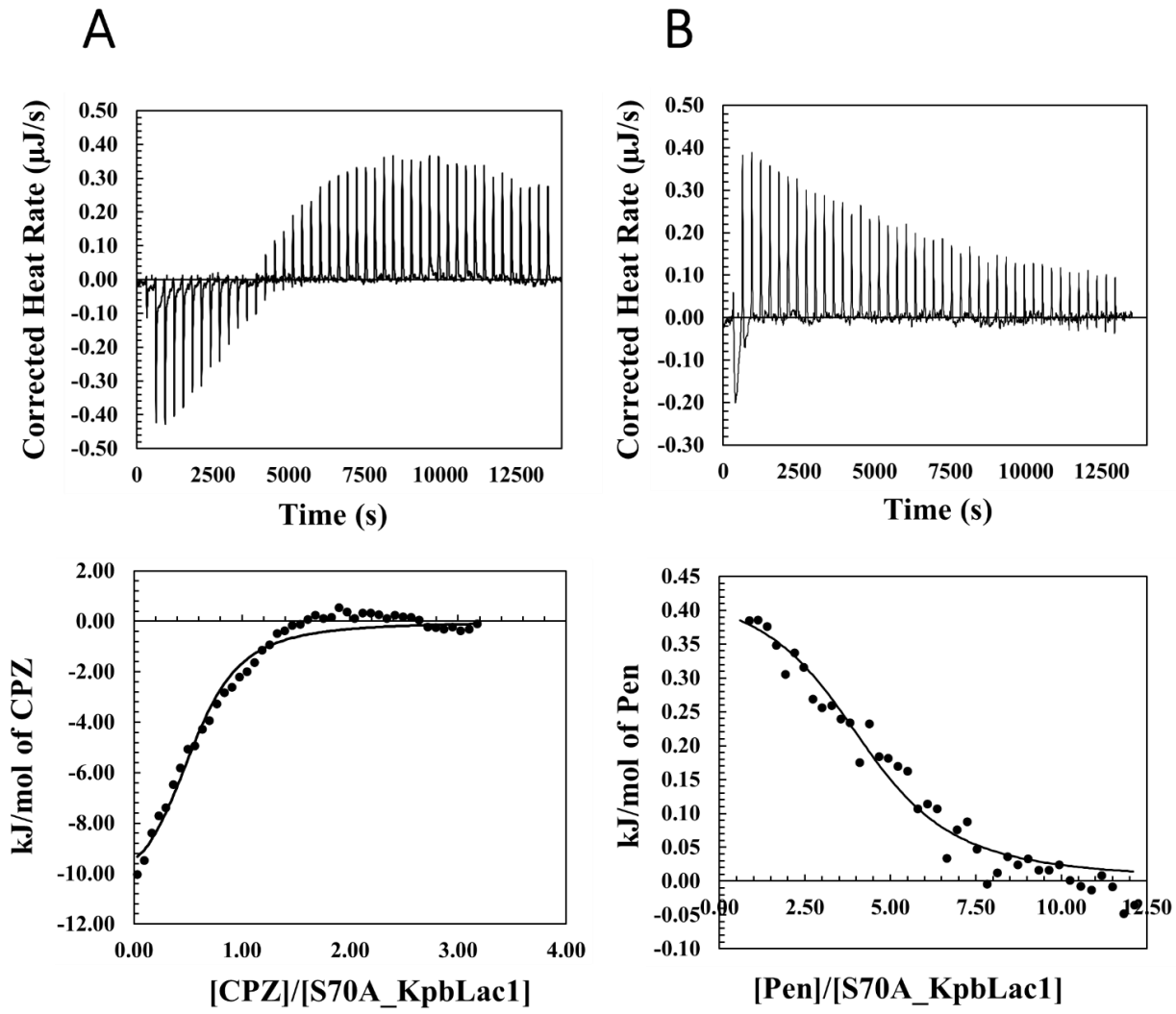

Figure 4. 10 Binding interaction between penicillin and CPZ to S70A-Kpβlac-1. The titration of penicillin and CPZ to S70A-Kpβlac-1 were conducted at 298.15 K. **A)** The interaction of 1 mM CPZ being titrated into 60 µM S70A-Kpβlac-1 was analysed with a thermogram (upper panel). The raw data was fitted to an independent model (single-site binding) to produce a fitted isotherm (bottom panel). The interaction was revealed to be entropically driven, exothermic, with stoichiometry of ~0.8, and K_D of 7.5µM. **B)** The interaction of 5 mM penicillin being titrated into 100 µM S70A-Kpβlac-1 was analysed with a thermogram (upper panel). The raw data was fitted to an independent model (single-site binding) to produce a fitted isotherm (bottom panel). The interaction was revealed to be entropically driven, endothermic, with stoichiometry of ~4, and K_D of 44 µM.

Table 4. 3 Thermodynamic parameters of the interaction between penicillin and CPZ with S70A-Kpβlac-1. The parameters were attained through a fitted independent model**.**

Parameter	S70A-KpβLac1-Cefoperazone	S70A-KpβLac1-Penicillin
K_D (μM)	7.58	44.92
n	0.76	4.45
K_a (M-1)	132000.00	20240.00
Δ*H*° (kJ/mol)	–8.32	0.44
Δ*S*° (kJ/mol)	20.41	24.61
Δ*G*° (kJ/mol)	–28.74	–24.17
Δ*S*° (J/mol.K)	69.64	83.93

Chapter 5
Discussion

Due to the surge of antibiotic resistance in bacteria, specifically, bacteria that cause nosocomial infections, such as *K. pneumoniae,* novel and effective drug treatment is paramount. *K. pneumoniae* has been reported to develop resistance to an array of antibiotics, more so the beta-lactam antibiotics (Youjun Yang et al., 1999). Since beta-lactam antibiotics are the most prescribed or first-line treatment for infections, this has become a threat globally (Youjun Yang *et al.*, 1999). Therefore, rational drug design with novel drug approaches against *Klebsiella pneumoniae* is explored. Drugs targeted against the bacterial metabolism or proteins vital for its activity, such as the Beta-Lactamase enzyme, which is responsible for the degradation of Beta-lactam antibiotics (Bush, 1989). Limited information is available on how β-lactamases can hydrolyse different kinds (i.e., different shapes and sizes) of β-lactams. In addition, no research has been conducted on the utilisation of Thermal shift assay and Isothermal titration calorimetry (ITC) on the binding of *Klebsiella pneumoniae* β-lactamase-1 to β-lactam; cefoperazone. Therefore, this research aims to provide structural and biophysical information on *Klebsiella pneumoniae* β-lactamase-1 binding stability and dynamics amongst two β-lactams (penicillin and cefoperazone). With this, vital information is obtained on the mechanism of β-lactamase resistance, which will help design new and improved β-lactamase inhibitors in *K. pneumoniae* which would ultimately reduce resistance of ESKAPE pathogens in nosocomial infections.

This study was conducted with a *K. pneumoniae* β-lactamase sequence extracted from a crystallised structure (UniProt code: W1DN50. GenBank ID: CDL10227.1) (Hinchliffe *et al*., 2022). The 28-amino acid signal sequence was removed, and this construct is denoted as Wild-type (WT)-Kpβlac-1. A mutant version S70A-Kpβlac-1 was constructed using WT-Kpβlac-1 as a template. The active site residues catalytically essential and conserved amongst β-lactamases were determined to be Serine-70, Lysine-73 Serine-130, Asparagine-132 and Threonine-237 (Hinchliffe *et al*., 2022). More importantly, Ser-70 and Lys-73 are involved in developing a lysinoalanine cross-linkage which is the basis of the hydrolytic capability of the enzyme (Hinchliffe *et al*., 2022), by induction of a mutation on Ser-70 to an alanine. This was done to inactivate the hydrolytic

potential of the enzyme. The alanine residues would not only inactive the mutant β-lactamase but would also introduce less steric hindrance in the protein sequence; therefore, the structural fold of the enzyme would not be disrupted (Sotomayor-Vivas *et al*., 2022). The two beta-lactam antibiotics in this research were penicillin and cefoperazone. Penicillin is a well-known, well-characterised beta-lactam and widely prescribed antibiotic (Wang *et al.*, 2017). Not much research is available on cefoperazone activity with Beta-lactamases. Due to size differences between the two antibiotics and the ability of the Beta-lactamase to recognise and hydrolyse both the beta-lactams is an essential aim of this research. Thus, a comparative study of the two antibiotics against the active and mutant Beta-lactamase was assessed.

The WT-KpBlac-1 and S70A-KpBlac-1 gene sequences were cloned in pET28a vectors with a hexahistidine tag and kanamycin resistance and were transformed in T7 *Escherichia coli* cells. *E. coli* cells are well-characterised, thus, easy to manipulate, and possess a fast generation time. Therefore, high amounts of transformative *E. coli* cells with the incorporated plasmid can be assured. The enzyme has been readily expressed in *E. coli* cells, more so in *E. coli* BL21 (DE3) (He *et al*., 2020)**.** Thus, introduce the novelty of the research with the utilisation of T7 transformed cells. The pET28a vector contains a T7 bacteriophage promoter and a T7 RNA polymerase which aid in optimal expression efficiencies. The vector confers resistance against kanamycin. The use of a pET28a was deliberate. If a pET11a vector had been used with ampicillin resistance, protein contamination would have been apparent upon expression and purification, as KpBLac-1 would hydrolyse the antibiotic. Therefore, antibiotic selection would be ineffective, as naturally occurring proteins of *E. coli* would also be expressed.

Expression of the enzyme with *E. coli* BL21 cells yielded protein amounts of 15-20 mg/mL (Crowder *et al*., 1998) (Toney *et al*., 1997) and even 50mg/mL (Butryn et al., 2021)**.** These yields were significantly higher than what was obtained in this research, which was revealed as; WT-Kpbalc-1 (3.4 mg/mL) and S70A-kpblac-1 (10.8 mg/mL) (Figure 4.3), regardless of the lower protein yields compared to previously published studies. The obtained protein was of high purity and large volumes to enable for analysis of downstream techniques. The signal sequence that was removed from *Klebsiella pneumoniae* β-lactamase to form the Wild-type (WT)-Kpβlac-1 is responsible for the membrane translocation of the enzyme (Kadonaga *et al.*, 1984). Removal of

the signal peptide ensured that the enzyme was immobile, thus ensuring that upon expression, all the enzyme is in the cytoplasm and upon cell lysis, all expressed enzyme is collected. The significance of this result is that Beta-lactamase can be expressed in other expression systems and vectors, and the signal peptide can be removed with good obtainable yields.

The expressed WT-Kpβlac-1 and S70A-Kpβlac-1was purified from the supernatant. This is to ensure that the his-tag is readily accessible and that protein is not clumped up in an aggregated state (Wong *et al.*, 1991). The his-tag was necessary to ensure that purification could be conducted using IMAC. This technique is effective and can purify pure proteins, whereas other purification techniques introduce contamination, and several purification steps are needed. The his-tag also aids in the solubility of the proteins and, due to their small size, does not hinder the structure or function of proteins (Kaur and Reinhardt, 2012). Obtained results from the SDS-PAGE (Figure 4.1) and UV-spectroscopy (Figure 4.2) of WT-Kpβlac-1 and S70A-Kpβlac-1suggested pure proteins, devoid of nucleic acid or protein contamination and no protein aggregation were obtained (Lindfors and Ylianttila, 2016). The his-tag aided in the selectivity of the purification technique, as the flow-through was devoid of recombinant proteins, which remained attached to the column by interacting with the nickel ions (Figure 4.1).

Nickel has a higher affinity for histidine tags than other divalent metal ions (Charlton and Zachariou, 2008). Thus, a nickel resin was used to ensure selective binding of WT-Kpβlac-1 and S70A-Kpβlac-1, minimal contaminants, and high protein yields. Cobalt-based resins are predominantly utilised if high-purity proteins are needed for sensitive techniques such as X-ray crystallography (Wong *et al.,* 1991). A cobalt resin only binds tagged proteins to its reactive core with specific spatial histidine positioning; therefore, it will result in low protein yields but higher purity (Wong *et al.*, 1991). Nickels' reactive core does not depend on the spatial histidine positioning and, thus, can bind to histidines in other areas of the protein but has a higher affinity for a poly-histidine arrangement (Wong *et al.*, 1991). This resin, therefore, results in possible lower purity but higher yields. However, to compensate for the non-specific binding of histidines to nickel columns. A small amount (~25 mM) of imidazole is included in the equilibration wash and wash buffers to ensure that only his-tagged proteins are bound to the column. Elution of the total proteins was obtained by adding high-concentration imidazole, which competitively displaced the

his-tagged WT-Kpβlac-1 and S70A-Kpβlac-1 from the nickel ions. Previous purification of the *Klebsiella pneumoniae* β-lactamase proved successful with the IMAC technique (Butryn *et al.*, 2021). From the size determination of WT-Kpβlac-1 and S70A-Kpβlac-1 from the calculated molecular weights from the SDS-PAGE, it was determined that purified WT-Kpβlac-1 and S70A-Kpβlac-1were 28 kDa and 27.7 kDa respectively (Figure 4.1 C), which corroborated with theoretical molecular weights of WT-Kpβlac-1 and S70A-Kpβlac-1 (29 kDa; ProtParam). The protein concentration of WT-Kpβlac-1 and S70A-Kpβlac-1 was 3.4 mg/mL and 10.8 mg/mL, respectively (Figure 4.3). The expression yield was revealed to be 3.4 mg of WT-Kpβlac-1 per g of wet *E. coli* cells; and 4.3 mg of S70A-Kpβlac-1 per g of wet *E. coli* cells. Due to a single step purification which minimised protein loss, the yield of the purification is reliable (Kaur and Reinhardt, 2012). However, compared to published data with relatively higher obtainable yields, could in future use *E. coli* BL21 as an expression host as seen in these published data (Butryn *et al.*, 2021).

The enzyme activity was assessed with a discontinuous assay technique. The reaction upon nitrocefin injection was automatically measured at different time intervals (every 5 seconds) for 60 seconds. This is due to the hydrolysis reaction occurring at a relatively fast rate, and measurements at different time points will allow for predetermining a reliable specific activity (Chow *et al*., 2013). Isothermal titration calorimetry was attempted to assess the activity of the WT-Kpβlac-1 and S70A-Kpβlac-1 using the Beta-lactam substrates (penicillin and CPZ) as opposed to a chromogenic substrate. However, with this technique, considerable optimisation must be conducted to achieve reliable results. Limitations of the spectroscopic technique with the FLUOstar Omega Multimode Microplate Reader (BMG LABTECH) is that the instrument could not read absorbances above 7 A.U. Therefore, the protein-ligand concentrations had to be reduced, and as a result, the activity of the enzyme was potentially underestimated. However, this technique revealed a high level of reactivity of WT-Kpβlac-1, and due to the mutation, S70A-Kpβlac-1 was proven inactive (Figure 4.4 and Supplementary Figure S1). In addition, it proves that the substitution mutation of S70A-Kpβlac-1 was successful, as significantly no enzyme activity (0.0028 mg/μmol/min) was observe (Figure 4.4), as well as no colour change in the presence of nitrocefin (Supplementary Figure S1). Specific activity obtained from the WT-Kpβlac-1 was relatively higher than previously published data for Beta-lactamases (Sharma *et al.*, 2004).

Far-UV CD was assessed to determine the secondary structure WT-Kpβlac-1 and S70A-Kpβlac-1 (Figure 4.5). The data were deconvoluted in DichroWeb to determine the percentage of secondary structure content of the proteins in the presence of penicillin and cefoperazone (CPZ) (Table 4.1). Another online prediction tool is AlphaFold Fill, which uses the AlphaFill algorithm which predicts conformations of the native enzymes with available ligands. However, this tool is only useful to predict protein conformations interacting with small molecules, metal ions and cofactors (Jumper *et al.*, 2021). It is necessary to validate the secondary structure to understand how it folds and functions and how it can be modified or targeted for drug design (Micsonai *et al.*, 2015). Penicillin and CPZ were included in the analysis to provide insight into the degree of secondary conformational changes these substrates confer on WT-Kpβlac-1 and S70A-Kpβlac-1. With these results, potential substrate-based inhibitors can be designed to inhibit Beta-lactamase competitively. It was determined that both the native WT-Kpβlac-1 and S70A-Kpβlac-1 were 63.4% and 60.9% alpha-helical, respectively (Figure 4.5. Table 4.1). This was expected from the deposited crystal structure (Hinchliffe *et al.*, 2022). The NRSMD values were in close agreement with a good fit. Therefore, attained structures are reliable (Table 4.1). In the presence of penicillin and CPZ, WT-Kpβlac-1 showed a ~60% reduction of alpha helices and adopted predominantly unordered conformations (Figure 4.5. Table 4.1). This structural change could be due to conformational changes occurring within the active site of WT-Kpβlac-1 as active hydrolysis of penicillin and CPZ are occurring.

For S70A-Kpβlac-1 assessment with penicillin, ~30% reduction in alpha helical content was noticed. However, the protein retained predominantly a helical conformation (44.9%) with a 33.9% unorder conformation (Figure 4.5. Table 4.1). This could have resulted due to the retention of penicillin in the active site of S70A-Kpβlac-1 conferring slight backbone conformations as covalent and ionic interactions occur to adjust the active site to accommodate penicillin. When CPZ was introduced to S70A-Kpβlac-1, the protein adopted a 100% β-stranded conformation (Figure 4.5. Table 4.1). This complete destabilisation of an alpha helical S70A-Kpβlac-1 to a β-stranded conformation, is similarly due to CPZ being retained to the active site. The correct conformation of the substrate must be achieved to perfectly sit in the active site, thus introducing backbone alterations within the protein. Changes within WT-Kpβlac-1 and S70A-Kpβlac-1 upon

penicillin and CPZ binding were expected. However, it was interesting to note the major shifts from alpha-helical to unorder to complete β-stranded protein. With these results, insight into structural backbone changes of WT-Kpβlac-1 and S70A-Kpβlac-1 when bound or actively hydrolyzing penicillin and CPZ are achieved. From this, structure-based inhibitors can be designed and targeted against Beta-lactamases. These drugs should confer a relative shape from which Beta-lactamases would recognise and interact with (Kaderabkova *et al.*, 2022). The inhibitor should then alter the structure of the enzyme away from its native structure, making it difficult for the Beta-lactamase to recognise and hydrolyse natural beta-lactam substrates. Therefore, from the findings, inhibitors conferring a similar structural shape, size, and stereochemistry as CPZ can be a possible therapeutic drug candidate against β-lactamases.

A major change in the secondary structure of proteins has been implicated in disease development, such as Amyloidosis and Prion disease (spongiform encephalopathies) (Moore *et al.*, 2009). These diseases develop due to misfolding of the protein into a β-sheeted conformation, which leads to tissue damage (Wille and Requena, 2018). However, β-lactamase is a bacterial protein and thus would not lead to chronic conditions in humans. The structural change would be harmful to the bacterium, and this would be useful as the research aims to find a suitable approach to inhibit the protein. Therefore, severe alterations to the bacterial β-lactamase secondary structure would obstruct it from performing its catalytic activity. The limitation of far-UV CD is that it is only a qualitative technique, and the proportion of secondary structural content must be obtained through either online tools or crystallography. Some components in buffers can absorb in the Far-UV region, causing signal interference (Micsonai *et al*., 2015). Another empirical technique used to assess the secondary structure is a method referred to as; Fourier Transform Infrared (FTIR) spectroscopy.

FTIR assess the differences in the dynamics of the hydrogen bonding between amide groups and their ability to absorb infrared light (Vonhoff *et al.,* 2010). Absorbance bands relating to amide bonds A, B, and I−VII are characteristic of the different structural regions within the protein (Sarver and Krueger, 1991) (Supplementary Figure S4). Amide I and II are of more importance as the hydrogen bonding of the backbone influences them. Thus, secondary structure conformations are assessed from these bonds (Surewicz *et al.*, 1993). The amide I band gives insight into the C=O

vibrational bond stretching. The Amide II band offers insights into the N=H vibrational bond bending (Yang *et al*., 2015) (Supplementary Figure S4). This technique has been used to characterise unfolding-folding processes and protein aggregation pathways in diseases such as Alzheimer's, Huntington's, and Parkinson's (Kong and Yu, 2007). However, this technique is not of high resolution as with X-ray crystallography or NMR; it does, however, allow for fast data outputs (Yang *et al*., 2015).

The primary sequence of amino acids interacts through the formation of hydrogen bonding. This hydrogen bonding drives the secondary structural features of the protein by forming alpha helices or β-sheets (Alberts *et al.,* 2002). Due to these secondary structures being in close proximity to one another, the R-groups of the amino acids between them will interact, forming dipole-dipole interactions, covalent bonding interactions, ionic or van der Waals interactions, London dispersion forces and driven by the hydrophobic effect (Alberts *et al.,* 2002). These formations of higher-ordered interactions drive the tertiary structure and determine the protein's fold. The three-dimensional fold of the protein is important for its function and is evolutionarily conserved between species (Sotomayor-Vivas *et al*., 2022). The assessment of the tertiary structure of a protein can give insights into the active site localisation and its function, which can be modified, controlled, or targeted (Moore *et al*., 2009). Tryptophan fluorescence assesses the local environment of tryptophan residues within the protein. Due to tryptophan exhibiting a significantly higher fluorescence yield than other aromatic residues (tyrosine and phenylalanine), this residue was solely excited at 295 nm (Ghisaidoobe and Chung, 2014). The indole ring of the amino acid act as a probe/fluorophore (Sindrewicz *et al.,* 2019). Tryptophan residues are predominantly situated in the hydrophobic pockets of proteins, and during protein unfolding, the tryptophan residues are exposed to the aqueous environment and subsequently, their fluorescence is quenched (Möller and Denicola, 2002).

The tertiary structure of WT-Kpβlac-1 and S70A-Kpβlac-1 was assessed with tryptophan fluorescence in the native and denatured protein states, as well as penicillin and cefoperazone (CPZ) bound states. It is expected that upon denaturation of WT-Kpβlac-1 and S70A-Kpβlac-1, tryptophan residues are solvent exposed, and therefore the fluorescence intensity is greatly quenched with a redshifted spectrum. This was seen for the unfolded WT-Kpβlac-1 and unfolded

S70A-Kpβlac-1 (Figure 4.6). Assessment of WT-Kpβlac-1 in the presence of penicillin and CPZ showed no quantum yield differences as the spectra overlap the native WT-Kpβlac-1 spectra (Figure 4.6A). This is due to WT-Kpβlac-1 actively hydrolyzing penicillin and CPZ; therefore, the substrates do not remain intact in the binding sites, thus resulting in a native-like spectrum. From an online modelling tool, Pymol, the crystal structure (UniProt code: W1DN50) of *Klebsiella pneumoniae* β-Lactamase was assessed, and it was observed that the three tryptophan residues (Trp195, Trp214, and Trp235) seem to be solvent exposed (supplementary Figure S5). This can also explain why there is no difference between the native and substrate- WT-Kpβlac-1 states. Assessment of S70A-Kpβlac-1 bound to penicillin and CPZ revealed changes in the fluorescence quantum yield. The penicillin-S70A-Kpβlac-1 state showed a slight decrease in fluorescence intensity which is not significant (Figure 4.6B). This could be because penicillin did not induce much of a significant difference in the protein conformation, and tryptophan residues remained intact. In addition, penicillin could possibly be weakly bound to the active site of WT-Kpβlac-1, thus, alluding to a slight decrease in the quantum yield. The CPZ-S70A-Kpβlac-1 bound state produced a significantly decreased quantum yield (Figure 4.6B). This could reveal that upon CPZ binding to the active site of S70A-Kpβlac-1, a conformational change is induced in the protein that causes tryptophan residues to be buried within the protein. Also, considering the large size of CPZ in which many structural changes are induced upon binding, these results correlate well with results obtained from Far-UV CD.

Extrinsic fluorescence was assessed with an anionic dye, 8-anilino-1-naphthalenesulfonic acid (ANS). ANS fluorescence gives insight into the hydrophobicity of the protein as a fluorescence signal is obtained when ANS binds to hydrophobic clefts (such as the active site/s) within the protein (Hawe *et al.*, 2008). The tertiary structure of WT-Kpβlac-1 and S70A-Kpβlac-1 was assessed with extrinsic ANS fluorescence for the native, denatured and penicillin and cefoperazone (CPZ) bound states (Figure 4.7). It is expected that upon denaturation of WT-Kpβlac-1 and S70A-Kpβlac-1, hydrophobic clefts are solvent exposed, and therefore, ANS has more accessibility to binding these pockets; as a result, the fluorescence intensity is increased. This is seen for both the unfolded WT-Kpβlac-1 and S70A-Kpβlac-1 (Figure 4.7). Assessment of WT-Kpβlac-1 in the presence of penicillin and CPZ showed no differences in fluorescence intensities as the spectra overlap the native WT-Kpβlac-1 spectra (Figure 4.7A). This is due to the highly reactive active

site whereby penicillin and CPZ are rapidly hydrolysed; therefore, the spectra resemble the native state as ANS can bind to the same positions as in the native state.

From the solved crystal structure (in the presence of an inhibitor; emmetazobactam) (PDBe ID: 6z7j), a surface structure was generated on PyMol, which revealed that the active site is solvent exposed (Hinchliffe *et al*., 2022) (Supplementary Figure S6). This could explain the similar quantum yields observed for the WT-Kpβlac-1 spectrums. Also, remembering that the enzyme is a hydrolase (EC 3.5.2.6) which requires water molecules for the hydrolyses, which is why the active site is solvent-exposed (He *et al.,* 2020). Assessment of the penicillin-S70A-Kpβlac-1 bound state revealed no significant change compared to the native spectra (Figure 4.7B). However, CPZ-S70A-Kpβlac-1 bound state showed a considerable fluorescence decrease. This represents that there is only one active site on the protein. Upon CPZ binding, the ANS is displaced into the aqueous solution resulting in the quenching of the fluorescence signal. However, this was not seen with penicillin-S70A-Kpβlac-1, which conferred a native-like spectrum. It can be speculated that penicillin weakly binds to the active site, and some proportion of ANS was bound to the active site as well, as the dye was not completely displaced into the aqueous environment. From these findings, it can empirically verify that the active site of β-lactamase is solvent exposed, there is only a single hydrophobic pocket (active site) on the protein, and penicillin binds weakly to the active site. Lastly, inhibitors can be designed with a similar structure resembling CPZ, which will tightly bind the active site, preventing water molecules from accessing the site. Since the hydrolysis reaction is dependent on water molecules, the function of the enzyme will be halted.

The 3D structure of the protein may or may not give rise to a quaternary structure due to the protein association of side-chain interactions forming subunits that are either similar or dissimilar (Alberts *et al.,* 2002). These subunits are held together by disulfide and non-covalent bonds (intermolecular forces) (Alberts *et al.*, 2002). The basis of SE-HPLC is to determine the oligomeric state of the protein by size determination. This is vital to understand how the native protein exists for designing targets that would either inhibit one or more subunit(s) (dimer/trimer etc.) or the complete protein (monomer) (Pérez-Escalante *et al.,* 2018). This technique is highly sensitive, and any interference (contaminants or protein aggregates) will influence the signal. The enzyme was expected to be monomeric based on the available crystal structure. From the investigation, the sizes of WT-

Kpβlac-1 and S70A-Kpβlac-1 were reported as 28.3 kDa and 31 kDa (Figure 4.8). This correlates closely to the theoretical sizes, and therefore the proteins are monomeric. These findings can deduce that the substitution mutation did not hinder the oligomeric structure of the protein. SE-HPLC can be coupled with Dynamic light scattering (DLS) in the future to validate the sizes of WT-Kpβlac-1 and S70A-Kpβlac-1. This technique requires optimisation to achieve reliable data; thus, this technique was not performed due to time constraints.

The thermal stability was assessed using a thermal shift assay in the presence of penicillin and cefoperazone (CPZ). This technique asses the melting temperature (T_m) which is the temperature where 50% of the protein is unfolded (Huynh and Partch, 2015). Proteins with a higher melting temperature are more stable, such as DNA polymerase, which is highly thermostable (Jafari *et al.*, 2014). X-ray crystallisation is more successful with proteins with higher melting temperatures (Weik and Colletier, 2010). The research revealed that no melting temperature shifts were observed for WT-Kpβlac-1 in the presence of penicillin and CPZ (Figure 4.9A. Table 4.2). This was expected since WT-Kpβlac-1 readily hydrolyses penicillin and CPZ; thus, the substrates are not bound to the active site, conferring a native-like spectrum. It is anticipated that the binding of penicillin and CPZ in S70A-Kpβlac-1 should stabilise the protein due to binding interactions of the active site residues with the substrates; therefore, the melting temperature should increase. However, this was not seen in the penicillin-S70A-Kpβlac-1 complex, as the melting temperature was identical to the native protein state (Figure 4.9B. Table 4.2). This can reveal that penicillin weakly binds to S70A-Kpβlac-1, and the enzyme's structural conformations are not entirely changed by penicillin. The CPZ-S70A-Kpβlac-1 state revealed a 5.5°C temperature increase (Figure 4.9B. Table 4.2). This indicates that S70A-Kpβlac-1 is greatly stabilised with CPZ by formation of tighter bonding interactions with the active site. Also due to CPZ being structurally larger than penicillin, S70A-Kpβlac-1 must adjust its binding pocket that would bind and fit the most stable configuration of CPZ. From these findings it can be revealed that CPZ increases the stability of S70A-Kpβlac-1 and therefore, inhibitors with similar structural features to CPZ should be designed. The data also revealed that penicillin binds weakly to the active site of S70A-Kpβlac-1. And lastly, co-crystallisation in the future of S70A-Kpβlac-1 would be more successful with CPZ compared to penicillin.

The thermodynamic parameters associated with penicillin and cefoperazone (CPZ) binding to S70A-Kpβlac-1 were assessed using isothermal titration calorimetry (ITC). Binding interactions with WT-Kpβlac-1 would not be achievable since the enzyme hydrolyses penicillin and CPZ. The technique provides thermodynamic parameters such as Gibbs free energy, dissociation/association constants, entropy, and enthalpy (Freire *et al.*, 1990). From these parameters, the binding mechanisms can be better understood. The enthalpy provides valuable information on the favorability of binding interactions (H-bonding, hydrophobic interactions, and electrostatic interactions). The entropy encompasses the degree of freedom of the protein and the solvent environment (Freire *et al.,* 1990).

From theory and published data on the binding of beta-lactams on β-lactamases, it was expected that the reaction be enthalpically favoured due to bond formations between the substrate and enzyme (Huynh and Partch, 2015). The binding interaction of cefoperazone (CPZ) with S70A-Kpβlac-1 was revealed to be an exothermic reaction (enthalpically favoured) (Figure 4.10A Table 4.3). Heat energy was given off as favourable active site bonds between CPZ and S70A-Kpβlac-1 were achieved, allowing for the stable and rigid binding of CPZ to the active site. In addition, the binding reaction was entropically favourable due to water molecules within the active site being displaced into the solvent to accommodate CPZ binding (Figure 4.10A. Table 4.3). This reaction is spontaneous at all temperatures. The binding interaction of penicillin with S70A-Kpβlac-1, revealed to be an endothermic reaction (enthalpically opposed) and heat energy was absorbed as bonds were broken (Figure 4.10B Table 4.3). This could be due to unfavorable weak active site bonding, whereby penicillin actively fall off and on the active site. This unstable attachment of penicillin within the active site is attributed through the increased entropy which is higher than CPZs entropy. This can be explained through the continually detachment and reattachment of penicillin due to weak binding, increased the “randomness” as well as the displacement of water therefore, a greater entropy was obtained. This binding reaction is spontaneous at higher temperatures. The dissociation and association constants for the two binding reactions were assessed. It was evident that S70A-Kpβlac-1 has a higher affinity for CPZ as lower amounts (7.577 μM) of CPZ is needed to occupy 50% of the active site. S70A-Kpβlac-1 has a lower affinity for penicillin as more significant amounts (44.92 μM) of penicillin is required to occupy 50% of the active site (Table 4.3). For drug discovery, molecules should be designed that possess high affinity

(thus lower inhibitor concentration is required) and tightly binds, thus forming strong bonds ($\Delta H<0$), which will ensure the drug does not fall off the active site and is rigidly attached; and increases the disorder of the solvent environment ($\Delta S>0$) (Ward and Holdgate, 2001). Therefore, from these findings, CPZ would be an attractive template for designing inhibitors against β-lactamases.

Chapter 6
Summary and conclusion

Successful expression and purification of pure WT-Kpβlac-1 and S70A-Kpβlac-1 were obtainable as this is often a bottleneck in protein biochemistry. Manipulation of the sequence by removal of the signal peptide, attachment of a non-cleavable histidine tag, substitution mutation, and use of an alternative expression host produced good and comparable WT-Kpβlac-1 and S70A-Kpβlac-1 yields. An activity assay proved that the substitution of Serine-70 to an Alanine inactivated the proteins' hydrolytic potential to hydrolyse β-lactam substrates, whereas WT-Kpβlac-1 was highly catalytic. The secondary structure of WT-Kpβlac-1 and S70A-Kpβlac-1 was disrupted upon penicillin and cefoperazone (CPZ) exposure from a native alpha-helical conformation to an unordered structure, to a complete β-stranded structure when bound to CPZ. The tertiary structure of WT-Kpβlac-1 and S70A-Kpβlac-1 empirically proved that the active site is solvent exposed and only a single catalytic site exists. From this study, penicillin-binding to the active site was speculated to be weak, whereas CPZ seemed to bind tighter.

The oligomeric state was revealed to be monomeric, and the mutation did not influence the protein's overall structure. Stability studies revealed that CPZ binding to S70A-Kpβlac-1 is more thermostable than penicillin-protein binding. The assumption of weak penicillin-binding was proven with a titration technique, which revealed that penicillin-binding to S70A-Kpβlac-1 is endothermic, and the protein has a lower affinity for the substrate. Therefore, potential novel inhibitor design should be focused on CPZ. Through substrate-based drug discovery, potential drugs should confer a similar shape, size, or stereochemistry as CPZ. This would change the conformation of the protein away from its native structure, as a result, water would not be freely available to assist in the catalytic activity. The potential inhibitor would also bind tightly to the active site with less need for high concentrations. Therefore, these findings contribute to the understanding of conformational changes during β-lactam binding to β-lactamases, the binding mechanism, and insights on potential novel inhibitors against these highly antibiotic-resistant bacteria. Future work may include differential scanning calorimery, hydrogen deuterium exchange

mass spectrometry and crystallography to obtain more information on protein unfolding stability, the dynamics of the protein, and protein ligand interactions.

References

Aditi Priyadarshini, B., Mahalakshmi, K., Naveen Kumar, V., 2019. Mutant Prevention Concentration of Ciprofloxacin against Klebsiella pneumoniae Clinical Isolates: An Ideal Prognosticator in Treating Multidrug-Resistant Strains. Int. J. Microbiol. 2019, 6850108. https://doi.org/10.1155/2019/6850108

Agaba, P., Tumukunde, J., Tindimwebwa, J.V.B., Kwizera, A., 2017. Nosocomial bacterial infections and their antimicrobial susceptibility patterns among patients in Ugandan intensive care units: a cross sectional study. BMC Res. Notes 10, 349. https://doi.org/10.1186/s13104-017-2695-5

Alberts, B., Johnson, A., Lewis, J., Raff, M., Roberts, K., Walter, P., 2002. The Shape and Structure of Proteins. Mol. Biol. Cell 4th Ed.

Ambler, R.P., Coulson, A.F.W., Frère, J.M., Ghuysen, J.M., Joris, B., Forsman, M., Levesque, R.C., Tiraby, G., Waley, S.G., 1991. A standard numbering scheme for the class A β-lactamases. Biochem. J. 276, 269–270. https://doi.org/10.1042/bj2760269

Arnold, R.S., Thom, K.A., Sharma, S., Phillips, M., Johnson, J.K., Morgan, D.J., 2011. Emergence of Klebsiella pneumoniae Carbapenemase (KPC)-Producing Bacteria. South. Med. J. 104, 40–45. https://doi.org/10.1097/SMJ.0b013e3181fd7d5a

Benítez-Chao, D.F., León-Buitimea, A., Lerma-Escalera, J.A., Morones-Ramírez, J.R., 2021. Bacteriocins: An Overview of Antimicrobial, Toxicity, and Biosafety Assessment by in vivo Models. Front. Microbiol. 12.

Blahová, J., Králiková, K., Krćméry, V., Vaculíková, A., Jezek, P., 2002. First occurrence of transferable extended-spectrum beta-lactamase hydrolyzing cefoperazone in multiresistant nosocomial strains of Klebsiella pneumoniae from two hospitals in Czech and Slovak Republics. J. Chemother. Florence Italy 14, 461–464. https://doi.org/10.1179/joc.2002.14.5.461

Boehle, K.E., Gilliand, J., Wheeldon, C.R., Holder, A., Adkins, J.A., Geiss, B.J., Ryan, E.P., Henry, C.S., 2017. Utilizing Paper-Based Devices for Antimicrobial-Resistant Bacteria Detection. Angew. Chem. 129, 6990–6994. https://doi.org/10.1002/ange.201702776

Boyd, S.E., Livermore, D.M., Hooper, D.C., Hope, W.W., 2020. Metallo-β-Lactamases: Structure, Function, Epidemiology, Treatment Options, and the Development Pipeline. Antimicrob. Agents Chemother. 64, e00397-20. https://doi.org/10.1128/AAC.00397-20

Bush, K., 1989. Characterization of beta-lactamases. Antimicrob. Agents Chemother. 33, 259–263.

Bush, K., Jacoby, G.A., 2010. Updated Functional Classification of β-Lactamases. Antimicrob. Agents Chemother. 54, 969–976. https://doi.org/10.1128/AAC.01009-09

Butryn, A., Simon, P.S., Aller, P., Hinchliffe, P., Massad, R.N., Leen, G., Tooke, C.L., Bogacz, I., Kim, I.-S., Bhowmick, A., Brewster, A.S., Devenish, N.E., Brem, J., Kamps, J.J.A.G., Lang, P.A., Rabe, P., Axford, D., Beale, J.H., Davy, B., Ebrahim, A., Orlans, J., Storm, S.L.S., Zhou, T., Owada, S., Tanaka, R., Tono, K., Evans, G., Owen, R.L., Houle, F.A., Sauter, N.K., Schofield, C.J., Spencer, J., Yachandra, V.K., Yano, J., Kern, J.F., Orville, A.M., 2021. An on-demand, drop-on-drop method for studying enzyme catalysis by serial crystallography. Nat. Commun. 12, 4461. https://doi.org/10.1038/s41467-021-24757-7

Charlton, A., Zachariou, M., 2008. Immobilized metal ion affinity chromatography of native proteins. Methods Mol. Biol. Clifton NJ 421, 25–35. https://doi.org/10.1007/978-1-59745-582-4_2

Chiou, J., Wan, S., Chan, K.-F., So, P.-K., He, D., Wai-chi Chan, E., Chan, T., Wong, K., Tao, J., Chen, S., 2015. Ebselen as a potent covalent inhibitor of New Delhi metallo-β-lactamase (NDM-1). Chem. Commun. 51, 9543–9546. https://doi.org/10.1039/C5CC02594J

Chow, C., Xu, H., Blanchard, J.S., 2013. Kinetic Characterizations of Nitrocefin, Cefoxitin, and Meropenem Hydrolysis by β-lactamase from Mycobacterium tuberculosis. Biochemistry 52, 4097–4104. https://doi.org/10.1021/bi400177y

Corbett, R.J., Roche, R.S., 1984. Use of high-speed size-exclusion chromatography for the study of protein folding and stability. Biochemistry 23, 1888–1894. https://doi.org/10.1021/bi00303a047

Crowder, M.W., Walsh, T.R., Banovic, L., Pettit, M., Spencer, J., 1998. Overexpression, Purification, and Characterization of the Cloned Metallo-β-Lactamase L1 fromStenotrophomonas maltophilia. Antimicrob. Agents Chemother. 42, 921–926. https://doi.org/10.1128/AAC.42.4.921

Dirar, M.H., Bilal, N.E., Ibrahim, M.E., Hamid, M.E., 2020. Prevalence of extended-spectrum β-lactamase (ESBL) and molecular detection of bla TEM, bla SHV and bla CTX-M genotypes among Enterobacteriaceae isolates from patients in Khartoum, Sudan. Pan Afr. Med. J. 37. https://doi.org/10.11604/pamj.2020.37.213.24988

Douminge, L., Feaugas, X., Bernard, J., Mallarino, S., 2013. Extrinsic fluorescence as a sensitive method for studying photo-degradation of high density polyethylene correlated with mechanical stresses. Curr. Appl. Phys. 13, 1751–1757. https://doi.org/10.1016/j.cap.2013.06.027

Elizabeth, M., Mboto, C., Agbo, B., 2019. Nosocomial Infections in Sub-Saharan Africa. pp. 90–102. https://doi.org/10.9734/bpi/rabr/v3

Fischbach, M.A., 2011. Combination therapies for combating antimicrobial resistance. Curr. Opin. Microbiol., Antimicrobials/Genomics 14, 519–523. https://doi.org/10.1016/j.mib.2011.08.003

Franceschini, N., Segatore, B., Perilli, M., Vessillier, S., Franchino, L., Amicosante, G., 2002. Meropenem stability to β-lactamase hydrolysis and comparative in vitro activity against several β-lactamase-producing Gram-negative strains. J. Antimicrob. Chemother. 49, 395–398. https://doi.org/10.1093/jac/49.2.395

Freire, E., Mayorga, O.L., Straume, M., 1990. Isothermal titration calorimetry. Anal. Chem. 62, 950A-959A. https://doi.org/10.1021/ac00217a002

Ghisaidoobe, A.B.T., Chung, S.J., 2014. Intrinsic Tryptophan Fluorescence in the Detection and Analysis of Proteins: A Focus on Förster Resonance Energy Transfer Techniques. Int. J. Mol. Sci. 15, 22518–22538. https://doi.org/10.3390/ijms151222518

Goh, H.C., Sobota, R.M., Ghadessy, F.J., Nirantar, S., 2017. Going native: Complete removal of protein purification affinity tags by simple modification of existing tags and proteases. Protein Expr. Purif. 129, 18–24. https://doi.org/10.1016/j.pep.2016.09.001

Grolier, J.-P.E., del Río, J.M., 2012. Isothermal titration calorimetry: A thermodynamic interpretation of measurements. J. Chem. Thermodyn. 55, 193–202. https://doi.org/10.1016/j.jct.2012.05.018

Gupta, S.K., Shukla, P., 2016. Advanced technologies for improved expression of recombinant proteins in bacteria: perspectives and applications. Crit. Rev. Biotechnol. 36, 1089–1098. https://doi.org/10.3109/07388551.2015.1084264

Hawe, A., Sutter, M., Jiskoot, W., 2008. Extrinsic fluorescent dyes as tools for protein characterization. Pharm. Res. 25, 1487–1499. https://doi.org/10.1007/s11095-007-9516-9

He, Y., Lei, J., Pan, X., Huang, X., Zhao, Y., 2020. The hydrolytic water molecule of Class A β-lactamase relies on the acyl-enzyme intermediate ES* for proper coordination and catalysis. Sci. Rep. 10, 10205. https://doi.org/10.1038/s41598-020-66431-w

Hinchliffe, P., Tooke, C.L., Bethel, C.R., Wang, B., Arthur, C., Heesom, K.J., Shapiro, S., Schlatzer, D.M., Papp-Wallace, K.M., Bonomo, R.A., Spencer, J., 2022. Penicillanic Acid Sulfones Inactivate the Extended-Spectrum β-Lactamase CTX-M-15 through Formation of a Serine-Lysine Cross-Link: an Alternative Mechanism of β-Lactamase Inhibition. mBio 13, e01793-21. https://doi.org/10.1128/mbio.01793-21

Huynh, K., Partch, C.L., 2015. Analysis of Protein Stability and Ligand Interactions by Thermal Shift Assay. Curr. Protoc. Protein Sci. 79, 28.9.1-28.9.14. https://doi.org/10.1002/0471140864.ps2809s79

Jablonski, A., 1933. Efficiency of Anti-Stokes Fluorescence in Dyes. Nature 131, 839–840. https://doi.org/10.1038/131839b0

Jafari, R., Almqvist, H., Axelsson, H., Ignatushchenko, M., Lundbäck, T., Nordlund, P., Molina, D.M., 2014. The cellular thermal shift assay for evaluating drug target interactions in cells. Nat. Protoc. 9, 2100–2122. https://doi.org/10.1038/nprot.2014.138

Jumper, J., Evans, R., Pritzel, A., Green, T., Figurnov, M., Ronneberger, O., Tunyasuvunakool, K., Bates, R., Žídek, A., Potapenko, A., Bridgland, A., Meyer, C., Kohl, S.A.A., Ballard, A.J., Cowie, A., Romera-Paredes, B., Nikolov, S., Jain, R., Adler, J., Back, T., Petersen, S., Reiman, D., Clancy, E., Zielinski, M., Steinegger, M., Pacholska, M., Berghammer, T., Bodenstein, S., Silver, D., Vinyals, O., Senior, A.W., Kavukcuoglu, K., Kohli, P., Hassabis, D., 2021. Highly accurate protein structure prediction with AlphaFold. Nature 596, 583–589. https://doi.org/10.1038/s41586-021-03819-2

Kaderabkova, N., Bharathwaj, M., Furniss, R.C.D., Gonzalez, D., Palmer, T., Mavridou, D.A.I., 2022. The biogenesis of β-lactamase enzymes. Microbiology 168, 001217. https://doi.org/10.1099/mic.0.001217

Kadonaga, J.T., Gautier, A.E., Straus, D.R., Charles, A.D., Edge, M.D., Knowles, J.R., 1984. The role of the beta-lactamase signal sequence in the secretion of proteins by Escherichia coli. J. Biol. Chem. 259, 2149–2154.

Kaur, J., Reinhardt, D.P., 2012. Immobilized Metal Affinity Chromatography Co-Purifies TGF-β1 with Histidine-Tagged Recombinant Extracellular Proteins. PLOS ONE 7, e48629. https://doi.org/10.1371/journal.pone.0048629

Khan, H.A., Baig, F.K., Mehboob, R., 2017. Nosocomial infections: Epidemiology, prevention, control and surveillance. Asian Pac. J. Trop. Biomed. 7, 478–482. https://doi.org/10.1016/j.apjtb.2017.01.019

King, D., Strynadka, N., 2011. Crystal structure of New Delhi metallo-β-lactamase reveals molecular basis for antibiotic resistance. Protein Sci. 20, 1484–1491. https://doi.org/10.1002/pro.697

Kong, J., Yu, S., 2007. Fourier transform infrared spectroscopic analysis of protein secondary structures. Acta Biochim. Biophys. Sin. 39, 549–559. https://doi.org/10.1111/j.1745-7270.2007.00320.x

Kram, K.E., Finkel, S.E., 2015. Rich Medium Composition Affects Escherichia coli Survival, Glycation, and Mutation Frequency during Long-Term Batch Culture. Appl. Environ. Microbiol. 81, 4442–4450. https://doi.org/10.1128/AEM.00722-15

Kumarasamy, K.K., Toleman, M.A., Walsh, T.R., Bagaria, J., Butt, F., Balakrishnan, R., Chaudhary, U., Doumith, M., Giske, C.G., Irfan, S., Krishnan, P., Kumar, A.V., Maharjan, S., Mushtaq, S., Noorie, T., Paterson, D.L., Pearson, A., Perry, C., Pike, R., Rao, B., Ray, U., Sarma, J.B., Sharma, M., Sheridan, E., Thirunarayan, M.A., Turton, J., Upadhyay, S., Warner, M., Welfare, W., Livermore, D.M., Woodford, N., 2010. Emergence of a new antibiotic resistance mechanism in India, Pakistan, and the UK: a molecular, biological, and epidemiological study. Lancet Infect. Dis. 10, 597–602. https://doi.org/10.1016/S1473-3099(10)70143-2

Laemmli, U.K., 1970. Cleavage of Structural Proteins during the Assembly of the Head of Bacteriophage T4. Nature 227, 680–685. https://doi.org/10.1038/227680a0

Lence, E., González-Bello, C., 2021. Bicyclic Boronate β-Lactamase Inhibitors: The Present Hope against Deadly Bacterial Pathogens. Adv. Ther. 4, 2000246. https://doi.org/10.1002/adtp.202000246

Li, Z., Cao, Y., Yi, L., Liu, J.-H., Yang, Q., 2019. Emergent Polymyxin Resistance: End of an Era? Open Forum Infect. Dis. 6, ofz368. https://doi.org/10.1093/ofid/ofz368

Lindfors, A.V., Ylianttila, L., 2016. Visualizing Rayleigh Scattering through UV Photography. Bull. Am. Meteorol. Soc. 97, 1561–1564. https://doi.org/10.1175/BAMS-D-14-00260.1

Marinescu, G.C., Popescu, R.-G., Dinischiotu, A., 2018. Size Exclusion Chromatography Method for Purification of Nicotinamide Mononucleotide (NMN) from Bacterial Cells. Sci. Rep. 8, 4433. https://doi.org/10.1038/s41598-018-22806-8

Mehta, S.C., Rice, K., Palzkill, T., 2015. Natural Variants of the KPC-2 Carbapenemase have Evolved Increased Catalytic Efficiency for Ceftazidime Hydrolysis at the Cost of Enzyme Stability. PLOS Pathog. 11, e1004949. https://doi.org/10.1371/journal.ppat.1004949

Micsonai, A., Wien, F., Kernya, L., Lee, Y.-H., Goto, Y., Réfrégiers, M., Kardos, J., 2015. Accurate secondary structure prediction and fold recognition for circular dichroism spectroscopy. Proc. Natl. Acad. Sci. U. S. A. 112, E3095-3103. https://doi.org/10.1073/pnas.1500851112

Möller, M., Denicola, A., 2002. Protein tryptophan accessibility studied by fluorescence quenching. Biochem. Mol. Biol. Educ. 30, 175–178. https://doi.org/10.1002/bmb.2002.494030030035

Moore, R.A., Taubner, L.M., Priola, S.A., 2009. Prion Protein Misfolding and Disease. Curr. Opin. Struct. Biol. 19, 14–22. https://doi.org/10.1016/j.sbi.2008.12.007

Mulani, M.S., Kamble, E.E., Kumkar, S.N., Tawre, M.S., Pardesi, K.R., 2019. Emerging Strategies to Combat ESKAPE Pathogens in the Era of Antimicrobial Resistance: A Review. Front. Microbiol. 10.

Munishkina, L.A., Fink, A.L., 2007. Fluorescence as a method to reveal structures and membrane-interactions of amyloidogenic proteins. Biochim. Biophys. Acta 1768, 1862–1885. https://doi.org/10.1016/j.bbamem.2007.03.015

Nordmann, P., Cuzon, G., Naas, T., 2009. The real threat of Klebsiella pneumoniae carbapenemase-producing bacteria. Lancet Infect. Dis. 9, 228–236. https://doi.org/10.1016/S1473-3099(09)70054-4

Nowakowski, A.B., Wobig, W.J., Petering, D.H., 2014. Native SDS-PAGE: High Resolution Electrophoretic Separation of Proteins With Retention of Native Properties Including Bound Metal Ions. Met. Integr. Biometal Sci. 6, 1068–1078. https://doi.org/10.1039/c4mt00033a

Oelschlaeger, P., 2021. β-Lactamases: Sequence, Structure, Function, and Inhibition. Biomolecules 11, 986. https://doi.org/10.3390/biom11070986

Pérez-Escalante, E., González-Olivares, L.G., Cruz-Guerrero, A.E., Galán-Vidal, C.A., Páez-Hernández, M.E., Álvarez-Romero, G.A., 2018. Size exclusion chromatography (SEC-HPLC) as an alternative to study thrombin inhibition. J. Chromatogr. B Analyt. Technol. Biomed. Life. Sci. 1074–1075, 34–38. https://doi.org/10.1016/j.jchromb.2017.12.037

Pierce, M.M., Raman, C.S., Nall, B.T., 1999. Isothermal Titration Calorimetry of Protein–Protein Interactions. Methods 19, 213–221. https://doi.org/10.1006/meth.1999.0852

Porath, J., Carlsson, J., Olsson, I., Belfrage, G., 1975. Metal chelate affinity chromatography, a new approach to protein fractionation. Nature 258, 598–599. https://doi.org/10.1038/258598a0

Prestinaci, F., Pezzotti, P., Pantosti, A., 2015. Antimicrobial resistance: a global multifaceted phenomenon. Pathog. Glob. Health 109, 309–318. https://doi.org/10.1179/2047773215Y.0000000030

Principi, N., Silvestri, E., Esposito, S., 2019. Advantages and Limitations of Bacteriophages for the Treatment of Bacterial Infections. Front. Pharmacol. 10.

Sacha, P., Wieczorek, P., Hauschild, T., Zórawski, M., Olszańska, D., Tryniszewska, E., 2008. Metallo-beta-lactamases of Pseudomonas aeruginosa--a novel mechanism resistance to beta-lactam antibiotics. Folia Histochem. Cytobiol. 46, 137–142. https://doi.org/10.2478/v10042-008-0020-9

Santajit, S., Indrawattana, N., 2016. Mechanisms of Antimicrobial Resistance in ESKAPE Pathogens. BioMed Res. Int. 2016, 2475067. https://doi.org/10.1155/2016/2475067

Sarver, R.W., Krueger, W.C., 1991. Protein secondary structure from fourier transform infrared spectroscopy: A data base analysis. Anal. Biochem. 194, 89–100. https://doi.org/10.1016/0003-2697(91)90155-M

Shapiro, A.B., 2017. Kinetics of Sulbactam Hydrolysis by β-Lactamases, and Kinetics of β-Lactamase Inhibition by Sulbactam. Antimicrob. Agents Chemother. 61, e01612-17. https://doi.org/10.1128/AAC.01612-17

Sharma, S., Ramnani, P., Virdi, J.S., 2004. Detection and assay of β-lactamases in clinical and non-clinical strains of Yersinia enterocolitica biovar 1A. J. Antimicrob. Chemother. 54, 401–405. https://doi.org/10.1093/jac/dkh365

Sindrewicz, P., Li, X., Yates, E.A., Turnbull, J.E., Lian, L.-Y., Yu, L.-G., 2019. Intrinsic tryptophan fluorescence spectroscopy reliably determines galectin-ligand interactions. Sci. Rep. 9, 11851. https://doi.org/10.1038/s41598-019-47658-8

Sotomayor-Vivas, C., Hernández-Lemus, E., Dorantes-Gilardi, R., 2022. Linking protein structural and functional change to mutation using amino acid networks. PLOS ONE 17, e0261829. https://doi.org/10.1371/journal.pone.0261829

Sunkwa-Mills, G., Rawal, L., Enweronu-Laryea, C., Aberese-Ako, M., Senah, K., Tersbøl, B.P., 2020. Perspectives and practices of healthcare providers and caregivers on healthcare-associated infections in the neonatal intensive care units of two hospitals in Ghana. Health Policy Plan. 35, i38–i50. https://doi.org/10.1093/heapol/czaa102

Surewicz, W.K., Mantsch, H.H., Chapman, D., 1993. Determination of protein secondary structure by Fourier transform infrared spectroscopy: A critical assessment. Biochemistry 32, 389–394. https://doi.org/10.1021/bi00053a001

Tenover, F.C., 2006. Mechanisms of Antimicrobial Resistance in Bacteria. Am. J. Med. 119, S3–S10. https://doi.org/10.1016/j.amjmed.2006.03.011

Tolera, M., Abate, D., Dheresa, M., Marami, D., 2018. Bacterial Nosocomial Infections and Antimicrobial Susceptibility Pattern among Patients Admitted at Hiwot Fana Specialized University Hospital, Eastern Ethiopia. Adv. Med. 2018, e2127814. https://doi.org/10.1155/2018/2127814

Toney, J.H., Wu, J.K., Overbye, K.M., Thompson, C.M., Pompliano, D.L., 1997. High-yield expression, purification, and characterization of active, soluble Bacteroides fragilis metallo-beta-lactamase, CcrA. Protein Expr. Purif. 9, 355–362. https://doi.org/10.1006/prep.1996.0718

Tooke, C.L., Hinchliffe, P., Bragginton, E.C., Colenso, C.K., Hirvonen, V.H.A., Takebayashi, Y., Spencer, J., 2019a. β-Lactamases and β-Lactamase Inhibitors in the 21st Century. J. Mol. Biol. 431, 3472–3500. https://doi.org/10.1016/j.jmb.2019.04.002

Tooke, C.L., Hinchliffe, P., Lang, P.A., Mulholland, A.J., Brem, J., Schofield, C.J., Spencer, J., 2019b. Molecular Basis of Class A β-Lactamase Inhibition by Relebactam. Antimicrob. Agents Chemother. 63, e00564-19. https://doi.org/10.1128/AAC.00564-19

Vaara, M., Sader, H.S., Rhomberg, P.R., Jones, R.N., Vaara, T., 2013. Antimicrobial activity of the novel polymyxin derivative NAB739 tested against Gram-negative pathogens. J. Antimicrob. Chemother. 68, 636–639. https://doi.org/10.1093/jac/dks438

Vivian, J.T., Callis, P.R., 2001. Mechanisms of Tryptophan Fluorescence Shifts in Proteins. Biophys. J. 80, 2093–2109. https://doi.org/10.1016/S0006-3495(01)76183-8

Vonhoff, S., Condliffe, J., Schiffter, H., 2010. Implementation of an FTIR calibration curve for fast and objective determination of changes in protein secondary structure during formulation development. J. Pharm. Biomed. Anal. 51, 39–45. https://doi.org/10.1016/j.jpba.2009.07.031

Wang, W.-J., Wang, Q., Zhang, Y., Lu, R., Zhang, Y.-L., Yang, K.-W., Lei, J.-E., He, Y., 2017. Characterization of β-lactamase activity using isothermal titration calorimetry. Biochim. Biophys. Acta BBA - Gen. Subj. 1861, 2031–2038. https://doi.org/10.1016/j.bbagen.2017.04.011

Wang, Z., Fast, W., Valentine, A.M., Benkovic, S.J., 1999. Metallo-β-lactamase: structure and mechanism. Curr. Opin. Chem. Biol. 3, 614–622. https://doi.org/10.1016/S1367-5931(99)00017-4

Ward, W.H., Holdgate, G.A., 2001. Isothermal titration calorimetry in drug discovery. Prog. Med. Chem. 38, 309–376. https://doi.org/10.1016/s0079-6468(08)70097-3

Weik, M., Colletier, J.-P., 2010. Temperature-dependent macromolecular X-ray crystallography. Acta Crystallogr. D Biol. Crystallogr. 66, 437–446. https://doi.org/10.1107/S0907444910002702

Wille, H., Requena, J.R., 2018. The Structure of PrPSc Prions. Pathogens 7, 20. https://doi.org/10.3390/pathogens7010020

Wong, J.W., Albright, R.L., Wang, N.-H.L., 1991. Immobilized Metal Ion Affinity Chromatography (IMAC) Chemistry and Bioseparation Applications. Sep. Purif. Methods 20, 49–106. https://doi.org/10.1080/03602549108021408

Yang, H., Yang, S., Kong, J., Dong, A., Yu, S., 2015. Obtaining information about protein secondary structures in aqueous solution using Fourier transform IR spectroscopy. Nat. Protoc. 10, 382–396. https://doi.org/10.1038/nprot.2015.024

Yang, H.Y., Nam, Y.S., Lee, H.J., 2014. Prevalence of plasmid-mediated quinolone resistance genes among ciprofloxacin-nonsusceptible Escherichia coli and Klebsiella pneumoniae isolated from blood cultures in Korea. Can. J. Infect. Dis. Med. Microbiol. J. Can. Mal. Infect. Microbiol. Medicale 25, 163–169. https://doi.org/10.1155/2014/329541

Yang, Youjun, Rasmussen, B.A., Shlaes, D.M., 1999. Class A β-lactamases—enzyme-inhibitor interactions and resistance. Pharmacol. Ther. 83, 141–151. https://doi.org/10.1016/S0163-7258(99)00027-3

Yang, Y., Rasmussen, B.A., Shlaes, D.M., 1999. Class A beta-lactamases--enzyme-inhibitor interactions and resistance. Pharmacol. Ther. 83, 141–151. https://doi.org/10.1016/s0163-7258(99)00027-3

Zhang, Y.-J., Wang, W.-M., Oelschlaeger, P., Chen, C., Lei, J.-E., Lv, M., Yang, K.-W., 2018. Real-Time Monitoring of NDM-1 Activity in Live Bacterial Cells by Isothermal Titration Calorimetry: A New Approach To Measure Inhibition of Antibiotic-Resistant Bacteria. ACS Infect. Dis. 4, 1671–1678. https://doi.org/10.1021/acsinfecdis.8b00147

Zharkova, M.S., Golubeva, O.Yu., Orlov, D.S., Vladimirova, E.V., Dmitriev, A.V., Tossi, A., Shamova, O.V., 2021. Silver Nanoparticles Functionalized With Antimicrobial Polypeptides: Benefits and Possible Pitfalls of a Novel Anti-infective Tool. Front. Microbiol. 12.

Zhu, S., Gong, C., Ren, L., Li, X., Song, D., Zheng, G., 2013. A simple and effective strategy for solving the problem of inclusion bodies in recombinant protein technology: His-tag deletions enhance soluble expression. Appl. Microbiol. Biotechnol. 97, 837–845. https://doi.org/10.1007/s00253-012-4630-y

Supplementary Figures and Tables

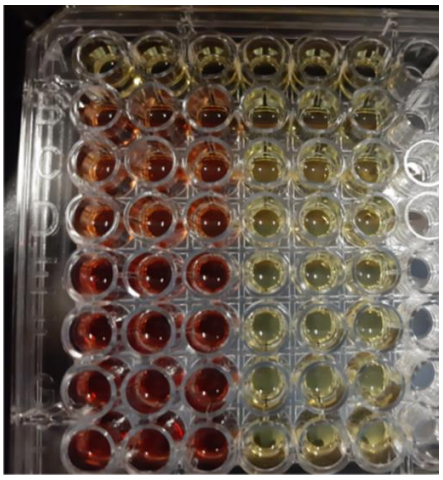

Figure S1: Specific activity of WT-*KpBlac-1* and S70A-*KpBlac-1* assessed with nitrocefin. The ability of WT-*KpBlac-1* and S70A-*KpBlac-1* to hydrolyse nitrocefin was assessed. The experiment was conducted with varied WT-*KpBlac-1* and S70A-*KpBlac-1* concentrations (0 µM to 1600 µM) and 0.5 mg/mL Nitrocefin at 482 nm, and setup as indicated on Figure 3.4 (methods section). Red color change indicts Nitrocefin hydrolysis by WT-*KpBlac-1* (Well Lane (triplicate) 1-3). Yellow color indicts intact Nitrocefin from which hydrolysis of nitrocefin by S70A-*KpBlac-1* was unsuccessful.

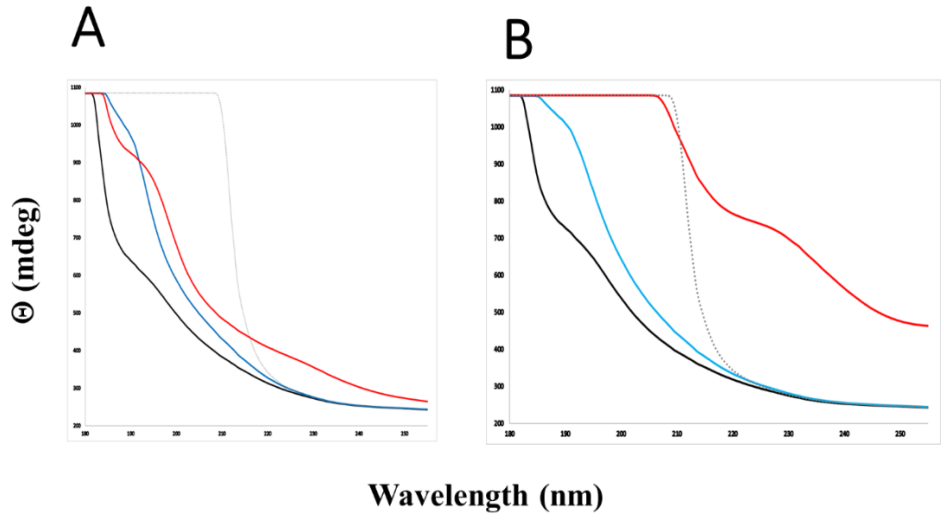

Figure S2: HT-voltage of secondary structural spectral analysis of WT-Kpβlac-1 and S70A-Kpβlac-1. The high tension (HT) voltage results from A) WT-Kpβlac-1; native (black), denatured (grey-dotted line), penicillin (blue) and CPZ (red); and B) S70A-Kpβlac-1; native (black), denatured (grey-dotted line), penicillin (blue) and CPZ (red).

Table S1: Intrinsic fluorescence emission spectrum shifts of WT-Kpβlac-1 and S70A-Kpβlac-1. Tryptophan fluorescence shifts and maximum emission wavelengths of WT-Kpβlac-1 and S70A-Kpβlac-1 analysis in the presence of penicillin and CPZ.

		Maximum emission wavelength (nm)	Type of shift relative to Native
WT-KpBLac-1	**Native**	339.5	Baseline
	Denatured	348.5	Redshift
	Penicillin	340.5	Redshift
	Cefoperazone	341.5	Redshift
S70A-KpBLac-1	**Native**	339.5	Baseline
	Denatured	350.0	Redshift
	Peniciilin	339.5	No shift
	Cefoperazone	340.5	Redshift

Table S2: Extrinsic fluorescence emission spectrum shifts of WT-Kpβlac-1 and S70A-Kpβlac-1. ANS fluorescence shifts and maximum emission wavelengths of WT-Kpβlac-1 and S70A-Kpβlac-1 analysis in the presence of penicillin and CPZ.

		Maximum emission wavelength (nm)	Type of shift relative to Native
WT-KpBLac-1	**Native**	509.0	Baseline
	Denatured	519.0	Redshift
	Penicillin	510.0	Redshift
	Cefoperazone	508.0	Blueshift
S70A-KpBLac-1	**Native**	520.5	Baseline
	Denatured	517.0	Blueshift
	Penicillin	512.0	Blueshift
	Cefoperazone	517.5	Blueshift

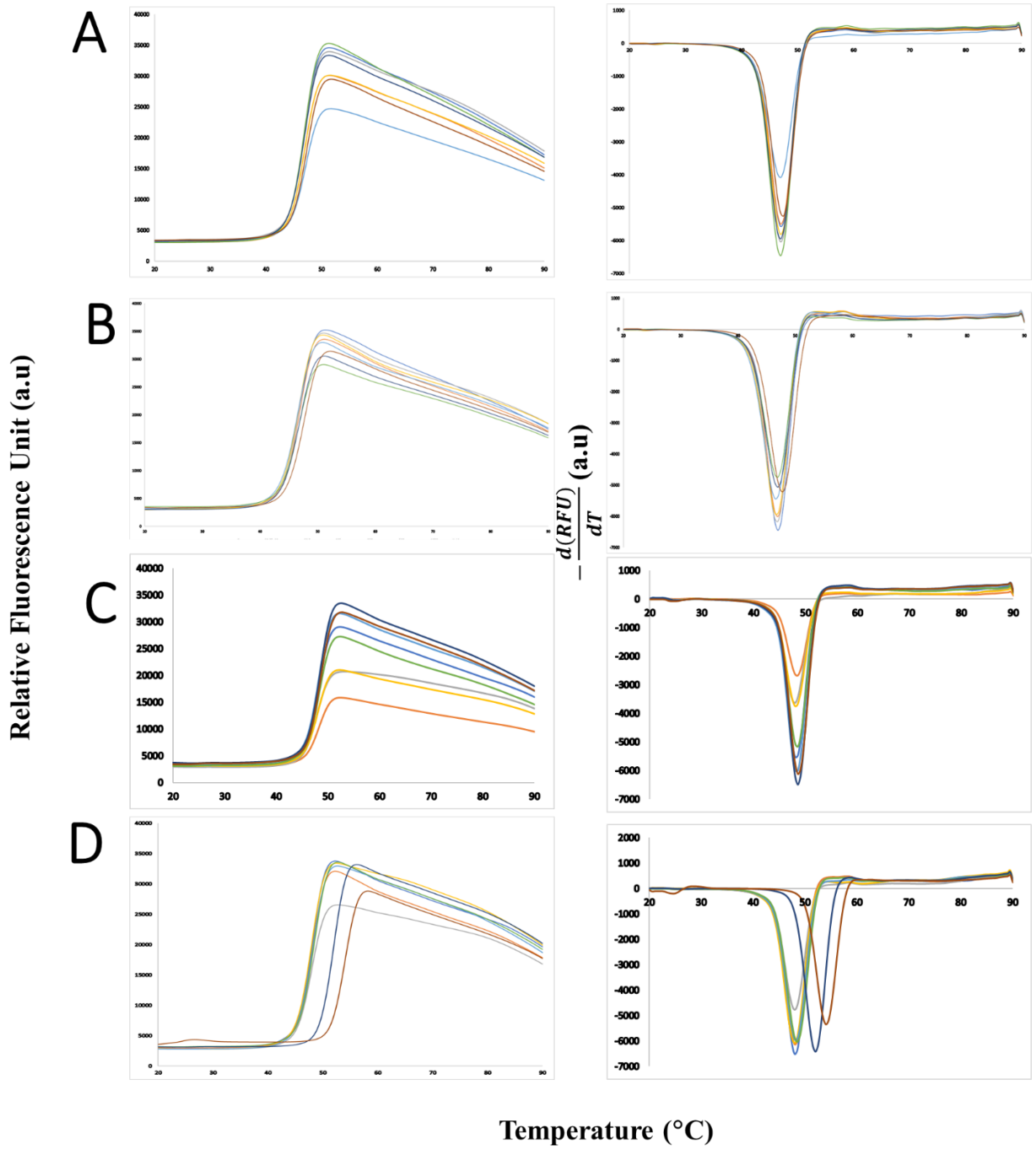

Figure S3: Thermal stability of WT-*KpBlac-1* and S70A-*KpBlac-1* with TSA. The thermal denaturation stability and of native WT-Kpβlac-1 and S70A-Kpβlac-1 in the presence of penicillin and CPZ were monitored using SYPRO orange dye from 20 to 90 °C The experiment was conducted with varied penicillin and CPZ concentrations (0 µM to 2000 µM), and setup as indicated on Figure 3.8 (methods section). The assessment of WT-Kpβlac-1 in the presence and absence of A) penicillin and B) CPZ. The assessment of S70A-Kpβlac-1 in the presence and absence of C) penicillin and D) CPZ. A shift of temperature was only noticed with S70A-Kpβlac-1 in the presence of CPZ (D).

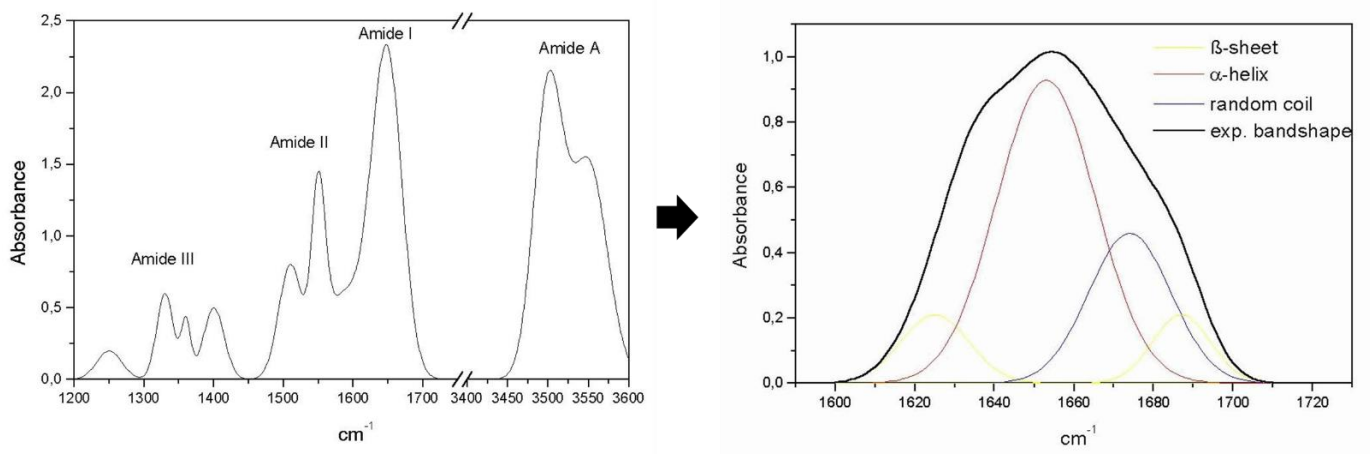

https://images.app.goo.gl/5Nz7A8cj75iq4hn7A
https://images.app.goo.gl/qZKcYmDVmqT1PeiE6

Figure S4: Fourier Transform Infrared Spectroscopy for determination of protein secondary structure. From a FTIR spectrum, Amide I and II provides information about hydrogen-bonding of the backbone. The Amide I and II spectra are deconvoluted to estimate the proportion of secondary structural content.

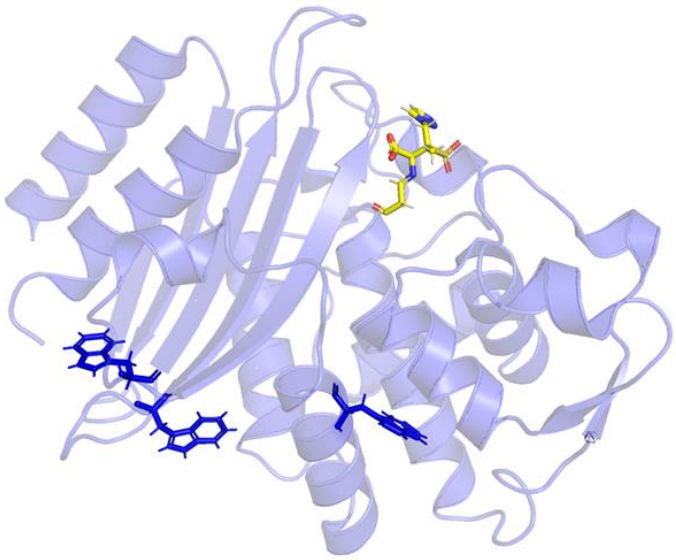

Figure S5: Crystal structure of CTX-M-15 indicting position of tryptophan residues. The structure was obtained through X-ray diffraction method with a resolution of 1.14 Å. Uniport ID: W1DN50, PDBe ID: 6z7j. Images generated with PyMol. Co-crystallised enzyme structure with emmetazobactam (yellow stick Figure) indicating location of tryptophan residues; Trp195, Trp214, and Trp235 (blue stick figures).

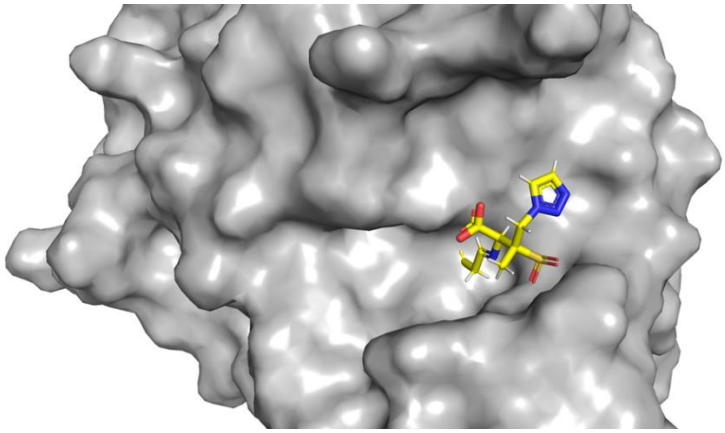

Figure S6: Crystal structure of CTX-M-15 indicating active site pocket. The structure was obtained through X-ray diffraction method with a resolution of 1.14 Å. Uniport ID: W1DN50, PDBe ID: 6z7j. Images generated with PyMol. A hydrophobic surface structure co-crystallised enzyme structure with emmetazobactam, outlining position of the active site and its hydrophobicity.